

LAMINAR NATURAL CONVECTION IN
RECTANGULAR CAVITIES

LAMINAR NATURAL CONVECTION IN AIR-FILLED RECTANGULAR
CAVITIES WITH AND WITHOUT PARTITIONS ON WALLS

By

WENJIANG WU, M.A.Sc., B.ENG.

A Thesis

Submitted to the School of Graduate Studies

in Partial Fulfilment of the Requirements

for the Degree

Doctor of Philosophy

McMaster University

©Copyright by Wenjiang Wu, December 2008

DOCTOR OF PHILOSOPHY (2008)
(Mechanical Engineering)

McMaster University
Hamilton, Ontario

TITLE: Laminar Natural Convection in Air-Filled Rectangular Cavities with and without Partitions on Walls

AUTHOR: Wenjiang Wu, M.A.Sc. (McMaster University)

SUPERVISOR: Dr. Chan Ching, Associate Professor
Department of Mechanical Engineering

NUMBER OF PAGES: xxviii; 189

To my parents

Abstract

The laminar natural convection in air-filled rectangular cavities with and without a partition on the wall was experimentally investigated. Temperature measurements and flow visualizations were performed for cases with heated and cooled vertical walls (corresponding to global Grashof numbers Gr_H of approximately 1.4×10^8 to 1.8×10^8) and non-dimensional top wall temperatures θ_T of 0.52 (insulated) to 2.3. In the rectangular cavities without the partition and with aspect ratios of 0.5, 1.0 and 2.0, the heated top wall caused the natural convection boundary layer flow to separate from either the top wall (for the cases with $\theta_T \lesssim 1.2$) or the heated vertical wall (for the cases with $\theta_T \gtrsim 1.2$) due to the negative buoyancy force. For the cases with $\theta_T \gtrsim 1.2$, there is an anti-clockwise recirculating flow in the upper left corner region. The extent of the recirculating flow decreased with an increase of the aspect ratio. The temperature gradient in the core region, $d\theta_\infty/d(y/H)$, increased with an increase of θ_T . For a given aspect ratio, $d\theta_\infty/d(y/H)$ changed more rapidly with the change in θ_T for the cases with $\theta_T \lesssim 1.2$ compared to the cases with $\theta_T \gtrsim 1.2$. The increase in $d\theta_\infty/d(y/H)$ was more significant for the smaller aspect ratio cavity. The temperature profiles predicted from the similarity solutions proposed by Kulkarni et al. [1] and from the non-similarity model developed by Chen and Eichhorn [2] for natural convection on an isothermal vertical wall in a stratified environment were compared to the measurements in the current cases. These models were not

able to accurately describe the characteristics of the natural convection flow in the rectangular cavities.

An aluminium partition with non-dimensional heights H_P/H of 0.0625 and 0.125 was attached either to the heated vertical wall or top wall at $y/H = 0.65, 0.95$ and $x/H = 0.1, 0.2, 0.4$ and 0.6 to study the effect of the partition on the laminar natural convection flow in a square cavity. The blockage and thermal effects of the partition resulted in changes in the temperature and flow fields, but were mainly limited in the vicinity of the partition. The effect of the partition changed with the height and location of the partition. When the partition was attached to the heated top wall, a recirculating flow was formed between the partition and the heated vertical wall. For a given partition height, the structure of this recirculating flow was dependent on the partition location and θ_T . A thermal boundary layer developed along the rear surface of the partition due to the thermal effect of the partition. The ambient temperature outside the boundary layer and Nu near the corner region were affected by the partition height due to the changes in the recirculating flow and the rear surface of the partition.

Acknowledgements

The author would like to express his gratitude to his supervisor Dr. Chan Ching for his valuable guidance and support throughout the course of this Ph.D. program. The author is grateful to other members of his supervisory committee, Dr. Gordon Irons and Dr. Sumanth Shankar, for their valuable suggestions and comments in the last few years. The author would also like to thank Dr. Dan Ewing for his advice and help with this work.

The author also appreciates his colleagues in the Thermal Management Research Laboratory (TMRL) for their kind help. Gratitude is also extended to the technicians, Mr. Ron Lodewyks, Mr. Mark MacKenzie, Mr. Dave Schick, Mr. Joe Verhaeghe and Mr. Jim McLaren, for their kind and patient help.

I would like to express my cordial appreciation to my best friend in Canada, Dr. Li Pan, for his selfless and sufficient help as well as support and encouragement in the past several years.

Last, but not the least, I would like to express my sincere gratitude to my parents, who always provided me with solid support and encouragement in all my endeavors, whether it was a success or failure. However, I was not able to repay their love in the last few years, to which I regret very much. I am also grateful to my older brother for his consideration, support and encouragement.

Table of Contents

Abstract	iv
Acknowledgements	vi
Table of Contents	vii
List of Tables	x
List of Figures	xii
Nomenclature	xxv
1 Introduction	1
2 Literature Review	6
2.1 Natural convection in rectangular cavities with smooth walls	6
2.1.1 Effect of the aspect ratio	7
2.1.2 Effect of the temperature difference between the top and bot- tom walls	16
2.1.3 Effect of the inclination	20
2.1.4 Summary and limitations	21

2.2	Natural convection in rectangular cavities with partitions attached to walls	23
2.2.1	Partitions attached to the vertical walls of rectangular cavities	23
2.2.2	Partitions attached to the horizontal walls of rectangular cavities	25
2.2.3	Effect of partition parameters on the natural convection flow .	32
2.2.4	Summary and Limitations	35
2.3	Theoretical Models	35
3	Experimental Methodology	37
3.1	Experimental Facility	37
3.2	Experimental Techniques	48
3.3	Data Reduction and Uncertainty Analysis	54
4	The effect of the top wall temperature on the laminar natural convection in rectangular cavities with smooth walls	63
4.1	The effect of a modest top wall temperature	64
4.2	The effect of a large top wall temperature	81
4.3	The effect of the large top wall temperature on the natural convection in rectangular cavities with different aspect ratios	99
5	Effect of a partition on the laminar natural convection in a square cavity with different top wall temperatures	116
5.1	Effect of a partition on the heated vertical wall	117
5.2	Effect of a partition on the top wall	134
6	Conclusions	166
7	Recommendations	173

List of Tables

2.1	Summary of investigations of natural convection in square cavities with smooth walls.	9
2.2	Summary of investigations of natural convection in rectangular cavities with smooth walls.	13
2.3	Summary of correlations for the natural convective heat transfer in rectangular cavities with the aspect ratio much larger or less than unity.	17
2.4	Summary of heat transfer correlations for the natural convection flow in tilted rectangular cavities.	22
2.5	Summary of investigations of natural convection in rectangular cavities with partitions attached to the vertical walls.	26
2.6	Summary of investigations of natural convection in rectangular cavities with partitions on the horizontal walls.	28
3.1	Summary of the uncertainties in the local heat flux, local heat transfer coefficient, local Nusselt number, local Rayleigh number and temperature gradient.	62
4.1	Summary of the wall temperatures, global Grashof numbers, and parameters in the correlation $Nu = C \cdot Ra^n$ for cases with modest top wall temperatures.	70

4.2	Summary of the wall temperatures, global Grashof numbers, and parameters in the correlation $Nu = C \cdot Ra^n$ for cases with large top wall temperatures.	85
5.1	Summary of the wall temperatures, global Grashof numbers, and parameters in the correlation $Nu = C \cdot Ra^n$ for the square cavity with a partition attached to the heated vertical wall at $y/H = 0.95$	121
5.2	Summary of the wall temperatures, global Grashof numbers, and parameters in the correlation $Nu = C \cdot Ra^n$ for the square cavity with a partition attached to the top wall at different locations.	139

List of Figures

3.1	Schematic of the rectangular cavity from (a) the side view and (b) the top view.	39
3.2	Schematic of the top wall.	41
3.3	Schematic of the heated vertical wall.	42
3.4	Detailed structure of the thermocouple embedded in the wall from (a) the top view and (b) the side view.	44
3.5	Schematic of the bottom wall with cooling channels.	46
3.6	Schematic of the cooled vertical wall with cooling channels.	47
3.7	Detailed structure of the corner between the heated vertical wall, heated vertical guard wall and the bottom wall.	49
3.8	Structure and dimensions of the thermocouple probe unit.	51
3.9	Photograph of the thermocouple probe unit.	51
3.10	Comparison of temperatures measured with \bigcirc : the 0.002" thermocouple and \bullet : the 0.010" thermocouple with the temperature measured by a platinum RTD.	53
3.11	Typical temperature distributions along the centreline of the heated vertical wall of the rectangular cavities with aspect ratios of Δ : 0.5, \bigcirc : 1.0 and \square : 2.0 for the top wall temperature of approximately $93^{\circ}C$ corresponding to the non-dimensional temperature of 1.14.	53

3.12	Temperature distributions on the insulated top wall of the rectangular cavities with aspect ratios of Δ : 0.5, \bigcirc : 1.0 and \square : 2.0.	55
3.13	Best linear fit used to determine the slope of the temperature profile at the non-dimensional height $y/H = 0.6$ of the square cavity with the top wall temperature of $79^{\circ}C$ corresponding to the non-dimensional temperature of 0.99.	55
3.14	Schematic of the central area of the heated vertical wall used to estimate energy balance.	58
3.15	Schematic of the control volume used to estimate energy balance for the entire system.	60
4.1	Non-dimensional temperature profiles in cavities (Left) and flow patterns in the upper left corner region (Right) for cases with aspect ratios of (a) 0.5, (b) 1.0 and (c) 2.0 for non-dimensional top wall temperatures of approximately 0.52 (insulated). Here, open and filled symbols were used to distinguish the temperature distributions at the different heights.	66
4.2	A schematic of the flow pattern in the upper left corner region of the square cavity with the non-dimensional top wall temperature of approximately 0.54 (insulated).	68
4.3	Non-dimensional temperature profiles in cavities (Left) and flow patterns in the upper left corner region (Right) for cases with aspect ratios of (a) 0.5, (b) 1.0 and (c) 2.0 for non-dimensional top wall temperatures of approximately 0.83. Here, open and filled symbols were used to distinguish the temperature distributions at the different heights.	71

4.4	Non-dimensional temperature profiles in cavities (Left) and flow patterns in the upper left corner region (Right) for cases with aspect ratios of (a) 0.5, (b) 1.0 and (c) 2.0 for non-dimensional top wall temperatures of approximately 1. Here, open and filled symbols were used to distinguish the temperature distributions at the different heights. . .	72
4.5	Non-dimensional temperature profiles in cavities (Left) and flow patterns in the upper left corner region (Right) for cases with aspect ratios of (a) 0.5, (b) 1.0 and (c) 2.0 for non-dimensional top wall temperatures of approximately 1.14. Here, open and filled symbols were used to distinguish the temperature distributions at the different heights. .	73
4.6	A typical schematic of the flow pattern in the upper left corner region of the rectangular cavity with the aspect ratio of 0.5 and non-dimensional top wall temperature of approximately 1.	74
4.7	Comparison of the non-dimensional local ambient temperature outside the boundary layer for cases with aspect ratios of (a) 0.5, (b) 1.0 and (c) 2.0. Here the non-dimensional top wall temperatures were Δ :0.52 (insulated), \bigcirc :0.83, \diamond :1 and \square :1.14.	76
4.8	Change in the vertical gradient of the temperature outside the boundary layer on the heated vertical wall with the change in the top wall temperature for cases with aspect ratios of Δ :0.5, \bigcirc :1.0 and \square :2.0. .	78
4.9	Comparison of the local heat flux along the heated vertical wall of cavities with aspect ratios of (a)0.5, (b) 1.0 and (c) 2.0. Here the non-dimensional top wall temperatures were Δ : 0.52 (insulated), \bigcirc : 0.83, \diamond : 1 and \square : 1.14.	79

4.10	Change in the local Nusselt number with the local Rayleigh number for cases with aspect ratios of (a)0.5, (b) 1.0 and (c) 2.0. Here the non-dimensional top wall temperatures were Δ : 0.52 (insulated), \circ : 0.83, \diamond : 1 and \square : 1.14.	82
4.11	Change in the local Nusselt number with the local Rayleigh number for the case with a non-dimensional top wall temperature of approximately 1. Here the error bars for local Nusselt numbers and local Rayleigh numbers are, respectively, set to (a) $\pm 6 - 9\%$ and $\pm 4 - 8\%$ for aspect ratio of 0.5, (b) $\pm 6 - 9\%$ and $\pm 4 - 6\%$ for aspect ratio of 1.0 and (c) $\pm 6 - 10\%$ and $\pm 4 - 9\%$ for aspect ratio of 2.0.	83
4.12	Flow patterns (Left) and temperature contours (Right) in the upper left region of the square cavity with non-dimensional top wall temperatures of (a) 1.4, (b) 1.9 and (c) 2.3.	87
4.13	A typical schematic of the flow pattern in the upper left corner region of the square cavity with the non-dimensional top wall temperature of 2.3.	88
4.14	Typical flow patterns in the upper left region of the square cavity with non-dimensional top wall temperature of 2.3. The images (a) and (b) were taken approximately 4 hours apart.	88
4.15	Changes in the local buoyancy force distributions along the heated vertical wall (Left) with an enlarged view in the corner region (Right) for non-dimensional top wall temperatures of (a) 1.4, (b) 1.9 and (c) 2.3.	90
4.16	Comparison of the non-dimensional temperature distributions at $x/H = 0.25$ for the square cavity with non-dimensional top wall temperatures of Δ : 1.4, \square : 1.9 and \circ : 2.3.	91

4.17	Comparison of the non-dimensional temperature distributions, θ_1 , predicted by the similarity model [1] with the measurements in the square cavity for non-dimensional top wall temperatures of (a) 1.4, (b) 1.9, and (c) 2.3 at the different heights.	94
4.18	Comparison of the non-dimensional temperature profiles - - -: predicted by the non-similarity solution [2] and —: from the measurements in the square cavity for non-dimensional top wall temperatures of (a) 1.4, (b) 1.9, and (c) 2.3.	96
4.19	Comparison of the non-dimensional temperature gradient at the surface of the heated vertical wall, $-\theta'_2(0, y/H)$, from the non-similarity model [2] (open) and the experimental data (solid) with the non-dimensional top wall temperatures of Δ : 1.4, \square : 1.9, and \circ : 2.3. . .	98
4.20	Comparison of the non-dimensional integral of the buoyancy force across the boundary layer flow along the heated vertical wall, $B(y)$, from the non-similarity model [2] (open) and the experimental data (solid) with the non-dimensional top wall temperatures of Δ : 1.4, \square : 1.9, and \circ : 2.3.	98
4.21	Comparison of the non-dimensional momentum flux of the boundary layer flow along the heated vertical wall, $M(y)$, predicted from the non-similarity model [2] for non-dimensional top wall temperatures of Δ : 1.4, \square : 1.9, and \circ : 2.3.	100
4.22	Non-dimensional temperature profiles in cavities (Left) and flow patterns in the upper left corner region (Right) for cases with aspect ratios of (a) 0.5, (b) 1.0 and (c) 2.0 for non-dimensional top wall temperature of approximately 2.3.	102

4.23	Non-dimensional temperature profiles in cavities (Left) and flow patterns in the upper left corner region (Right) for cases with aspect ratios of (a) 0.5, (b) 1.0 and (c) 2.0 for non-dimensional top wall temperature of approximately 1.9.	105
4.24	Non-dimensional temperature profiles in cavities (Left) and flow patterns in the upper left corner region (Right) for cases with aspect ratios of (a) 0.5, (b) 1.0 and (c) 2.0 for non-dimensional top wall temperature of approximately 1.4.	106
4.25	Comparison of the non-dimensional local ambient temperature outside of the boundary layer for cases with aspect ratios of (a) 0.5, (b) 1.0 and (c) 2.0. Here the non-dimensional top wall temperatures were Δ : 1.4, \square : 1.9 and \bigcirc : 2.3.	108
4.26	Change in the vertical gradient of the temperature outside the boundary layer on the heated vertical wall with the change in the top wall temperature for cases with aspect ratios of Δ : 0.5, \bigcirc : 1.0 and \square : 2.0.	109
4.27	Comparison of the local Nusselt number along the heated vertical wall for cases with aspect ratios of (a) 0.5, (b) 1.0 and (c) 2.0. Here the non-dimensional top wall temperatures were Δ : 1.4, \square : 1.9 and \bigcirc : 2.3.	111
4.28	Change in the local Nusselt number with the local Rayleigh number for cases with aspect ratios of (a) 0.5, (b) 1.0 and (c) 2.0. Here the non-dimensional top wall temperatures were Δ : 1.4, \square : 1.9 and \bigcirc : 2.3.	113

4.29	Change in the local Nusselt number with the local Rayleigh number along the heated vertical wall from $y/H = 0.2$ to 0.7 for cases with aspect ratios of 0.5 (small size symbols), 1.0 (mid size symbols) and 2.0 (large size symbols) under the non-dimensional top wall temperatures of $+$: 0.52 (insulated), \times : 0.83 , \diamond : 1 , $*$: 1.14 , Δ : 1.4 , \square : 1.9 and \bigcirc : 2.3	115
4.30	Change in the average Nusselt number for the heated vertical wall with the vertical Rayleigh number for cases with aspect ratios of Δ : 0.5 , \bigcirc : 1.0 and \square : 2.0	115
5.1	Flow patterns (Left) and the corresponding schematics (Right) in the upper left region of the square cavity with a partition on the heated vertical wall at $y/H = 0.65$ for the non-dimensional top wall temperatures of approximately (a) 0.57 (insulated), (b) 1.4 and (c) 2.3 . The non-dimensional height of the partition here was 0.0625	118
5.2	Flow patterns in the upper left region of the square cavity (Left) and non-dimensional temperature profiles in the square cavity for cases (a) without a partition and (b) with a partition on the heated vertical wall at $y/H = 0.95$ for non-dimensional top wall temperatures of approximately 0.59 (insulated). The non-dimensional height of the partition was 0.0625	122
5.3	Flow patterns in the upper left region of the square cavity (Left) and non-dimensional temperature profiles in the square cavity for cases (a) without a partition and (b) with a partition on the heated vertical wall at $y/H = 0.95$ for non-dimensional top wall temperatures of approximately 1.4 . The non-dimensional height of the partition was 0.0625	123

5.4	Flow patterns in the upper left region of the square cavity (Left) and non-dimensional temperature profiles in the square cavity for cases (a) without a partition and (b) with a partition on the heated vertical wall at $y/H = 0.95$ for non-dimensional top wall temperatures of approximately 2.3. The non-dimensional height of the partition was 0.0625.	124
5.5	Flow pattern in the upper left region of the square cavity (Left) and non-dimensional temperature profiles in the square cavity with a partition attached on the heated vertical wall at $y/H = 0.95$ for the non-dimensional top wall temperature of approximately 1.4. The non-dimensional height of the partition was 0.125.	127
5.6	Flow pattern in the upper left region of the square cavity (Left) and non-dimensional temperature profiles in the square cavity with a partition attached on the heated vertical wall at $y/H = 0.95$ for the non-dimensional top wall temperature of approximately 2.3. The non-dimensional height of the partition was 0.125.	127
5.7	Comparison of the non-dimensional ambient temperature outside of the boundary layer for cases with or without a partition on the heated vertical wall at $y/H = 0.95$. Smooth wall cavity with θ_T of +: 0.54 (insulated). Partition with the non-dimensional height of 0.0625 and θ_T of \circ : 0.59 (insulated), \triangle : 1.4, and \square : 2.3. Partition with the non-dimensional height of 0.125 and θ_T of \times : 1.4 and \diamond : 2.3.	128

5.8	Comparison of the non-dimensional ambient temperature outside of the boundary layer for cases with the non-dimensional top wall temperatures of (a) 1.4 and (b) 2.3. ○: without partition, △: the partition with the non-dimensional height of 0.0625 on the heated vertical wall at $y/H = 0.95$, □: the partition with the non-dimensional height of 0.125 on the heated vertical wall at $y/H = 0.95$	130
5.9	Comparison of the local Nusselt number along the heated vertical wall of the square cavity with or without a partition on the heated vertical wall at $y/H = 0.95$. Smooth wall cavity with θ_T of +: 0.54 (insulated), ▲: 1.4 and ■: 2.3. Partition with the non-dimensional height of 0.0625 and θ_T of ○: 0.59 (insulated), △: 1.4, and □: 2.3. Partition with the non-dimensional height of 0.125 and θ_T of ×: 1.4 and ◇: 2.3.	132
5.10	Change in the local Nusselt number with the local Rayleigh number for cases with a partition on the heated vertical wall at $y/H = 0.95$. Partition with the non-dimensional height of 0.0625 and θ_T of ○: 0.59 (insulated), △: 1.4 and □: 2.3. Partition with the non-dimensional height of 0.125 and θ_T of ×: 1.4 and ◇: 2.3.	135
5.11	Flow patterns across the entire width of the partitioned square cavity for non-dimensional top wall temperature of approximately 0.56 (insulated) with the partition ($H_P/H = 0.0625$) attached at (a) $x/H = 0.1$, (b) $x/H = 0.2$, (c) $x/H = 0.4$ and (d) $x/H = 0.6$	136
5.12	Flow patterns across the entire width of the partitioned square cavity for non-dimensional top wall temperature of approximately 1.4 with the partition ($H_P/H = 0.0625$) attached at (a) $x/H = 0.1$, (b) $x/H = 0.2$, (c) $x/H = 0.4$ and (d) $x/H = 0.6$	137

5.13	Flow patterns across the entire width of the partitioned square cavity for non-dimensional top wall temperature of approximately 2.3 with the partition ($H_P/H = 0.0625$) attached at (a) $x/H = 0.1$, (b) $x/H = 0.2$, (c) $x/H = 0.4$ and (d) $x/H = 0.6$	138
5.14	Flow patterns across the entire width of the partitioned square cavity for non-dimensional top wall temperature of approximately 1.4 with the partition ($H_P/H = 0.125$) attached at (a) $x/H = 0.1$, (b) $x/H = 0.2$, (c) $x/H = 0.4$ and (d) $x/H = 0.6$	143
5.15	Flow patterns across the entire width of the partitioned square cavity for non-dimensional top wall temperature of approximately 2.3 with the partition ($H_P/H = 0.125$) attached at (a) $x/H = 0.1$, (b) $x/H = 0.2$, (c) $x/H = 0.4$ and (d) $x/H = 0.6$	144
5.16	Flow pattern across the entire width of the partitioned square cavity for non-dimensional top wall temperature of approximately 1.4 with a wooden partition ($H_P/H = 0.125$) attached on the top wall at $x/H = 0.2$.	146
5.17	Non-dimensional temperature profiles along the heated vertical wall of the square cavity (a) without the partition and with the partition on the top wall (b) at $x/H = 0.2$ and (c) at $x/H = 0.6$ for non-dimensional top wall temperature of approximately 0.56 (insulated). Here, the non-dimensional height of the partition was 0.0625.	147
5.18	Non-dimensional temperature profiles along the heated vertical wall of the square cavity (a) without the partition and with the partition on the top wall (b) at $x/H = 0.2$ and (c) at $x/H = 0.6$ for non-dimensional top wall temperature of approximately 1.4. Here, the non-dimensional height of the partition was 0.0625.	148

5.19	Non-dimensional temperature profiles along the heated vertical wall of the square cavity (a) without the partition and with the partition on the top wall (b) at $x/H = 0.2$ and (c) at $x/H = 0.6$ for non-dimensional top wall temperature of approximately 2.3. Here, the non-dimensional height of the partition was 0.0625.	149
5.20	Non-dimensional temperature profiles along the heated vertical wall of the square cavity with the partition on the top wall (a) at $x/H = 0.2$ and (b) at $x/H = 0.6$ for non-dimensional top wall temperature of approximately 1.4. Here, the non-dimensional height of the partition was 0.125.	153
5.21	Non-dimensional temperature profiles along the heated vertical wall of the square cavity with the partition on the top wall (a) at $x/H = 0.2$ and (b) at $x/H = 0.6$ for non-dimensional top wall temperature of approximately 2.3. Here, the non-dimensional height of the partition was 0.125.	154
5.22	Comparison of the non-dimensional temperature outside of the boundary layer for cases with the non-dimensional top wall temperature of approximately 0.56 (insulated). \circ : without the partition, \square : the partition on the top wall at $x/H = 0.2$, and \triangle : the partition on the top wall at $x/H = 0.6$. Here, the non-dimensional height of the partition was 0.0625.	155
5.23	Comparison of the non-dimensional temperature outside of the boundary layer for cases with non-dimensional top wall temperatures of (a) 1.4 and (b) 2.3. \circ : without the partition, \square : the partition on the top wall at $x/H = 0.2$, and \triangle : the partition on the top wall at $x/H = 0.6$. Here, the non-dimensional height of the partition was 0.0625.	157

5.24	Comparison of the non-dimensional temperature outside of the boundary layer for cases with the partition on the top wall at (a) $x/H = 0.2$ and (b) $x/H = 0.6$. The non-dimensional heights of the partitions were 0.0625 (open symbols) and 0.125 (filled symbols), respectively. \bigcirc : under the non-dimensional top wall temperature of 1.4, and \triangle : under the non-dimensional top wall temperature of 2.3.	158
5.25	Comparison of the local Nusselt number along the heated vertical wall of the square cavity with the non-dimensional top wall temperature of approximately 0.56 (insulated). \bigcirc : without the partition, \square : the partition on the top wall at $x/H = 0.2$, and \triangle : the partition on the top wall at $x/H = 0.6$. Here, the non-dimensional height of the partition was 0.0625.	160
5.26	Comparison of the local Nusselt number along the heated vertical wall of the square cavity for cases with non-dimensional top wall temperatures of (a) 1.4 and (b) 2.3. \bigcirc : without the partition, \square : the partition on the top wall at $x/H = 0.2$, and \triangle : the partition on the top wall at $x/H = 0.6$. Here, the non-dimensional height of the partition was 0.0625.	161
5.27	Comparison of the local Nusselt number along the heated vertical wall of the square cavity for cases with the partition on the top wall at (a) $x/H = 0.2$ and (b) $x/H = 0.6$. The non-dimensional heights of the partitions were 0.0625 (open symbols) and 0.125 (filled symbols), respectively. \bigcirc : under the non-dimensional top wall temperature of 1.4, and \triangle : under the non-dimensional top wall temperature of 2.3. .	162

5.28	Change in the local Nusselt number with the local Rayleigh number for cases with the partition on the top wall at (a) $x/H = 0.2$ and (b) $x/H = 0.6$. Partition with the non-dimensional height of 0.0625 and θ_T of \bigcirc : 0.56 (insulated), \triangle : 1.4 and \square : 2.3. Partition with the non-dimensional height of 0.125 and θ_T of \times : 1.4 and \diamond : 2.3.	165
7.1	Preliminary velocity measurements by a pulsed-wire for the upward boundary layer flow along the heated vertical wall at non-dimensional heights y/H of \triangle : 0.2, \bigcirc : 0.5 and \square : 0.8. These measurements were performed in the square cavity with smooth walls and non-dimensional top wall temperature θ_T of approximately 2.3.	175

Nomenclature

a	stratification rate of the ambient air, $a = dT_{\infty}/dy$
AR	aspect ratio of the cavity, $AR = H/L$
$B(y)$	non-dimensional integral of the buoyancy force along the heated vertical wall, $B(y) = \frac{\int_0^y \rho_{\infty}(y)g\beta(y) \cdot [T(x,y) - T_{\infty}(y)] \cdot dx}{(T_H - T_{\infty,0})\rho_{\infty}(y)\beta(y)g} \cdot \left(\frac{g\beta(y)a}{4\nu^2\xi}\right)^{1/4}$
c_p	specific heat, $J/kg \cdot ^{\circ}C$
C	constant in the Nusselt-Rayleigh number correlation, $Nu = C \cdot Ra^n$
$F_B(y)$	local buoyancy force along the heated vertical wall, $F_B(y) = \rho_{\infty}(y) \cdot g \cdot \beta(y) \cdot [T(x, y) - T_{\infty}(y)]$
g	gravity constant, m/s^2
Gr	local Grashof number, $Gr = \frac{g\beta(T_H - T_{\infty})y^3}{\nu^2}$
Gr_H	global Grashof number based on the height of the cavity, $Gr_H = \frac{g\beta(T_H - T_C)H^3}{\nu^2}$
Gr_L	global Grashof number based on the width of the cavity, $Gr_L = \frac{g\beta(T_H - T_C)L^3}{\nu^2}$
h	local heat transfer coefficient, $W/m^2 \cdot ^{\circ}C$
\bar{h}	average heat transfer coefficient for the heated vertical wall, $W/m^2 \cdot ^{\circ}C$
H	height of the cavity, m
H_P	height of the partition, m

k	thermal conductivity of the air, $W/m \cdot ^\circ C$
L	width of the cavity, m
\dot{m}	mass flow rate of the water, kg/s
$M(y)$	non-dimensional momentum flux of the boundary layer flow along the heated vertical wall, $M(y) = \frac{\int_0^{\delta} V \rho_{\infty}(y) V \cdot dx}{\rho_{\infty}(y) \cdot 2^{5/2} \cdot \nu^{1/2} \cdot [g\beta(y)]^{3/4} \cdot (T_H - T_{\infty,0})^{3/4} \cdot y^{5/4}}$
n	index in the Nusselt-Rayleigh number correlation, $Nu = C \cdot Ra^n$
Nu	local Nusselt number, $Nu = \frac{hy}{k}$
Nu_H	Nusselt number based on the height of the cavity, $Nu_H = \frac{hH}{k}$
\overline{Nu}_H	average Nusselt number for the heated vertical wall, $\overline{Nu}_H = \frac{\overline{h}H}{k}$
Nu_L	Nusselt number based on the width of the cavity, $Nu_L = \frac{hL}{k}$
\overline{Nu}_L	average Nusselt number based on the width of the cavity, $\overline{Nu}_L = \frac{\overline{h}L}{k}$
Pr	Prandtl number, $Pr = \frac{\nu}{\alpha}$
q''	local heat flux, W/m^2
Q	heat transfer rate, W
Ra	local Rayleigh number, $Ra = \frac{g\beta(T_H - T_{\infty})y^3}{\alpha\nu}$
Ra_H	global Rayleigh number based on the height of the cavity, $Ra_H = Gr_H \cdot Pr = \frac{g\beta(T_H - T_C)H^3}{\alpha\nu}$
Ra_L	global Rayleigh number based on the width of the cavity, $Ra_L = \frac{g\beta(T_H - T_C)L^3}{\alpha\nu}$
Ra_V	vertical Rayleigh number based on the temperature difference between the top and bottom walls, $Ra_V = \frac{g\beta(T_T - T_B)H^3}{\alpha\nu}$
T_B	average temperature of the bottom wall in the cavity, $^\circ C$
T_C	average temperature of the cooled vertical wall in the cavity, $^\circ C$
T_{edge}	temperature at the edge of the conduction layer, $^\circ C$

T_H	average temperature of the heated vertical wall in the cavity, $^{\circ}C$
T_T	average temperature of the top wall in the cavity, $^{\circ}C$
T_{∞}	local ambient temperature outside of the thermal boundary layer, $^{\circ}C$
$T_{\infty,0}$	temperature of the ambient air at the height of $y = 0$ extrapolated from the measured temperature gradient dT_{∞}/dy , $^{\circ}C$
$T_{w,i}$	temperature of water measured at the inlet of the cooling channel, $^{\circ}C$
$T_{w,o}$	temperature of water measured at the outlet of the cooling channel, $^{\circ}C$
V	vertical velocity component of the upward flow along the heated vertical wall, m/s
x	distance from the heated vertical wall, m
y	height above the bottom wall, m
α	thermal diffusivity, m^2/s
β	volume expansion coefficient at constant pressure, K^{-1}
η_1	a non-dimensional distance from the heated vertical wall in the similarity solution [1], $\eta_1 = (g\beta/4\nu^2)^{1/4}a^{1/4}x$
η_2	a non-dimensional distance from the heated vertical wall in the non-similarity solution [2], $\eta_2 = (g\beta/4\nu^2)^{1/4}(a/\xi)^{1/4}x$
ν	kinematic viscosity, m^2/s
ρ_{∞}	density of the ambient air, kg/m^3
θ	non-dimensional temperature, $\theta = (T - T_C)/(T_H - T_C)$
θ_B	non-dimensional temperature of the bottom wall in the cavity, $\theta_B = (T_B - T_C)/(T_H - T_C)$

θ_C	non-dimensional temperature of the cooled vertical wall in the cavity, $\theta_C = (T_C - T_C)/(T_H - T_C)$
θ_H	non-dimensional temperature of the heated vertical wall in the cavity, $\theta_H = (T_H - T_C)/(T_H - T_C)$
θ_T	non-dimensional temperature of the top wall in the cavity, $\theta_T = (T_T - T_C)/(T_H - T_C)$
θ_∞	non-dimensional local ambient temperature outside the boundary layer, $\theta_\infty = (T_\infty - T_C)/(T_H - T_C)$
θ_1	a non-dimensional temperature in the similarity solution [1], $\theta_1 = (T - T_\infty)/(T_H - T_\infty)$
θ_2	a non-dimensional temperature in the non-similarity solution [2], $\theta_2 = (T - T_\infty)/(T_H - T_{\infty,0})$
$d\theta_\infty/d(y/H)$	vertical gradient of the non-dimensional temperature outside the boundary layer on the heated vertical wall
ϕ	cavity tilt angle from horizontal
ξ	non-dimensional vertical distance, $\xi = ay/(T_H - T_{\infty,0})$
δ	thickness of the boundary layer, m

Subscripts

B	bottom wall of the cavity
C	cooled vertical wall of the cavity
H	heated vertical wall of the cavity
P	partition
T	top wall of the cavity

Chapter 1

Introduction

The importance of natural convection in cavities can be found in many engineering applications, such as heating and ventilating of living space, cooling in nuclear reactors and electronic packaging, as well as energy transfer in solar collectors. For example, natural convection has been extensively used to transfer residual heat from the fins attached to electronic parts to the walls of enclosed electronics cabinets due to the low cost as well as high durability and reliability of this technique. Therefore, natural convection in cavities has been extensively investigated over the past several decades. Most of these studies have been mainly focused on the natural convection in two generic configurations: (1) rectangular cavities with smooth walls [3][4][5][6], and (2) rectangular cavities with partitions attached to walls to simulate engineering applications [7][8][9][10].

There have been numerous experimental [11][5][6] and numerical [12][13] investigations of the natural convection in rectangular cavities driven by a temperature difference across the vertical walls. The natural convection, however, is extremely sensitive to changes in thermal boundary conditions and the cavity geometry [14]. For example, Ostrach and Raghavan [15] and Shiralkar and Tien [16] observed that

the temperature of the top and bottom walls had a significant effect on the stratification inside the cavity that, in turn, affected the flow pattern and the heat transfer characteristics. Ravi et al. [17] and Wu et al. [18] found that an increase in the top wall temperature resulted in a significant change in the flow pattern in the cavity. When the temperature of the top wall was close to or larger than that of the heated vertical wall, the flow separated from the top wall near the upper corner between the heated vertical wall and the top wall due to the formation of a negatively buoyant plume. Emery and Chu [19] and MacGregor and Emery [20] showed that the aspect ratio of a rectangular cavity had a significant effect on the natural convection heat transfer. As the aspect ratio was increased or decreased, secondary flow cells formed in the core region with an increase in the Rayleigh number [21][22][23][13]. Cormack et al. [4] observed that the natural convection flow in the cavity was reduced as the aspect ratio of the cavity decreased and the viscous force on the top and bottom walls became more prevalent.

Compared to the extensive investigations of the natural convection in cavities with smooth walls, studies on the natural convection in cavities with partitions on the walls are limited. The characteristics of the natural convection flow significantly changed when partitions were added to the walls of rectangular cavities [24][25][26][27]. For example, Shi and Khodadadi [28] indicated that a partition attached to the heated vertical wall of a square cavity degraded the heat transfer capacity on the wall since the presence of the partition modified the boundary layer flow along the walls of the cavity. Bilgen [29] observed that the natural convection flow circulation was blocked by partitions which were attached to the adiabatic horizontal walls of a rectangular cavity.

Heretofore, most previous studies of the natural convection in rectangular cavities have mainly focused on cavities with differentially heated vertical walls and

either insulated or adiabatic horizontal walls and aspect ratios either very much less or larger than unity. There have been fewer investigations on the laminar natural convection in rectangular cavities with different horizontal wall temperatures, particularly for the case where the top wall temperature is significantly larger than the heated vertical wall. There are no studies on the effect of the top wall temperature on the characteristics of laminar natural convection in rectangular cavities with relatively modest aspect ratios. Similarly, most previous investigations of the natural convection in partitioned rectangular cavities have focused on the cases with either adiabatic or insulated horizontal walls. Under these thermal boundary conditions, the partition directly suppressed the motion of the boundary layer flow along the walls or had an extra heating effect, resulting in changes in natural convection flow compared to that in cavities without partitions. There have been no studies on partitioned cavities with temperature differences in both the horizontal and vertical directions, although results from cavities with smooth walls suggest that the temperature difference across the horizontal walls of a partitioned cavity would result in changes in the characteristics of natural convection in the cavity.

Thus, the overall objective of this investigation is to characterize the laminar natural convection air flow in rectangular cavities with and without a partition on the wall. This study is important to further develop theoretical and numerical models of laminar natural convection in rectangular cavities with different thermal boundary conditions and geometries. Experiments were performed for a fixed non-dimensional temperature difference across the vertical walls for different vertical temperature differences between the top and bottom walls for cavities with aspect ratios of 0.5, 1.0 and 2.0. The specific objectives of the current investigation are:

1. To experimentally characterize the effect of the top wall temperature on the

laminar natural convection in rectangular cavities with aspect ratios of 0.5, 1.0 and 2.0.

2. To investigate the mechanisms of the laminar natural convection flow separation on the vertical wall of a square cavity with a heated top wall, in particular for the cases with very large top wall temperatures.
3. To compare the predictions from previous theoretical models to the results from the experiments to examine if these models can accurately predict the development of the natural convection flow in rectangular cavities.
4. To experimentally investigate the effect of a partition, including its position and height, on the laminar natural convection flow in a square cavity with large top wall temperatures.

The study would yield a more fundamental understanding of the mechanisms of the laminar natural convection in rectangular cavities with different thermal boundary conditions and geometries, especially that of a large temperature difference between the top and bottom walls. The effect of partitions on the natural convection in an air-filled square cavity would be useful for designing engineering applications such as optimizing the energy transfer in enclosed electronics cabinets, rooms and buildings. It is also expected that the experimental data from this investigation could be used to benchmark numerical simulations.

This thesis contains six chapters. The previous investigations on natural convection in cavities are reviewed and summarized in Chapter 2. The experimental facility and techniques, as well as data analysis method are then described in Chapter 3. The results for the laminar natural convection in rectangular smooth wall cavities with different top wall temperatures and relatively modest aspect ratios are

discussed in Chapter 4, while the effects of a partition and its parameters on the laminar natural convection in a square cavity with large top wall temperatures are presented in Chapter 5. Finally, the conclusions of the current study are summarized in Chapter 6, and the recommendations are given in Chapter 7.

Chapter 2

Literature Review

The natural convection in cavities has been extensively investigated over the past several decades. It has been shown that the natural convection is extremely sensitive to changes in the thermal boundary condition [15][16][17] and the cavity configuration [19][30][13]. Most previous investigations have mainly focused on the natural convection in two generic configurations: rectangular cavities with smooth walls and rectangular cavities with partitions attached to the walls. The literature pertaining to these two configurations are discussed in details in the sections one and two, respectively. Existing theoretical models used to predict the natural convection flow are finally reviewed in the third section.

2.1 Natural convection in rectangular cavities with smooth walls

A number of investigations have been numerically and experimentally performed to study the natural convection flow in cavities with smooth walls. These studies can be broadly divided into two categories: (1) cavities heated from the side and (2) cavities

heated from below. In the first type, the natural convection flow is formed due to the temperature difference across the two vertical walls of the cavity [20][12][17][6]. In the second type, the natural convection flow (the Benard flow) is generated as the temperature of fluid in the lower layer increases above the higher layer [31][32][33][34].

While several investigations have focused on the natural convection in cavities where the bottom wall temperatures were higher than the top wall, most investigations have mainly focused on the natural convection flow driven by a temperature difference between the two vertical walls, as summarized by Hoogendoorn [35], Ostrach [36][14] and Hyun [37]. The current investigation only focuses on the natural convection formed by a temperature difference across the cavity, therefore previous investigations with this type of thermal boundary condition are discussed here. Previous investigations have shown that the aspect ratio [3][21][4], thermal boundary condition [15][16][17] and the inclination [38][39][40] affect the natural convection in rectangular cavities with smooth walls.

2.1.1 Effect of the aspect ratio

Heretofore, most investigations of natural convection in rectangular cavities with smooth walls have focused on the case where the two vertical walls are at different temperatures, with the horizontal walls either insulated or adiabatic. For example, Emery and Chu [19] theoretically and experimentally showed that the ratio of the height to the width of the rectangular cavity had a significant effect on the natural convection heat transfer in the cavity. MacGregor and Emery [20] later showed that the difference in aspect ratio of the enclosure had a significant effect on the temperature fields and streamlines inside the cavity. Ostrach [14] summarized the previous studies and indicated that the natural convection is very sensitive to the change in the

configuration of the cavity. The studies where the aspect ratio of the cavity was approximately unity are discussed first, followed by the investigations where the height was significantly larger or less than the width.

2.1.1.1 Natural convection in square cavities

Previous investigations in square cavities with smooth walls are summarized in Table 2.1. The flow patterns and temperature distributions with heated and cooled vertical walls have been characterized for a range of Grashof numbers. MacGregor and Emery [20] numerically and experimentally examined the effect of the temperature difference between the two vertical walls of a square cavity for Grashof numbers, Gr_L , in the range 10^2 to 10^5 . The temperature and flow fields changed significantly with an increase of Gr_L . For $Gr_L \approx 10^2$, the isotherms were approximately evenly spaced vertical lines indicating the heat was transferred primarily by conduction. There was a circulatory motion but the streamlines were evenly spaced showing there was not a particularly strong natural convection flow near the wall. When Gr_L was increased to 10^5 , the isotherms and the streamlines distorted, indicating the heat was transferred by convection. Later, Cormack et al. [4] and Ravi et al. [17] investigated the natural convection for a similar order of Grashof number and found similar streamlines and isotherms in the cavity.

Tian and Karayiannis [6] recently measured the temperature and velocity distributions near the walls of an air-filled square cavity with isothermal heated and cooled vertical walls and highly conducting horizontal walls for Gr_L of 2.22×10^9 . A boundary layer developed along the vertical walls. In the core region, the flow was stably stratified, with the flow primarily in boundary layers along the walls driven by the buoyancy force. The temperature profiles had an undershoot near the edge of the boundary layer, where the local temperature fell below the local temperature in

Table 2.1: Summary of investigations of natural convection in square cavities with smooth walls.

Investigators	Approach	Study Area	Major Findings
MacGregor and Emery (1969) [20]	Numerical and experimental approaches	Natural convection in rectangular cavities with isothermal and constant-heat-flux vertical walls, as well as insulated horizontal walls. The aspect ratios are from 1 to 40; the Grashof numbers are in the range of $10^2 - 10^5$ and Prandtl numbers are from 1 to 20,000.	(1). The effects of the Prandtl number, Grashof number and aspect ratio were described. (2). Some heat transfer correlations were presented.
Newell and Schmidt (1970) [12]	Numerical technique	Two-dimensional laminar natural convection in an air-filled rectangular cavity with isothermal vertical walls and insulated horizontal walls. The aspect ratios are ranging from 1 to 20, and Grashof numbers are in the range of 4×10^3 to 1.4×10^5 .	(1). Heat transfer correlations were given.
Ostrach and Raghavan (1979) [15]	Experiment using thermocouples and particles	Laminar natural convection in silicone oil-filled rectangular cavities with aspect ratios of 1 and 3, Grashof numbers up to 20. Temperature differences were imposed in vertical and horizontal directions.	(1). The vertical temperature difference slowed down the flow. (2). The reduction in flow velocities depends on the aspect ratio and the Grashof number.
Sernas and Lee (1981) [41]	Experiment using an interferometer	Natural convection heat transfer and flow patterns in air-filled rectangular cavities with two types of horizontal walls. The aspect ratios are from 0.1 to 1.0, Grashof numbers are in the range of $2.64 \times 10^6 - 5.45 \times 10^6$.	(1). The heat transfer characteristics and flow patterns were changed significantly with the changes in the thermal boundary conditions on the horizontal walls.
Shiralkar and Tien (1982) [16]	Numerical technique with exponential difference scheme	Laminar natural convection flow and heat transfer in an air-filled square cavity with Rayleigh number up to 10^6 . A stabilizing and variable vertical temperature difference was imposed to the cavity.	(1). A stabilizing vertical temperature difference can decrease the vertical velocities along the heated vertical wall, while increase the horizontal heat transfer.
Briggs and Jones (1985) [42]	Experiment using a laser-doppler velocimeter	Two-dimensional periodic natural convection in an air-filled square cavity with conducting horizontal walls. Rayleigh numbers are from 0.1×10^7 to 1.2×10^7 .	(1). The existence of periodic laminar natural convection flow was detected at Rayleigh numbers above 0.3×10^7 . (2). The effect of Rayleigh number on frequency of flow was reported.
Viskanta et al. (1986) [43]	Numerical and experimental approaches	3-D laminar natural convection in a square cavity with insulated horizontal walls. Rayleigh number is 10^6 , and Prandtl number is 0.02.	(1). For low-Prandtl-number fluids, three-dimensional effects develop not only near the walls but also in the center of the cavity. (2). Three-dimensional effects on the convective heat transfer throughout the cavity.
Bohn and Anderson (1986) [44]	Experiment using thermocouples	Three-dimensional natural convection flow in a water-filled cubical cavity with adiabatic horizontal walls. The Rayleigh number is of the order of 10^{10} .	(1). A three-dimensional cavity exhibits core stratification, and the temperature in the core varies only in the vertical direction.
Ravi et al. (1994) [17]	Numerical technique	Laminar natural convection flow in a square cavity with variable horizontal wall temperatures. Prandtl numbers are from 0.71 to 70, and Rayleigh numbers are in the range of $10^4 - 10^8$.	(1). At high Rayleigh number, a recirculating pocket appears near the corners downstream of the vertical walls, and the flow separates and reattaches at the horizontal walls. (2). The corner structure is caused by thermal effects. (3). The horizontal wall temperatures affect the corner flow.

Table 2.1: Summary of investigations of natural convection in square cavities with smooth walls (con'd).

Investigators	Approach	Study Area	Major Findings
Tian and Karayiannis (2000) [6][45]	Experiment using thermocouple and LDA probes	Low level turbulence natural convection in an air-filled square cavity with highly conducting horizontal walls. Rayleigh number is 1.58×10^9 .	<ol style="list-style-type: none"> (1). The temperature and velocity distributions were measured at different locations in the cavity. (2). A contour plot of the thermal field and a vector plot of the air flow in the cavity were reported. (3). The temperature and velocity fluctuations were limited in the boundary layers along the walls and were not in Gaussian distribution. (4). The temperature and the velocity components fluctuate separately.
Ramesh and Venkateshan (2001) [46]	Experimental study using a differential interferometer	Laminar natural convection heat transfer in an air-filled square cavity with adiabatic horizontal walls. Grashof numbers are in the range of $5 \times 10^4 - 2 \times 10^6$.	<ol style="list-style-type: none"> (1). A correlation for average convective Nusselt number was given. (2). The contribution of surface radiative heat transfer to the total heat transfer from the heated vertical wall was negligibly small. (3). Even for a perfectly adiabatic case, the horizontal walls varied linearly over a significant part excepting near the two corners.
Ampofo and Karayiannis (2003) [47]	Experimental study using thermocouple and LDA probes	Low-level turbulence natural convection in an air-filled square cavity with highly conducting horizontal walls. The isothermal heated and cooled vertical walls gave a Rayleigh number of 1.58×10^9 .	(1). Experimental benchmark data for turbulent natural convection in an air filled square cavity were presented, which will be useful for validation of computational fluid dynamics codes.
Salat et al. (2004) [48]	Experimental and numerical studies	Turbulent natural convection flow develops in an air-filled square cavity with adiabatic horizontal walls. Rayleigh number is equal to 1.5×10^9 .	<ol style="list-style-type: none"> (1). 2-D numerical simulation is not the critical ingredient for explaining the discrepancy observed between numerical simulations and experiments for the thermal stratification. (2). Introducing experimental temperature measurements in numerical simulations is not the definitive answer to the discrepancy observed on the thermal stratification in the cavity core.
Wu et al. (2006) [18]	Experiment using a thermocouple probe and incense smoke	Laminar natural convection in an air-filled square cavity with a Grashof number of 1.9×10^8 . The non-dimensional top wall temperature was changed from 0.54(insulated) to 1.4.	<ol style="list-style-type: none"> (1). Increasing the top wall temperature resulted in a separated flow region on the top wall causing a secondary flow that had a significant effect on the heat transfer. (2). A natural convective heat transfer correlation was presented.

the core region of the cavity. Cheesewright [49] noted that this occurred in natural convection boundary layers in non-isothermal surroundings because the heat flux to the fluid in the outer region of the boundary layer was not sufficient to change its temperature as quickly as the temperature outside the boundary layer.

Newell and Schmidt [12] performed a numerical simulation of the two-dimensional laminar natural convection in an air-filled square cavity with isothermal vertical walls and insulated horizontal walls and developed a correlation for the average Nusselt number along the heated vertical wall based on the width of the cavity, given by

$$\overline{Nu}_L = 0.145(Gr'_L)^{0.397}. \quad (2.1)$$

Here the Grashof number was based on the width of the cavity L and was defined as

$$Gr'_L = \frac{g\beta[T_H - (\frac{T_H+T_C}{2})]L^3}{\nu^2}. \quad (2.2)$$

2.1.1.2 Natural convection in rectangular cavities

There have been a number of investigations of the effect of the cavity aspect ratio on the natural convection in rectangular cavities as summarized in Table 2.2. In this study, the aspect ratio is defined as the ratio of height to width of the cavity ($AR = H/L$). For aspect ratios much larger or less than unity, the flow pattern in the cavity becomes significantly different from that in a square cavity as the Rayleigh number is increased. For example, Elder [21] studied the natural convection flows in a rectangular cavity with aspect ratios of 1 to 60 using paraffin and silicone oil with Prandtl numbers approximately equal to 1000. The flows were visualized using aluminum powder suspended in the working fluid. A transition of the flow in the

core region of the cavity was observed for Rayleigh number Ra_L above 3×10^5 . In particular, for a Rayleigh number Ra_L of 3.6×10^5 , a second cell of circular flow appeared in the core region, and the number of flow cells changed with an increase of the Rayleigh number. Later, Seki et al. [11] observed the same phenomenon in a cavity with aspect ratio of 15. Similar results were reported by Ostrach et al. [30] and Drummond and Korpela [13] in rectangular cavities with aspect ratios much less than the unity.

The characteristics of the secondary flow cells have been further investigated in [22][23][54]. Wakitani [22] numerically investigated the flow patterns and noted that for the onset of secondary flow cells, the critical value of the aspect ratio was 11.5 and the Rayleigh number Ra_L was 8.5×10^3 . With an increase of the aspect ratio, the critical value of the Rayleigh number decreased and reached an approximately constant value. For a given aspect ratio, with an increase of the Rayleigh number, the number of the secondary cells first increased and then decreased. Lartigue et al. [23] and Zhu and Yang [54] corroborated these results in air-filled rectangular cavities with aspect ratios of 40 and 16, respectively. Lartigue et al. [23] confirmed the presence of secondary flow cells, and the number of secondary flow cells decreased as the Rayleigh number Ra_L increased from 6800 to 17750. Zhu and Yang [54] indicated that the number of secondary flow cells was mainly determined by the Rayleigh number.

Cormack et al. [55] theoretically analyzed the natural convection flow in a rectangular cavity with aspect ratio $AR \ll 1$ and found that the flow consisted of a parallel flow in the core region and a second non-parallel flow near the vertical walls. This was corroborated by Cormack et al. [4] and Imberger [56] through simulations and experiments, respectively. The simulations of Cormack et al. [4] showed streamlines and isotherms for cavities with a Rayleigh number Ra_H of 1.4×10^5 and aspect ratios ranging from 0.05 to 0.2 became more parallel to the horizontal walls

Table 2.2: Summary of investigations of natural convection in rectangular cavities with smooth walls.

Investigators	Approach	Study Area	Major Findings
Eckert and Carlson (1961) [3]	Experiment using a Zehnder-Mach interferometer	Natural convection in air-filled rectangular cavities with aspect ratios of 10, 20 and 46.7. The horizontal walls of cavities were adiabatic and Grashof numbers are in the range of $10^3 \sim 10^5$.	(1). Grashof number and aspect ratio determined the natural convection characteristics in the cavity. (2). Relations for local and average heat transfer were presented.
Emery and Chu (1965) [19]	Theoretical analysis and experiments	Natural convection heat transfer in rectangular cavities with aspect ratios of 10 and 20. The horizontal walls were Micarta. The Prandtl numbers of working fluids are from 3 to 30,000. Rayleigh numbers are up to 10^7 .	(1). The heat transfer was a function of temperature difference in the horizontal direction, the aspect ratio of cavity and Prandtl number of working fluid. (2). Nusselt number correlations were presented.
Elder (1965) [21]	Experiment using thermocouples and aluminium powder	Laminar natural convection in rectangular cavities with aspect ratios of 1 to 60, Rayleigh numbers less than 10^8 . Prandtl numbers of working fluids were around 1000. The horizontal walls of cavities were insulated.	(1). The Rayleigh number has a significant effect on the temperature field and flow pattern of the natural convection flows in cavities.
Gill (1966) [50]	Theoretical analysis	Two-dimensional convective motion in rectangular cavities with aspect ratios of 2.5 to 18.8. The horizontal walls of cavities were adiabatic and Rayleigh number is of the order of 10^6 .	(1). An approximate solution was obtained for the case of large values of the Prandtl number, and that was in agreement with experimental results reported by Elder (1965) [21].
Davis (1968) [51]	Numerical approach	Steady laminar natural convection in rectangular cavities with aspect ratios of 1 – 5. The thermal boundary conditions on the horizontal walls were adiabatic and linear. Rayleigh numbers were up to 2×10^5 , and Prandtl numbers were in the range 10^{-1} to 10^3 .	(1). Some details of the flow at high Rayleigh numbers were revealed. (2). It was observed that high Prandtl numbers exert a stabilizing influence on the numerical solution, while they have only a small effect on the final results.
Seki et al. (1978) [11]	Experimental visualization	Natural convection flow in narrow vertical rectangular cavities with insulated horizontal walls. Aspect ratios were from 6 to 30, Prandtl number were in the range 4 – 12500, and Rayleigh numbers were up to 10^9 .	(1). The flow patterns were changed by the Rayleigh numbers. (2). The flow pattern was easily shifted from laminar flow to transition flow with decreasing Prandtl number and increasing cavity width. (3). Experimental measurements of the net heat transfer were given.
Yin et al. (1978)[5]	Experiment using thermocouple probes	Natural convection in air-filled rectangular cavities with aspect ratios ranging from 4.9 to 78.7 and Grashof numbers ranging from 1.5×10^3 to 7.0×10^6 . The horizontal walls of cavities were insulated.	(1). Two Nusselt-Grashof correlations were presented.
Schinkel et al. (1980) [52]	Numerical technique with a finite difference method	Natural convection in vertical air-filled rectangular cavities with aspect ratios from 1 – 18 and Rayleigh numbers varied from $10^4 - 10^6$. The horizontal walls of cavities were both perfectly conducting and adiabatic.	(1). The effect of stratification on the natural convection flow and heat transfer was discussed.
Farhangnia et al. (1996) [53]	Numerical simulation	Two-dimensional turbulent natural convection in an air-filled rectangular cavity with aspect ratio of 4 and Rayleigh number of 10^9 . The horizontal walls of the cavity were insulated.	(1). Both mean and fluctuating quantities provided good agreement with experimental results.

Table 2.2: Summary of investigations of natural convection in rectangular cavities with smooth walls (con'd).

Investigators	Approach	Study Area	Major Findings
Wakitani (1998) [22]	Numerical simulations based on a finite difference method	Flow patterns of two-dimensional natural convection in vertical air-filled rectangular cavities with aspect ratios of 10 to 24 and Rayleigh numbers up to 10^6 . The horizontal walls were insulated.	(1). The critical value of aspect ratio is 11.5 for the onset of secondary cells and the Rayleigh number is 8.5×10^3 . (2). With the increase of the aspect ratio, the critical Rayleigh number trends to decrease and becomes almost constant. (3). The reverse transition from multicellular to unicellular can be explained from the predictions of stability analysis.
Lartigue et al. (2000) [23]	Experimental and numerical studies	Laminar natural convection in an air-filled rectangular cavity with aspect ratio of 40 and Rayleigh numbers ranging from 3550 to 17750. The horizontal walls of the cavity were adiabatic.	(1). The numerical and experimental results showed the presence of secondary cells. (2). The number of cells decreases as the Rayleigh number increases.
Zhu and Yang (2003) [54]	Numerical study	Transient laminar natural convection in an air-filled rectangular cavity with adiabatic horizontal walls. The aspect ratio is 16, and Rayleigh numbers are ranging from 10^3 to 6×10^5 .	(1). The number of cells was found to be dominated by Rayleigh number.
Cormack et al. (1974) [55]	Theoretical analysis	Natural convection in a shallow cavity with differentially heated vertical walls and insulated horizontal walls.	(1). The flow consisted of two regimes: a parallel flow in the core region and a non-parallel flow near the ends of cavity.
Cormack et al. (1974) [4]	Numerical study	Natural convection in rectangular cavities with aspect ratios from 0.05 to 1, and Rayleigh numbers ranging from 70 to 1.4×10^5 . The horizontal walls of cavities were insulated.	(1). The natural convection flow was reduced as the aspect ratio decreased and the viscous force on the horizontal walls became more prevalent. (2). The heat was transferred mainly by conduction at the lowest Rayleigh number.
Imberger (1974) [56]	Experimental study	The steady motion of water in an enclosed rectangular cavity with differentially heated vertical walls and insulated horizontal walls. The aspect ratios of the cavity were 10^{-2} and 1.9×10^{-2} , and the Rayleigh numbers were from 1.31×10^6 to 1.11×10^8 .	(1). The results of streamlines were in qualitative agreement with the results presented by Cormack et al. (1974) [4]. (2). The correlation of heat transfer from the heated vertical wall to the opposite cooled vertical wall was given.
Cormack et al. (1975) [57]	Theoretical analysis	Natural convection in Newtonian fluid-filled shallow cavities with differentially heated vertical walls and an insulated bottom wall. Different boundary conditions were imposed on top walls of cavities.	(1). Changes in boundary conditions on top wall have an important influence in the temperature and flow structure within the cavity.
Ostrach et al. (1980) [30]	Experiment by visualizing flow patterns	Natural convection in rectangular cavities with differentially heated vertical walls and highly conducting horizontal walls. Aspect ratios of cavities ranged from 0.05 to 0.5, Grashof numbers from 27.7 to 10^6 and Prandtl numbers from 0.72 to 1.38×10^3 .	(1). Specially detailed information on the flow patterns was presented. (2). The effect of aspect ratio on the flow patterns and velocity distributions in the cavities was observed for a wide range of Grashof numbers.
Bejan et al. (1981) [58]	Experiment to study the temperature and flow pattern	High-Rayleigh-number convection in a water-filled rectangular cavity with differentially heated vertical walls and adiabatic horizontal walls. The aspect ratio was 0.0625, and Rayleigh numbers were from 2×10^8 to 2×10^9 .	(1). Contrary to lower Rayleigh number flows, the core flow structure was not parallel to the horizontal walls. (2). There were horizontal wall jet flows along the horizontal walls, there were two secondary flows outside of these wall jets. (3). A heat transfer correlation between the two vertical walls was presented.

Table 2.2: Summary of investigations of natural convection in rectangular cavities with smooth walls (con'd).

Investigators	Approach	Study Area	Major Findings
Yewell et al. (1982) [59]	Experiment using thermocouples and velocity probes	Transient natural convection in water-filled rectangular cavities with aspect ratios of 0.0625 and 0.112. The vertical walls were differentially heated and horizontal walls were adiabatic. Rayleigh numbers were 1.28×10^9 and 1.49×10^9 .	(1). Thin intrusion layers along the horizontal walls were observed. (2). The core was thermally stratified. (3). The equation for the time to reach the steady state was given.
Hart (1983) [60]	Theoretical analysis	Two-dimensional convection in a shallow rectangular cavity with differentially heated vertical walls.	(1). Conditions for which a parallel core flow will exist at low Prandtl number working fluids were found.
Ozoe et al. (1983) [61]	Experiment using a LDA, phenolphthalein and a thermocouple	Natural convection in a water-filled rectangular cavity with aspect ratio of 0.54, Rayleigh number of 1.52×10^8 and Prandtl number of 9.08. The two vertical walls were kept at different temperatures and the horizontal walls were insulated.	(1). The horizontal and vertical velocity profiles near the heated vertical wall were measured. (2). The horizontal temperature profiles were measured.
Kamotani et al. (1983) [62]	Experiment using a thermocouple probe and dye	Laminar natural convection heat transfer in water and silicone oils-filled rectangular cavities with insulated horizontal walls. The aspect ratios were from 0.043 to 1.0, Prandtl numbers between 5.5 and 19280, and Rayleigh numbers from 10^4 to 4×10^7 .	(1). In square cavity, the Nusselt number was nearly independent of Prandtl number. (2). In the cavity with aspect ratio of 0.2, the heat transfer rate depended strongly on Prandtl number due to the effect of Prandtl number on secondary cells. (3). The relation between Nusselt number and Rayleigh number in cavities with different aspect ratios were presented.
Drummond and Korpela (1987) [13]	Numerical study	Laminar natural convection flow in rectangular cavities with aspect ratios of 0.05 to 0.125, Prandtl numbers less than 2 and Grashof numbers less than 30000. The horizontal walls of cavities were both conducting and insulated.	(1). For fluids of small Prandtl number the differences in the flow patterns in these two cases are slight, the strength of the circulation in the cells being somewhat weaker when the horizontal walls were insulated. (2). For a given Prandtl number, more secondary cells formed in the core region with the increase of the Grashof number. (3). For a given Grashof number, more secondary cells appeared in the core region with the decrease of the Prandtl number.

and parallel to the vertical walls, respectively, with a decrease of the aspect ratio of the cavity. Thus, the natural convection flow in the cavity was reduced as the aspect ratio of the cavity decreased and the viscous forces on the top and bottom walls became more prevalent. Imberger [56] measured the steady motion of water in a shallow rectangular cavity with differentially heated vertical walls for Rayleigh numbers Ra_H ranging from 1.31×10^6 to 1.11×10^8 and aspect ratios of 10^{-2} to 1.9×10^{-2} . The results were in qualitative agreement with the results obtained by Cormack et al. [4]. However, with an increase of the Rayleigh number, the characteristics of the core flow changed. Bejan et al. [58] measured the natural convection in rectangular cavities with $AR = 0.0625$ and Rayleigh numbers, Ra_H , of 2×10^8 to 2×10^9 . The flow patterns indicate that, contrary to lower Rayleigh number flows [55][4][56], the core flow structure was not parallel to the horizontal walls. There were horizontal wall jet flows along the two insulated horizontal walls, but similar to larger aspect ratio cavities there were two secondary flows outside of these wall jets. Yewell et al. [59] later observed similar horizontal velocity profiles in experiments in water-filled rectangular cavities with aspect ratios of 0.0625 and 0.112 at Rayleigh numbers Ra_H of 1.28×10^9 and 1.49×10^9 .

The correlations for the convective heat transfer are different from that in a square cavity when the aspect ratio was larger or less than the unity, and are summarized in Table 2.3.

2.1.2 Effect of the temperature difference between the top and bottom walls

Compared with studies of the natural convection in rectangular cavities with adiabatic or insulated horizontal walls, there are only limited investigations with differen-

Table 2.3: Summary of correlations for the natural convective heat transfer in rectangular cavities with the aspect ratio much larger or less than unity.

Investigators	Approach	Thermal Boundary Conditions of the Top and Bottom Walls	Working Fluid	Aspect Ratio (AR)	Grashof or Rayleigh Number	Correlations
Eckert and Carlson (1961) [3]	Experimental measurements	Adiabatic	Air	10, 20 and 46.7	Gr_L : $10^3 - 10^5$	(1). for the conduction regime: $Nu_L = 1$, for $Gr_L \sim 10^3$; (2). for the boundary layer regime: $Nu_L = 0.119 \cdot (Gr_L)^{0.3} \cdot (\frac{L}{H})^{0.1}$, for $Gr_L \sim 10^5$.
Emery and Chu (1965) [19]	Theoretical analysis and experiments	Adiabatic	$Pr = 3 - 30,000$	10 and 20	Ra_L : up to 10^7	(1). $Nu_L = 1$, for $Ra_L < 10^3$; (2). $Nu_L = 0.280 \cdot (\frac{L}{H})^{\frac{1}{4}} \cdot Ra_L^{\frac{1}{4}}$, for $10^3 < Ra_L < 10^7$.
Yin et al. (1978) [5]	Experimental measurements	Insulated	Air	4.9 - 78.7	Gr_L : $1.5 \times 10^3 - 7.0 \times 10^6$	(1). $Nu_L = 0.091 \cdot Gr_L^{0.307}$, neglected the effect of the aspect ratio; (2). $Nu_L = 0.210 \cdot Gr_L^{0.269} \cdot (\frac{L}{H})^{0.131}$, considered the effect of the aspect ratio.
Bejan et al. (1981) [58]	Experimental measurements	Adiabatic	Water	0.0625	Ra_H : $2 \times 10^8 - 2 \times 10^9$	$Nu_L = 0.014 \cdot Ra_H^{0.38}$.

tial heated vertical walls and a vertical temperature difference between the top and bottom walls. The temperature of the top and bottom walls of a rectangular cavity has a significant effect on the stratification inside the cavity that in turn affects the flow and heat transfer characteristics. Ostrach and Raghavan [15] visualized the flow patterns in square and rectangular cavities containing silicone oil with a heated top wall and cooled bottom wall as well as a temperature difference across the vertical walls. The flow patterns became more asymmetric as the temperature difference between the horizontal walls increased to approximately 2 times of that between the vertical walls. Eventually, a secondary recirculating flow region developed near the top of the vertical wall when the vertical temperature difference was approximate 6 times that of the horizontal temperature difference. Shiralkar and Tien [16] performed a similar numerical investigation of the heat transfer in an air-filled square cavity for cases where the top and bottom walls were heated or cooled, respectively. In this case, the temperature difference in the vertical direction was 2 to 5 times that in the horizontal direction. There was again a significant secondary flow near the top corner of the heated vertical wall. Somewhat surprisingly, the heat transfer from the heated vertical wall increased when the top wall was heated and the bottom wall was cooled even though the vertical velocity of the boundary layer flow along the vertical walls decreased. Experimental results reported by Sernas and Lee [41] also showed that characteristics of the natural convection in air-filled rectangular cavities with aspect ratios of 0.1 to 1.0 were dependent on the thermal boundary conditions of the horizontal walls.

Ravi et al. [17] and Wu et al. [18] numerically and experimentally investigated how the change in the temperatures of the top and bottom walls affected the laminar natural convection flow in an air-filled square cavity with a moderate temperature difference in the vertical direction ($\theta_T - \theta_B \lesssim 1.4$). They found that an increase in

the temperature of the top wall resulted in a significant change in the flow pattern in the cavity. This was true particularly near the upper corner between the heated walls when the temperature of the top wall was close to or larger than that of the heated vertical wall. In this case, the flow separated from the top wall near the corner due to the formation of a negatively buoyant plume, resulting in an undulating flow near the corner region. Baines [63] observed a very similar phenomenon for a two-dimensional plume adjacent to a vertical wall in a density-stratified environment due to the effect of the buoyancy force. The flow passed through several stages, from an inertial jet to a buoyant plume, to a neutrally buoyant jet and then a negatively buoyant plume. Finally, the negative buoyancy force caused the flow to turn over. The development of the natural convection boundary layer flow for higher top wall temperatures has not been investigated experimentally for air flows, though the results from the numerical study by Shiralkar and Tien [16] suggested the upward boundary layer flow may separate from the heated vertical wall below the corner when the temperature of the top wall was much larger than the vertical wall. In particular, the flow formed a recirculating region near the corner when the temperature difference in the vertical direction was five times that in the horizontal direction. There was no evidence of significant undulation in the flow after the upward boundary layer flow separated from the heated vertical wall and turned over, similar to the observations by Ravi et al. [17] and Wu et al. [18] for the cases with more moderate top wall temperatures.

Wu et al. [18] presented a correlation for the local heat transfer along most of the heated vertical wall ($0.1 \leq y/H \leq 0.7$) of the air-filled square cavity with a moderate temperature difference in the vertical direction ($\theta_T - \theta_B \lesssim 1.4$) by

$$Nu = CRa^{0.32}. \quad (2.3)$$

Here, the value of the constant C increased as the temperature of the top wall on the cavity was increased, and decreased when the temperature of the bottom wall was decreased.

2.1.3 Effect of the inclination

Natural convection flow is a buoyancy-driven flow due to the presence of gravitational acceleration and density variations from one fluid layer to another. Therefore, the inclination of a cavity can significantly affect the natural convection in the cavity. The flow along the wall is driven by the component of the buoyant force which is directly related to the inclination angle.

Ozoe et al. [38], Arnold et al. [39], Meyer et al. [64], Elsherbiny et al. [40] and Hamady et al. [65] studied the effect of inclination on the heat transfer and flow pattern of two-dimensional laminar natural convection in inclined side-heated rectangular cavities with adiabatic or conducting top and bottom walls. They all indicated that the characteristics of the natural convection were affected by the angle of inclination of cavities. For example, Hamady et al. [65] experimentally and numerically studied the effect of inclination on the steady natural convection local heat transfer characteristics. Their investigation was carried out in an air-filled square cavity with differentially heated vertical walls and insulated top and bottom walls. Measurements were performed at various inclination angles, ranging between 0° (heated from above) and 180° (heated from below), for Rayleigh numbers Ra_H between 10^4 and 10^6 . The heat flux at the heated and cooled vertical walls were strongly dependent on the angle of inclination due to the change in the flow pattern. Sharif and co-workers [66][67] numerically studied the natural convection in side-heated square cavities with adiabatic top and bottom walls at various angles of inclination up to 90° . The angle of

inclination changed both laminar and turbulent natural convection flow patterns that caused significant changes in heat transfer characteristics. It was noted that the heat transfer characteristics became significantly different for inclinations greater than 45° due to the change in the flow field.

Several heat transfer correlations have been developed by researchers based on results of their investigations and these are summarized in Table 2.4.

2.1.4 Summary and limitations

The natural convection in rectangular cavities has been extensively investigated both numerically and experimentally. However, most of these studies have mainly focused on characterizing the natural convection air flow in rectangular cavities with differentially heated vertical walls with either adiabatic, insulated or conducting horizontal walls. There are only few investigations of the laminar natural convection in rectangular cavities with different top and bottom wall temperatures, particularly for the case where the top wall temperature is significantly larger than the heated vertical wall. There does not appear to have been any experimental investigations to clarify the natural convection flow in a cavity driven by a temperature difference in the vertical walls where the temperature of the top wall of the cavity was changed, in particular for top wall temperatures greater than the heated vertical wall.

The effect of aspect ratio on the natural convection in rectangular cavities has been studied mainly for the cases where the aspect ratio is much less or larger than unity. In such cases, the change in the aspect ratio caused significant changes in natural convection due to changes in flow patterns, in particular in the core region of the cavities. There are very few investigations on the effect of the top wall temperature, especially a larger top wall temperature ($\theta_T \gtrsim 1.2$), on the characteristics of laminar

Table 2.4: Summary of heat transfer correlations for the natural convection flow in tilted rectangular cavities.

Investigators	Approach	Thermal Boundary Conditions of the Top and Bottom Walls	Working Fluid	Inclination	Aspect Ratio (AR)	Grashof or Rayleigh Number	Correlations
Dropkin and Somerscales (1965) [68]	Experimental measurements	Insulated	Pr : 0.02 - 11,560	$0^\circ \leq \phi \leq 90^\circ$	4.41 - 16.56	Ra_L : 5×10^4 - 7.17×10^8	$Nu_L = C \cdot (Ra_L)^{\frac{1}{3}} \cdot Pr^{0.074}$, with $C = 0.069$, for $\phi = 0^\circ$ and $C = 0.049$ for $\phi = 90^\circ$.
Randall et al. (1979) [69]	Experimental measurements	Insulated	Air	$45^\circ \leq \phi \leq 90^\circ$	9 - 36	Gr_L : 4×10^3 - 3.1×10^5	$Nu_L = 0.118 \cdot [Gr_L \cdot Pr \cdot \cos^2(\phi - 45)]^{0.29}$.
Elsherbiny (1996) [70]	Experimental measurements	Conducting	Air	$0^\circ \leq \phi \leq 180^\circ$	20	Ra_L : 10^2 - 2×10^6	(1). for $\phi = 180^\circ$: $Nu_L = [1 + (0.212 \cdot Ra_L^{0.136})^{11}]^{\frac{1}{11}}$; (2). for $\phi = 120^\circ$: $Nu_L = [1 + (0.0566 \cdot Ra_L^{0.332})^{4.76}]^{\frac{1}{4.76}}$; (3). for $120^\circ \leq \phi \leq 180^\circ$: $Nu_L(\phi) = Nu_L(180^\circ) + \left(\frac{180-\phi}{60}\right) \cdot [Nu_L(120^\circ) - Nu_L(180^\circ)]$.

natural convection flow in rectangular cavities with relatively modest aspect ratios.

2.2 Natural convection in rectangular cavities with partitions attached to walls

Investigations that have focused on the natural convection in enclosures with partitions attached to the walls are limited [7][8][9][10]. In recent years, there is increasing attention on enclosures with partitions on walls, largely due to the needs of engineering applications. It is evident that industrial applications, such as heating and ventilating of living spaces, solar thermal collector systems and electronic cooling devices, do not conform to an enclosure with smooth walls. Several investigations [24][25][26][27] have indicated that the characteristics of the natural convection flow were significantly changed due to the partitions on the walls. Most investigations have focused on partitions attached to vertical walls and horizontal walls.

2.2.1 Partitions attached to the vertical walls of rectangular cavities

The main investigations of natural convection in rectangular cavities with partitions attached to the vertical walls are summarized in Table 2.5. Scozia and Frederick [9] numerically studied the laminar natural convection flow, with Rayleigh numbers Ra_L ranging from 10^3 to 10^5 , in an air-filled slender rectangular cavity with aspect ratios ≥ 20 , with angles of inclination of 45° and 90° . The vertical walls of the cavity were isothermal but with different temperatures, while the horizontal walls were insulated. Conducting partitions were attached to the cooled vertical wall of the cavity. It was found that the natural convection flow was blocked by the partitions, resulting in

changes in the temperature field. The characteristics of the natural convection flow were dependent on the Rayleigh number, height and number of the partitions, as well as the aspect ratio and angle of inclination of the cavity. Ampofo [27] experimentally studied the natural convection of air in a square cavity with five partitions on the heated vertical wall, with differentially heated vertical walls and conducting horizontal walls. Velocity profiles and temperature distributions showed the natural convection flow in the partitioned cavity differed significantly from the corresponding results in the non-partitioned cavity under the same experimental conditions due to the blockage effect of the partitions. As a result, the heat transfer rate along the heated vertical wall was decreased. Shi and Khodadadi [28] corroborated that a partition attached to the heated vertical wall of a square cavity can decrease the heat transfer on the wall. They numerically investigated the laminar natural convection heat transfer within a differentially heated air-filled partitioned square cavity with adiabatic horizontal walls. In this case, the Rayleigh numbers Ra_L were in the range of 10^4 to 10^7 . A single highly conductive thin partition with variable height was placed at 7 different locations of the heated vertical wall. It was found that the presence of the partition modified the clockwise rotating boundary layer flow along the walls of the cavity. However, heat transfer on the cooled vertical wall without the partition can be promoted for high Rayleigh numbers and with the partition placed close to the insulated top and bottom walls. It was noted that significant energy was routed through the partition as the partition was placed on the lower half of the heated vertical wall. The authors indicated that two competing mechanisms were responsible for the flow and thermal modifications. One is the hydrodynamic blockage due to the partition that directly depends on the height of the partition, while the other is the extra heating effect by the partition which is promoted as the Rayleigh number increases. The extra heating effect offsets the hydrodynamic blockage effect and can

contribute to the strengthening of the flow field as the Rayleigh number increases. Bilgen [10] performed numerical simulations for Rayleigh number Ra_L up to 10^9 . When the height and conductivity of the partition were increased, with the partition at or near the center of the cavity, the conduction through the cavity was enhanced while the suppression of the natural convection flow was intensified. The Nusselt number increased with an increase of the Rayleigh number Ra_L , while it decreased with an increase of the height and conductivity of the partition.

2.2.2 Partitions attached to the horizontal walls of rectangular cavities

When partitions are placed on the adiabatic or insulated horizontal walls of a rectangular cavity, the natural convection flow and heat transfer changed due to the suppression of the boundary layer flow along the wall. A summary of investigations for this geometry is provided in Table 2.6. Bilgen [29] numerically studied the laminar and turbulent natural convection in air-filled rectangular cavities with partitions attached to adiabatic horizontal walls. The aspect ratios of the cavities were 0.3 and 0.4, and the Rayleigh numbers Ra_L were in the range of 10^4 to 10^{11} . It was observed that the flow circulation was blocked by the partitions, resulting in a reduction of the heat transfer.

Nansteel and Greif [7] experimentally investigated the natural convection in a water-filled rectangular cavity with aspect ratio of 0.5 and Rayleigh numbers Ra_L in the range of 2.3×10^{10} to 1.1×10^{11} . A partition attached to the top wall of the cavity significantly decreased the overall heat transfer, especially when the partition was non-conducting. Three relatively distinct regions, i.e. an inactive core region, a region of very weak recirculation and a peripheral boundary layer flow, were observed

Table 2.5: Summary of investigations of natural convection in rectangular cavities with partitions attached to the vertical walls.

Investigators	Approach	Study Area	Major Findings
Bilgen (2005) [10]	Numerical approach with SIMPLER algorithm	Natural convection heat transfer in an air-filled differentially heated square cavity with a horizontal thin fin attached to the heated vertical wall. The horizontal walls were adiabatic. The dimensionless height, position and the relative conductivity ratio of the fin were variable. Rayleigh numbers were from 10^4 to 10^9 .	(1). Nusselt number is an increasing function of Rayleigh number, and a decreasing function of partition height and relative conductivity ratio. (2). The heat transfer may be suppressed up to 38% by choosing appropriate thermal and geometrical parameters.
Ampofo (2005 and 2004) [26][27]	Experiment using a thermocouple probe and a 2-D LDA	Natural convection of air in a non-partitioned or partitioned square cavity with differentially heated vertical and conducting horizontal walls under the Rayleigh number with 1.58×10^9 . Five partitions were installed on the heated vertical wall.	(1). Partitions tend to reduce the heat transfer rates along the heated vertical wall compared with similar cavities with smooth walls. (2). The velocity and temperature fields results obtained in the partitioned cavity differ substantially from the corresponding results in the non-partitioned cavity with the same dimensions and under the same experimental conditions.
Shi and Khodadadi (2003) [28]	A finite-volume-based computation study	Steady laminar natural convection heat transfer in an air-filled differentially heated square cavity with insulated top and bottom walls. A single highly conductive thin fin with variable height was attached to the heated vertical wall of the cavity at 7 different locations. The Rayleigh number is in the range of $10^4 - 10^7$.	(1). Two competing mechanisms, i.e. the hydrodynamic blockage effect and the extra heating effect offered by the fin, are responsible for flow and thermal modifications. (2). The fin on the heated vertical wall modified the clockwise rotating boundary layer flow. (3). A correlation among the mean Nu, Ra, height and position of the fin was proposed.
Yucel and Turkoglu (1998) [71]	Control volume approach and SIMPLE algorithm	Laminar natural convection in air-filled vertical slender cavities (aspect ratio = 10) with conducting fins attached to the cold vertical wall. The horizontal walls were insulated. The Rayleigh numbers are in the range of 10^3 to 10^4 .	(1). The fin height and the number of fins are important parameters for optimization of the heat transfer rate. (2). At low Rayleigh numbers, the mean Nu increases with increasing number of fins and the fin heights; while at high Rayleigh numbers, the heat transfer rate can be decreased or increased based on the number of fins and the fin heights.
Frederick and Valencia (1995) [72]	Numerical technique with a spacewise periodical approach	Laminar natural convection of air in the central microcavities of vertical enclosures with equally spaced baffles attached either to one of the vertical walls or both vertical walls. The Rayleigh numbers are in the range of 10^4 to 10^5 .	(1). The flow pattern is significantly different as the fins are attached to both vertical walls, rather than to only one of vertical walls that resulted in a different heat transfer characteristic.
Nag et al. (1994) [73]	Numerical technique with the finite element method	The effect of a partial horizontal partition, attached to the heated vertical wall of an air-filled square cavity with adiabatic horizontal walls. The Rayleigh numbers are in the range of 10^3 to 10^6 .	(1). The effects of the thickness and conductivity of the partition on the laminar natural convection heat transfer were presented.
Scozia and Frederick (1991) [9]	Numerical technique	Laminar natural convection in air-filled, inclined, slender cavities (aspect ratio > 20) with insulated top and bottom walls. Partitions were attached to the cold vertical wall. Rayleigh numbers are in the range of 10^3 to 10^5 .	(1). The flow and heat transfer mechanisms and their dependence on Rayleigh number, microcavity aspect ratio, overall aspect ratio, and angle of inclination were discussed.

Table 2.5: Summary of investigations of natural convection in rectangular cavities with partitions attached to the vertical walls (con'd).

Investigators	Approach	Study Area	Major Findings
Frederick (1989) [74]	Numerical technique	Natural convection in an air-filled, differentially heated, inclined square cavity, with a diathermal partition on its cold wall, at Rayleigh numbers of $10^3 - 10^5$. The horizontal walls of the cavity were insulated.	(1). The partition causes convection suppression and heat transfer reduction. (2). Heat transfer reduction depends on Rayleigh number, partition height and inclination of the cavity.
Frederick and Valencia (1989) [75]	Numerical technique	Natural convection in an air-filled square cavity with a conducting partition on its heated vertical wall. The horizontal walls of the cavity were perfectly conducting. Rayleigh numbers are in the range of 10^3 to 10^6 .	(1). The effects of the height and conductivity of the partition on the laminar natural convection were reported.
Shakerin et al. (1988) [76]	Experimental approach with the dye visualization and a Mach-Zehnder interferometer	Laminar natural convection flow in an enclosure with single and repeated, two-dimensional, rectangular roughness elements on the heated vertical wall. $1 \leq \text{aspect ratio} \leq 3$; $10^5 \leq Ra_L \leq 10^8$, and $Pr = 0.7$ and 7.0 .	(1). The steady natural convection boundary layers tend to follow the wall contour very closely. (2). With conducting, closely spaced, multiple roughness elements, the total heat transfer is not significantly different from that for a smooth surface.

Table 2.6: Summary of investigations of natural convection in rectangular cavities with partitions on the horizontal walls.

Investigators	Approach	Study Area	Major Findings
Ambarita et al. (2006) [77]	Numerical technique with the finite volume method	Laminar natural convection heat transfer in an air-filled partitioned square cavity. Two insulated partitions were attached to the adiabatic horizontal walls of the cavity. The Rayleigh numbers are from 10^4 to 10^8 .	(1). The Nusselt number is a function of Rayleigh number, partitions height and position. (2). The two partitions trap some fluid in the cavity and affect the flow fields.
Yucel and Ozdem (2003) [78]	Numerical technique with control volume approach and SIMPLE algorithm	Laminar natural convection fluid flow and heat transfer in air-filled partially divided square cavities, of which the horizontal walls are adiabatic or perfectly conducting. The partitions were attached to the bottom and top walls of the cavities in-line. Rayleigh numbers are in the range of 10^3 to 5×10^5 .	(1). The heat transfer rate depends on the partition height, the number of in-line partitions and the Rayleigh number.
Bilgen (2002) [29]	Numerical technique with SIMPLER method	Laminar and turbulent natural convection in air-filled cavities with partial partitions on the adiabatic horizontal walls. The aspect ratios of the cavities were from 0.3 to 0.4, and Rayleigh numbers are from 10^4 to 10^{11} .	(1). The flow regime was laminar for Ra up to 10^8 thereafter turbulent. (2). The flow circulation is choked by the partitions. (3). The heat transfer was affected by the partition number and location, as well as the aspect ratio of the cavity.
Turkoglu and Yucel (1996) [79]	Numerical technique with SIMPLER algorithm	Laminar natural convection heat transfer in air-filled rectangular cavities (aspect ratios of 0.5 – 1.5) with insulated horizontal walls. Conducting multiple complete partitions were placed vertically. Rayleigh numbers are from 5×10^5 to 5×10^6 .	(1). The mean Nusselt number was affected by the partition number and Rayleigh number. (2). The cavity aspect ratio does not affect the heat transfer to a considerable extent for considered aspect ratios in the study.
Nowak and Novak (1994) [80]	Numerical technique with the finite-difference approach	Laminar natural convection heat transfer in air-filled slender rectangular cavities with two partial partitions located in the adiabatic horizontal walls. The aspect ratio of cavities was up to 45, and Grashof number was up to 5×10^8 .	(1). The flow pattern was changed by the height of the partitions. (2). The two partitions can appreciably reduce the heat transfer rate.
Ciofalo and Karayiannis (1991) [81]	Numerical technique with the computer code Harwell-FLOW3D	Laminar natural convection heat transfer in air-filled partially or completely partitioned rectangular cavities with aspect ratios of 0.5 to 10. The horizontal walls of cavities were adiabatic or LTP. The Rayleigh number is varied from 10^4 to 10^7 .	(1). The partitions can reduce heat transfer rates in cavities due to two different basic mechanisms for different aspect ratios.
Acharya and Jetli (1990) [82]	Numerical technique with control volume approach	Laminar natural convection in an air-filled square cavity with perfectly conducting horizontal walls. A partial poorly conducting partition was attached to the bottom wall. Rayleigh numbers are from 10^4 to 3.55×10^5 .	(1). The influences of partition position and height have been studied. (2). The existence of three distinctly different flow regimes at different Rayleigh number ranges was confirmed.
Olson et al. (1990) [83]	Experimental approach with thermocouples and the smoke flow visualization	Steady state natural convection in an air-filled rectangular room with insulated horizontal walls. The aspect ratio of the cavity was 0.32. A vertical partition extended from the bottom wall to midheight. Rayleigh number is of the order of 10^{10} .	(1). The partition caused a modest decrease of heat transfer rate, while substantial changes in flow patterns and core temperature field. (2). Under the same conditions, the results from water and air are significantly different.

Table 2.6: Summary of investigations of natural convection in rectangular cavities with partitions on the horizontal walls (con'd).

Investigators	Approach	Study Area	Major Findings
Chen et al. (1990) [84]	Experimental approach with a thermocouple probe, a laser-Doppler velocimeter and the dye flow visualization	Natural convection in a water-filled, partially divided rectangular cavity with aspect ratio of 0.5. An adiabatic partition plate with/without an opening was attached to the insulated top wall of the cavity. Rayleigh numbers are ranging from 10^6 to 10^8 .	(1). The opening in the partition plate has the effect of increasing heat transfer by allowing the flow of the entrapped hot fluid through the opening.
Kelkar and Patankar (1990) [8]	Numerical technique with the finite-difference method and SIMPLER algorithm	Laminar natural convection flows in air-filled square cavities with vertical partitions. The horizontal walls are adiabatic, and the Rayleigh numbers are ranging from 0 to 10^6 .	(1). When a single partition is placed at the center, the boundary layers on the horizontal walls remain relatively unaffected; while partitions located at the top and bottom walls make the flow negotiate around them, resulting in the hot and cold streams in direct contact.
Nishimura et al. (1988) [85]	Experimental and numerical approaches	Laminar natural convection in water-filled rectangular cavities divided by complete multiple vertical partitions. The cavities with aspect ratios of 10 and 4 have the adiabatic horizontal walls. Rayleigh numbers are ranging from 10^6 to 10^8 .	(1). A heat transfer correlation was presented. (2). A useful number of partitions is 2 – 5, which can reduce the heat transfer rate by 70 – 90%.
Jetli and Acharya (1988) [86]	Numerical technique with the control volume approach	Laminar natural convection in air-filled square cavities with adiabatic or perfectly conducting horizontal walls. Two offset partitions were attached to the horizontal walls. Rayleigh numbers are 10^4 , 10^5 and 3.55×10^5 .	(1). The effect of horizontal wall conditions on the natural convection in the cavities was studied. (2). Correlations for Nusselt number have been presented.
Zimmerman and Acharya (1987) [87]	Numerical technique with the SIMPLER algorithm	Laminar natural convection in a square cavity with perfectly conducting horizontal walls. Partial partitions were mounted in the center of the cavity on the top and bottom walls. Rayleigh numbers are in the range of $10^4 - 3.55 \times 10^5$.	(1). The effects of the thickness and conductivity of the partitions on the natural convection flow and heat transfer have been investigated.
Nishimura et al. (1987) [88]	Experiment with a thermocouple probe	Natural convection heat transfer in water-filled rectangular cavities with adiabatic horizontal walls and a complete vertical partition. Aspect ratios are 4 and 10. Rayleigh numbers are from 10^6 to 10^8 .	(1). When the partition deviates from the center of the cavities, the heat transfer rate is identical with that for the partition in the central position.
Shaw et al. (1987) [89]	Numerical technique with cubic spline collection method	Laminar natural convection in a partially divided square cavity with adiabatic horizontal walls. Rayleigh numbers are in the range of $10^3 - 10^6$ and $Pr = 1$.	(1). An increase in the height of the partition decreased the heat transfer efficiently, while the effect of location of the partition on the mean Nusselt number is small.

Table 2.6: Summary of investigations of natural convection in rectangular cavities with partitions on the horizontal walls (con'd).

Investigators	Approach	Study Area	Major Findings
Jetli et al. (1986) [90]	Numerical technique with the finite-difference method SIMPLER	Laminar natural convection in a partially divided square cavity with perfectly conducting horizontal walls. Two offset partitions were attached to horizontal walls. Rayleigh numbers are 10^4 , 10^5 and 3.55×10^5 .	(1). The position and conductivity of the partitions have significant effects on the natural convection in the cavity.
Tong and Gerner (1986) [91]	Numerical technique with the finite-difference method	Laminar natural convection in air-filled partitioned rectangular cavities with insulated horizontal walls. A thin vertical partition separates the cavity into two regions. Aspect ratios of the cavities are from 5 to 15, and Rayleigh numbers are 10^4 and 10^5 .	(1). The partition can reduce heat transfer rate, and the maximum reduction occurred when the partition was placed midway between the vertical walls of cavities.
Nansteel and Greif (1984) [92]	Experiment using thermocouples and dye injection	Natural convection flow and heat transfer in a water-filled rectangular cavity with insulated horizontal walls. A vertical partition was oriented parallel to the vertical walls. Aspect ratio is 0.5, and Rayleigh numbers are from 10^{10} to 10^{11} .	(1). The dependence of the natural convection flow and heat transfer on the Rayleigh number and the size of the opening in the partition was studied.
Lin and Bejan (1983) [25]	Experimental and numerical study	Natural convection heat transfer in rectangular cavities with a partial vertical partition. The horizontal walls were adiabatic, and aspect ratios are 0.305 and 0.5. The working fluids include water and air. Rayleigh numbers are in the range of $10^9 - 10^{10}$.	(1). The partial partition reduces significantly the net heat transfer between the vertical walls of the cavity.
Bajorek and Lloyd (1982) [24]	Experimental study using a Mach-Zehnder interferometer	Laminar natural convection in a partitioned square cavity with insulated horizontal walls. Insulated partitions were placed both on the floor and ceiling of the cavity. Air and carbon dioxide were working fluids. Grashof numbers are from 1.7×10^5 to 3×10^6 .	(1). The partitions affected significantly the convective heat transfer, and the effect is dependent on the Grashof number. (2). The partitions appeared to have an unsettling effect on the flow field.
Nansteel and Greif (1981) [7]	Experiment using dye injection and thermocouple probes	Natural convection in a water-filled rectangular cavity with insulated horizontal walls. Aspect ratio of the cavity is 0.5. A partial vertical partition was placed on the top wall. Rayleigh numbers are in the range of $2.3 \times 10^{10} - 1.1 \times 10^{11}$.	(1). Three distinct regions were observed in the cavity. (2). The partition decreased significantly the overall heat transfer, especially when the partition was non-conducting.

due to the presence of the partition. The boundary layer flow along the heated vertical wall did not extend over the entire surface since most of the flow separated from the heated vertical wall at approximately mid-height of the wall, and then moved across the cavity horizontally until reaching the lower edge of the partition. This flow pattern differed substantially from that reported by Duxbury [93] in an air-filled partially divided enclosure with Rayleigh number approaching 10^6 . There was no distinct recirculating region and also little or no flow separation from the heated vertical wall. This discrepancy is likely due to the different working fluids. Olson et al. [83] experimentally studied the natural convection in an air-filled partitioned rectangular cavity with aspect ratio of 0.32 and Rayleigh number Ra_H of 10^{10} . The results of their study were different to previous investigations using water as the working fluid, both in temperature profiles and flow patterns. The authors indicated that water experiments at the same geometry and Rayleigh number tend to have higher thermal stratification and reduced flow recirculation.

Ciofalo and Karayiannis [81] numerically investigated the laminar natural convection heat transfer in air-filled rectangular cavities with aspect ratios of 0.5 to 10 and Rayleigh numbers Ra_L of 10^4 to 10^7 . The vertical walls of the cavities were isothermal with different temperatures, and the horizontal walls were adiabatic or with a linear temperature profile. Two symmetric partial partitions protruded centrally from the horizontal walls. The investigation showed that two basic mechanisms are responsible for the heat transfer reduction in cavities. At low aspect ratios, partitions do not alter the unicellular flow pattern. The effect of the partitions on the fluid flow rate along the walls was limited resulting in moderately reducing the local Nusselt number. However, at high aspect ratios, the presence of partitions caused the break down of the unicell, and resulted in the formation of secondary cells that were particularly intense near the bottom of the heated vertical wall and the top of

the cold vertical wall that resulted in a strong local reduction of Nusselt number.

2.2.3 Effect of partition parameters on the natural convection flow

The effect of partition parameters on natural convection characteristics have been studied, mainly focusing on the effect of the height, position and number of partitions. Frederick and Valencia [75] numerically studied the laminar natural convection heat transfer in an air-filled square cavity with conducting horizontal walls and a conducting partition on the heated vertical wall. With an increase of the partition height, the reduction of the heat transfer rate became more significant due to the increased blockage effect of the partition on the flow. A similar result was reported by Nowak and Novak [80] from numerical simulations of the laminar natural convection in air-filled slender rectangular cavities with two partial vertical partitions located in the middle of adiabatic horizontal walls. With an increase of the partition height, the flow pattern changed from multicellular to the unicellular transition regime. Lin and Bejan [25] experimentally investigated the natural convection heat transfer in a water-filled partitioned rectangular cavity with adiabatic horizontal walls with a vertical non-conducting partition at the center of the bottom wall. A heat transfer correlation was developed that took into account the partition height

$$Nu_H = 0.336 \frac{Ra_H^{1/4}}{(1 - \frac{H_P}{H})^{-3/4} + 0.5}. \quad (2.4)$$

Ambarita et al. [77] numerically studied the effect of offset partitions on the laminar natural convection in an air-filled square cavity. In their study, two insulated offset partitions with non-dimensional partition heights H_P/H of 0.6, 0.7 and 0.8

were respectively attached to the adiabatic top and bottom walls of the cavity at variable positions. For the global Rayleigh number $Ra_H < 10^6$, there was a single cell occupying the square cavity. While, for $Ra_H \geq 10^6$, the two partitions resulted in two separated and distinct flow regions with no interaction between the two flow zones. The phenomenon was not present in similar investigations in which the non-dimensional height of partitions was less than 0.5 [24][90][29].

Jetli et al. [90] numerically investigated the effect of two offset partitions on the laminar natural convection in a partially divided square cavity with conducting horizontal walls, and reported that the position of the partitions had a significant effect on the heat transfer and flow characteristics of the cavity. Shaw et al. [89] and Acharya and Jetli [82] numerically compared the effects of the partition height and position. Shaw et al. [89] investigated the laminar natural convection in a square cavity with a movable partial vertical adiabatic partition placed on the adiabatic bottom wall of the cavity. An increase in the height of the partition decreased the heat transfer, while the effect of the location of the partition on the mean Nusselt number was small. Acharya and Jetli [82] corroborated the conclusions of Shaw et al. [89]. They indicated that the partition height had a much stronger effect on the cavity heat transfer than the partition position based on their investigation of the laminar natural convection heat transfer in an air-filled square cavity with a single partial partition on the conducting bottom wall of the cavity. Recently, Shi and Khodadadi [28] developed correlations to describe the effects of the partition height and location on the natural convection heat transfer in an air-filled square cavity with a partition attached to the heated vertical wall

for $Ra_L = 10^4 \sim 10^5$

$$\overline{Nu_C} = (0.1213S_p^2 - 0.1202S_P + 0.1807) \cdot Ra_L^{0.2979} \cdot \left(\frac{H_P}{H}\right)^{0.0656}, \quad (2.5)$$

for $Ra_L = 10^6 \sim 10^7$

$$\overline{Nu_C} = (0.0163S_p^2 - 0.0129S_p + 0.1598) \cdot Ra_L^{0.2979} \cdot \left(\frac{H_P}{H}\right)^{0.0656}. \quad (2.6)$$

Here $\overline{Nu_C}$ is the mean Nusselt number on the cooled vertical wall and S_P represents the dimensionless position of the partition.

Yucel and Turkoglu [71] and Yucel and Ozdem [78] indicated that the number of partitions is an important parameter for optimization of the natural convection heat transfer rate. Yucel and Ozdem [78] found that when the number of partitions was increased, the partitions partially blocked the motion of the fluid flow resulting in the mean Nusselt number to be decreased.

Effects of the thickness and conductivity of partitions as well as the aspect ratio and the inclination of partitioned cavities on the natural convection have been studied. For example, Nag et al. [73] indicated that the thickness of a partition substantially affected the laminar natural convection heat transfer in an air-filled square cavity with a partition on the heated vertical wall. Zimmerman and Acharya [87] indicated that with an increase of the conductivity of partitions, the natural convection flow strength and the average Nusselt number were decreased. Bilgen [29] studied the effect of the aspect ratio on the natural convection heat transfer in partitioned rectangular cavities and concluded that with a decrease of the aspect ratio, the heat transfer was reduced since the cavity became more elongated. Frederick [74] performed an investigation on natural convection in an air-filled inclined square cavity with a partial partition on cold wall, and indicated that the heat transfer reduction depends on the angle of the inclination.

2.2.4 Summary and Limitations

Most previous experimental and numerical investigations on the natural convection in partitioned rectangular cavities have focused on cavities with adiabatic, insulated or conducting horizontal walls. Under these thermal boundary conditions, the partition directly suppressed the motion of the boundary layer flow along the walls or had an extra heating effect, resulting in significant changes in natural convection flow compared to that in cavities without partitions. There are no investigations on partitioned cavities with temperature differences in both horizontal and vertical directions simultaneously, in particular with larger top wall temperatures. Wu et al. [18] and Ravi et al. [17] reported that the temperature difference between the horizontal top and bottom walls significantly changed the flow pattern in a cavity with smooth walls due to the change in the stratification rate in the core region of the cavity. It is particular true for cases with larger top wall temperatures. These results suggest that characteristics of the natural convection flow in partitioned cavities are likely to be changed with an increase of the top wall temperature.

2.3 Theoretical Models

Only a few theoretical models have been developed compared with the numerous experimental and numerical investigations of natural convection in cavities. The existing theoretical models have mainly focused on the natural convection flow along a single vertical wall rather than in cavities.

A number of models have been developed for the natural convection flows on isolated isothermal vertical walls in stratified environments. Early studies were mainly focused on seeking similarity solutions. Cheesewright [49] developed similarity solutions for the flow along an isothermal plate in non-isothermal ambient air. This

included solutions for a range of ambient temperature distributions, but not a linear stable ambient temperature distribution like those observed for the natural convection flows in cavities driven by a temperature difference between the vertical walls [18][6]. Chen and Eichhorn [2], later, concluded that a similarity solution to the problem of an isothermal heated vertical wall in a linearly stratified stable medium was not possible, and used a local non-similarity approach to solve the problem. The local non-similarity method that included a second term to account for the changes in the streamwise direction was proposed by Sparrow and coworkers [94][95][96]. Chen and Eichhorn [2] compared the solutions from this non-similarity approach to the experimental measurements of natural convection from a cylinder in a stratified fluid with a Prandtl number of 6.0 and found good agreement between the experiment and the solution. They examined the flow with a Prandtl number of 0.7 but did not compare the results with experiments. Kulkarni et al. [1] later suggested that there were similarity solutions for the natural convection flow along a vertical wall in a stratified environment with a linear temperature distribution, but did not compare their results with experiments, instead comparing with other similarity and non-similarity solutions. Heretofore, there does not appear to have been any attempts to compare these solutions to experimental results for natural convection of air flows in cavities.

Chapter 3

Experimental Methodology

The experiments were performed in an air-filled rectangular cavity with differentially heated vertical walls and an adjustable aspect ratio. The experimental facilities are described first. The experimental techniques used to measure the temperature distributions and visualize the flow in the cavity are then discussed in detail. Finally, the data analysis procedures are presented.

3.1 Experimental Facility

The laminar natural convection air flow in rectangular cavities with and without a partition on the wall were experimentally investigated in an air-filled rectangular cavity shown schematically in Figure 3.1. The cavity had a height of 305mm (12") and a width that could be adjusted from 100 to 610mm (3.9" to 24") by moving one vertical wall. Experiments were performed with the width of the cavity set to 152.5, 305 and 610mm (6", 12" and 24"), corresponding to aspect ratios AR of 2, 1 and 0.5. The depth of the cavity was 914mm (36"), which was 3 times the height, so that the flow should be approximately two-dimensional as suggested in a number

of previous studies [6][15]. The walls of the cavity were designed so that one of the vertical walls and the top wall could be heated independently; while the other vertical wall, which was the movable wall, and the bottom wall could be cooled. The ends of the cavity were sealed using walls with large glass windows so the flow in the cavity could be visualized. The cavity was insulated using OFI-48 insulation with a thermal conductivity of $0.035W/m \cdot ^\circ C$ to reduce heat transfer to the ambient. The cavity was supported on a $1.5m(5')$ high frame constructed from rectangular tubing. A two-dimensional traversing system was mounted on this frame, which was used to move a thermocouple probe unit in both horizontal and vertical directions to measure the temperature distributions in the cavity.

The walls of the cavity were constructed from a series of sections and instrumented using thermocouples that were used to monitor the surface temperature. The top wall and the heated vertical wall were constructed using $12.7mm$ ($0.5''$) thick aluminium plates. The heated vertical wall had three silicone rubber heaters, with a maximum capacity of $180W$, while the top wall had four heaters which were attached on the outside surface of these plates. To minimize heat losses from the heated walls to the ambient, the walls were insulated using aluminium guard heater walls constructed similar to the heated walls following a number of previous studies [3][11]. The walls were separated by a $25mm$ thick layer of OFI-48 insulation. The heat transfer between the heated vertical wall and its guard wall was less than $3W$, corresponding to approximately 15% of the heat transfer into the cavity from the heated vertical wall. This heat loss was estimated from the temperature difference between the heated vertical wall and its guard wall, and knowing the thermal conductivity of the insulation. The surface radiation effects from the cavity walls were estimated using an emissivity of 0.04 for the aluminium plates and were found to be negligible compared to the natural convection heat transfer along the heated vertical wall.

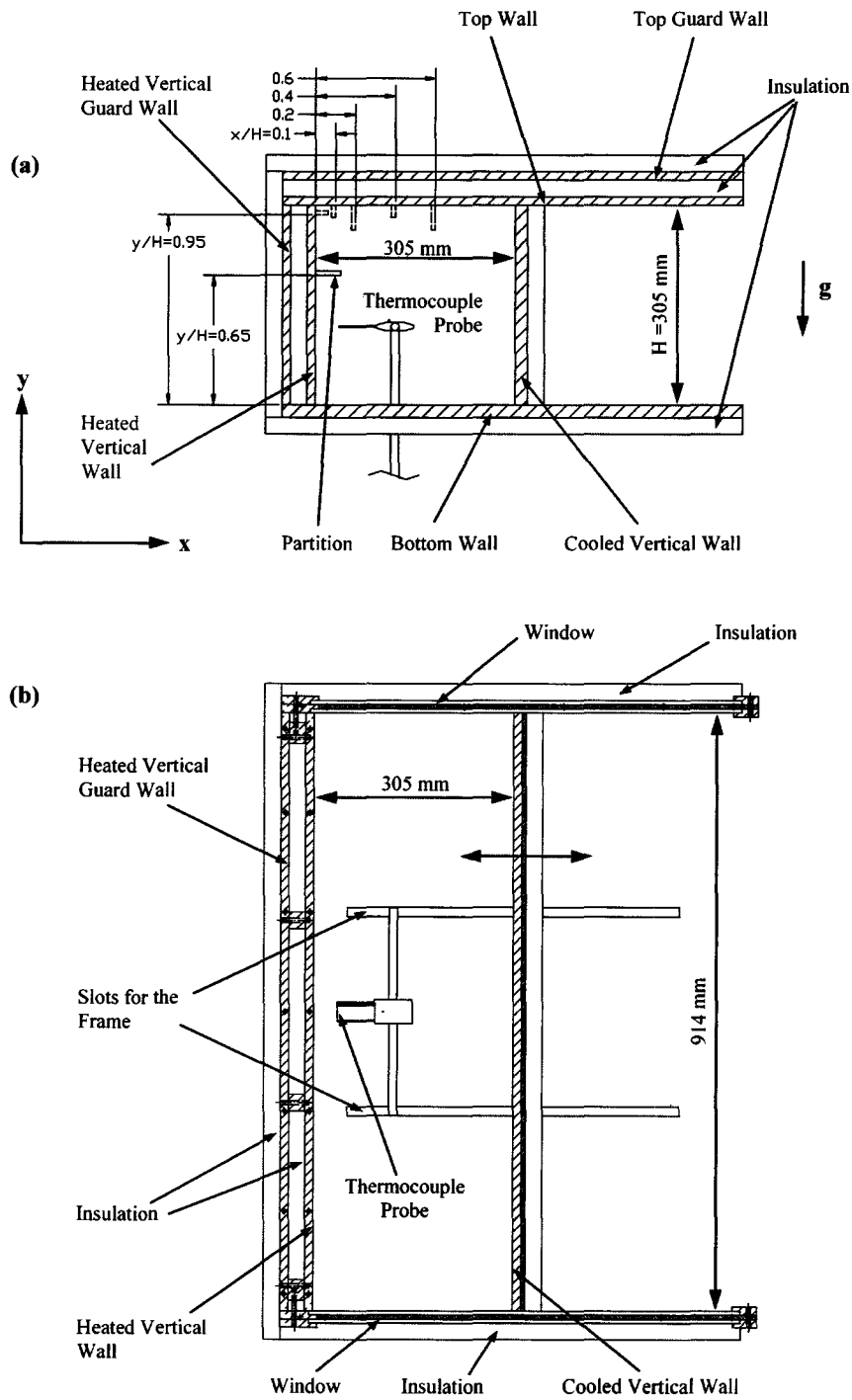


Figure 3.1: Schematic of the rectangular cavity from (a) the side view and (b) the top view.

Schematics of the top wall and the heated vertical wall are shown in Figures 3.2 and 3.3. The walls were divided into sections by milling 6mm grooves on the outside surface of these plates. The top wall was divided into four equal size sections, while the vertical wall was divided into three sections that were 89mm , 102mm , and 114mm high, respectively, with the smallest section at the bottom of the wall where the heat flux into the cavity was the largest. Silicone rubber heaters were embedded into 25mm wide grooves machined in the center of each section and powered using a multi-channel variable duty controller that could vary the duty cycle for each of the heaters independently, so the heated walls could be maintained at a uniform temperature.

The temperature distributions on the top wall and the heated vertical wall were measured using T-type thermocouples embedded in these plates at the locations shown in Figures 3.2 and 3.3. Each section of the wall contained 12 thermocouples. Six thermocouples embedded in holes with a depth of 3.2mm ($0.125''$) from the rear surface were used to measure the outside temperature of the plate, while the other six embedded in holes with a depth of 11.1mm ($0.4375''$) were used to measure the temperature of the inner surface of the wall. The detailed schematic showing how the thermocouples were embedded in the surface is shown in Figure 3.4. The thermocouples were bare wire thermocouples with a diameter of 0.254mm ($0.010''$). They were insulated using ceramic tubing and Teflon tubing as shown in Figure 3.4. The thermocouple was held in place using thermally conductive epoxy adhesive that was used to fill the hole. The thermocouple leads were connected to 24 AWG T-type thermocouple wire at a phenolic terminal block that can withstand temperatures up to 150°C . The six thermocouples located on the outer surface in each section were connected together to determine the average outside temperature of the wall, which was used to estimate the heat transfer from the top wall and the heated vertical wall

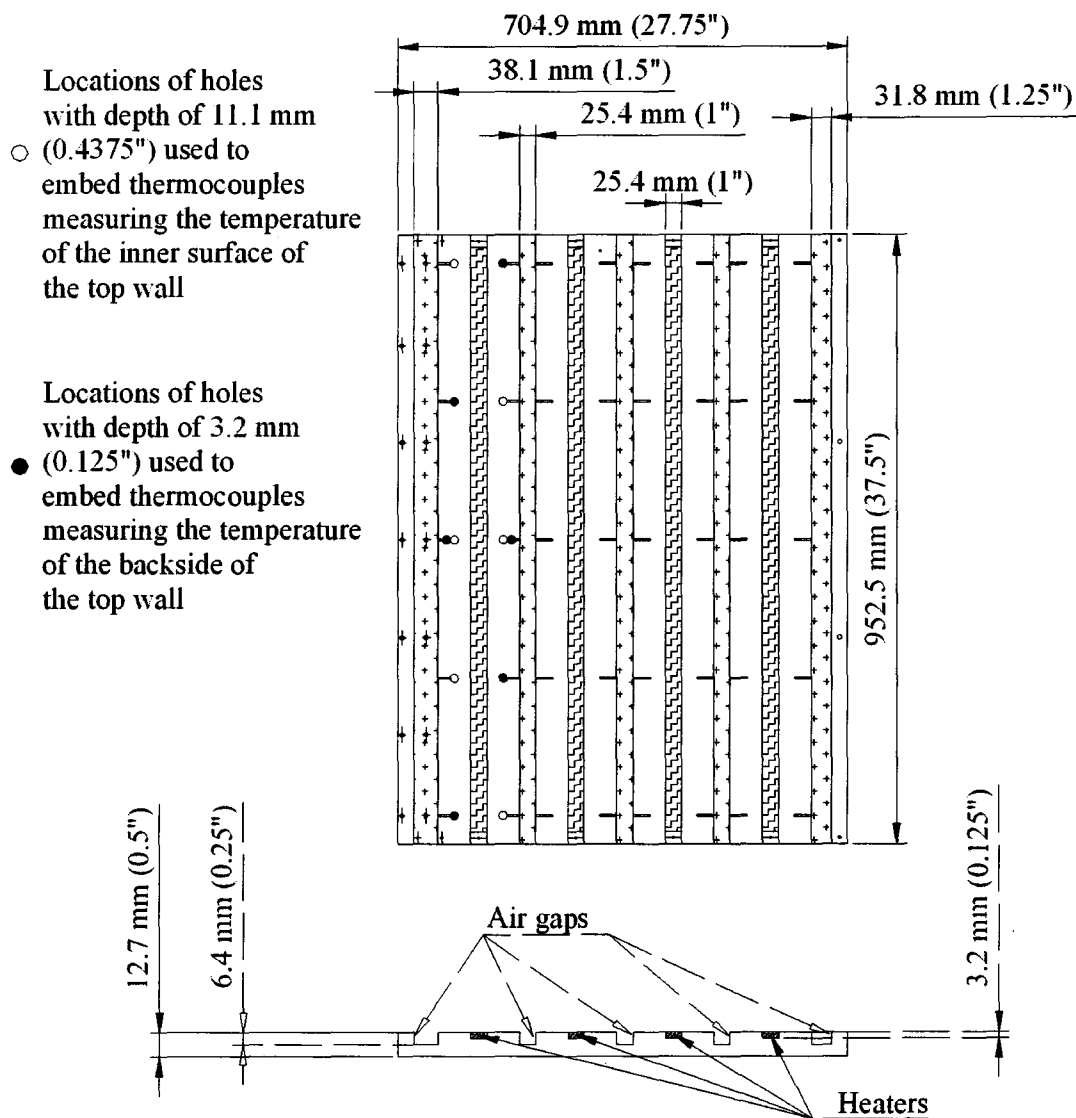


Figure 3.2: Schematic of the top wall.

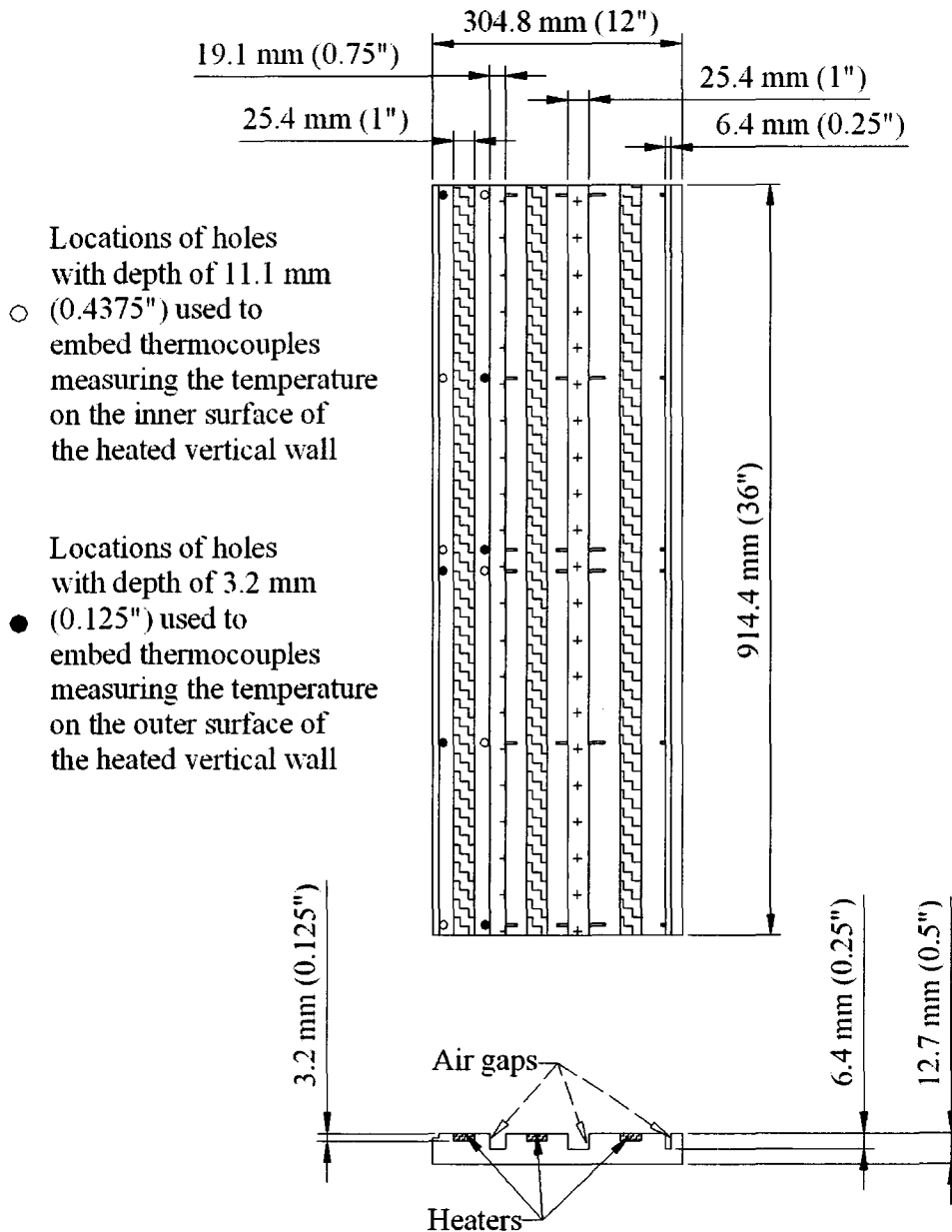


Figure 3.3: Schematic of the heated vertical wall.

to their respective guard walls. The thermocouples mounted on the inside of the wall were connected individually to the thermocouple meter. There were, respectively, 6 and 8 thermocouples embedded along the centerlines of the heated vertical wall and the top wall to continuously monitor the changes in the temperatures so that the average wall temperatures reported here can be calculated.

The structure of the guard walls for the top wall and the heated vertical wall are similar to that of the heated walls. The four heaters on the top guard wall were connected in parallel and powered using a variable transformer with maximum current of 10 amps. The output voltage of the transformer was adjusted so that the average temperature on the inner surface of the guard wall can be approximately equal to that on the outside of the top wall. Similarly, three heaters on the heated vertical guard wall were connected in parallel to a transformer with maximum current of 7.5 amps. The guard walls included 6 T-type thermocouples embedded in each of the sections at the same locations as the thermocouples on the outside of the heated walls. The six thermocouples in each of the sections were connected together so the average temperature of each section in the guard walls could be determined.

The bottom wall and the cooled vertical wall were also constructed from 12.7mm (0.5") thick aluminium plates that contained serpentine cooling channels as shown in Figures 3.5 and 3.6. The cooling channels were grooves with a width of 25.4mm (1") and depth of 6.4mm (0.25") machined into the rear surface of the plates. The channels were closed using 6.4mm (0.25") thick outer aluminium plates that were insulated from the outside using a 25mm (1") thick layer of insulation. Two slots with width of 14mm (0.55") were machined into the bottom wall so the frame for the movable thermocouple probe could pass through the wall. The temperature of the bottom wall was measured using 16 T-type thermocouples located as shown in Figure 3.5. These thermocouples were embedded using the same approach as in the heated

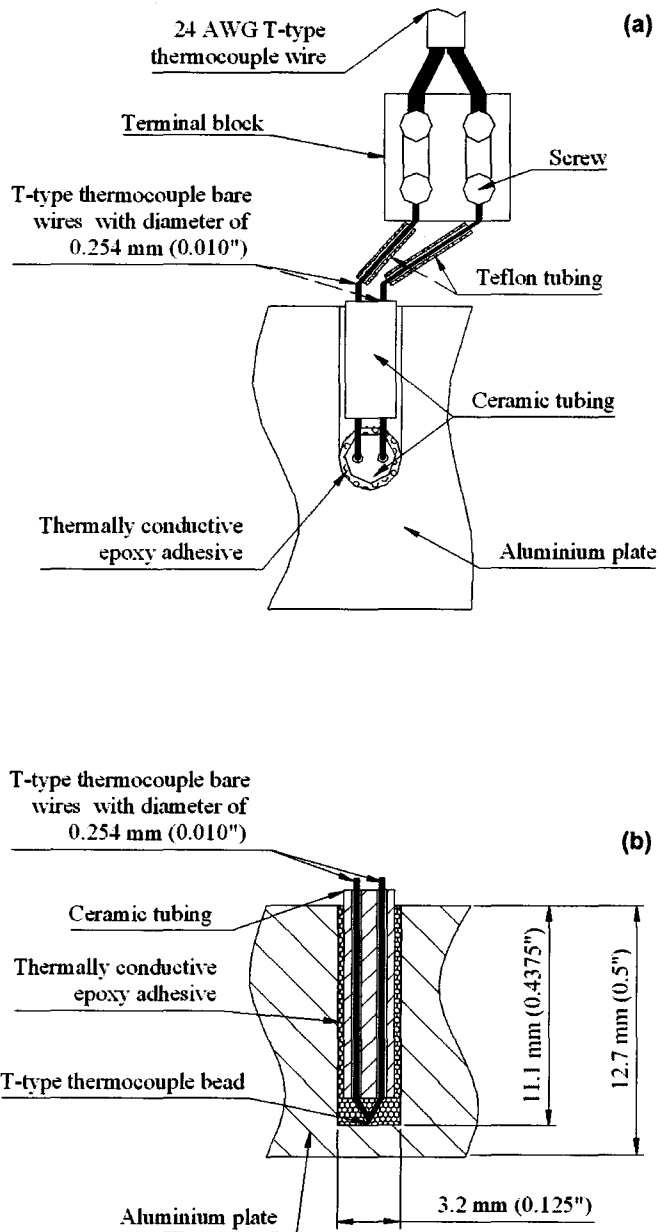


Figure 3.4: Detailed structure of the thermocouple embedded in the wall from (a) the top view and (b) the side view.

walls. Four of these thermocouples were located in the centerline of the bottom wall to calculate the average wall temperature and the others were distributed throughout the remaining area. The temperature on the cooled vertical wall was monitored using 11 T-type thermocouples as shown in Figure 3.6, three of which were on the centerline. Municipal water was circulated through the channels to remove the heat from these two plates following Randall et al. [69] and Tian and Karayiannis [6]. The cold water was first passed through a bank of four flow meters with accuracy of $\pm 1.69 \times 10^{-4} L/s$. The water temperature at the inlet and outlet of the channels was measured using eight T-type thermocouples mounted at the beginning and the end of the flow loops. The energy removed from the cavity was estimated as

$$Q = \dot{m}c_p(T_{w,o} - T_{w,i}), \quad (3.1)$$

where \dot{m} is the mass rate of the water and c_p is the specific heat of the water, while $T_{w,o}$ and $T_{w,i}$ are the outlet and inlet temperatures of the water, respectively. The temperature of these two walls in the current investigation was kept approximately uniform by maintaining the cooling water flow rate relatively high at approximately $0.9 L/min$. This was facilitated by the fact that the heat flux through the walls was relatively low, approximately less than $480 W/m^2$ in the current study.

The temperature difference between the walls will result in a singularity in temperature at the junctions, which has been studied by Nansteel et al. [97]. In order to minimize the heat transfer between the heated vertical wall and the top wall, the junction between the walls was insulated using a thin layer of mineral fibre paper. The maximum temperature difference across the mineral fibre paper, in the current investigation, was approximately $48^\circ C$. The maximum temperature gradients in the vicinity of the junction on the heated vertical wall and the top

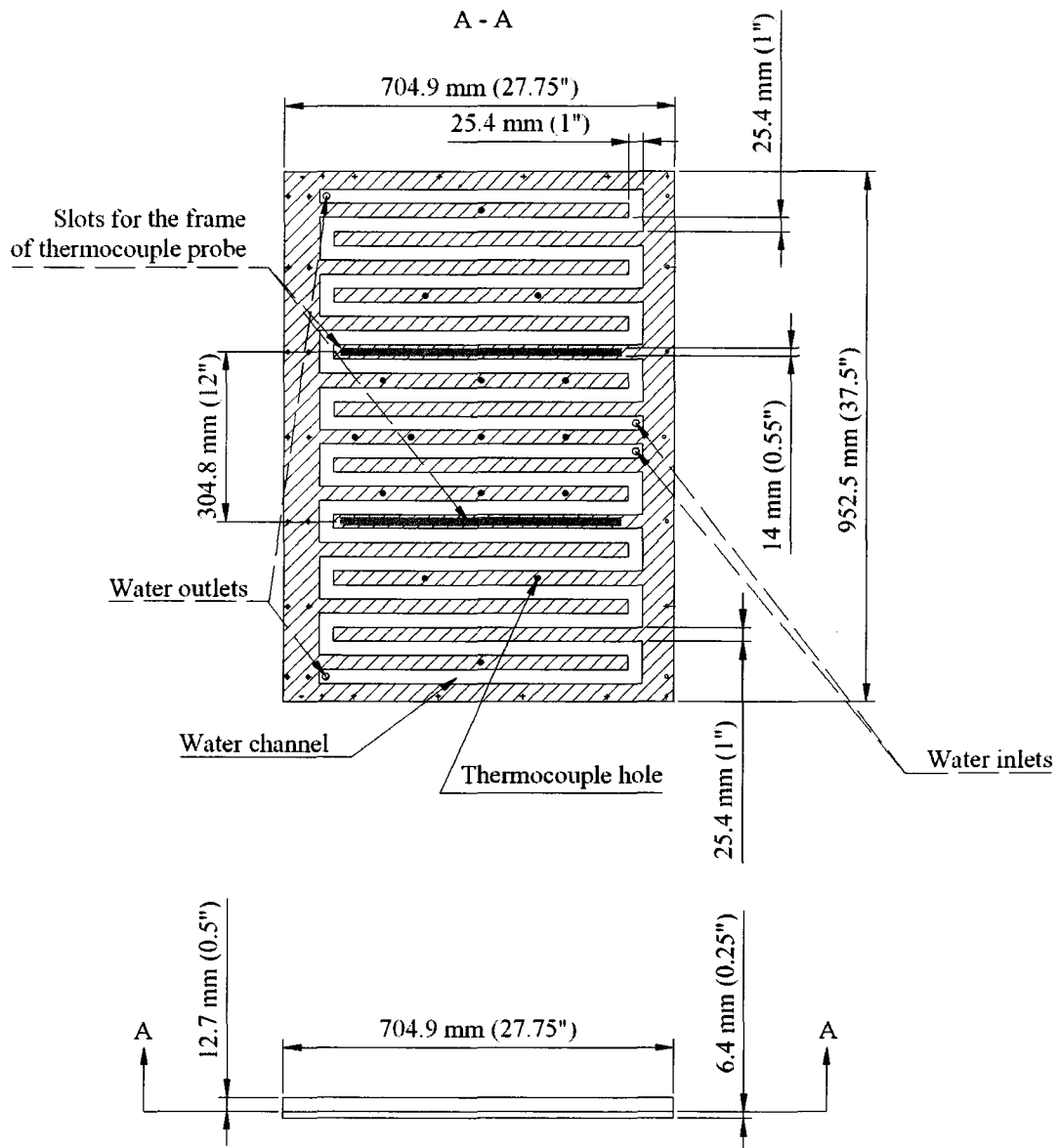


Figure 3.5: Schematic of the bottom wall with cooling channels.

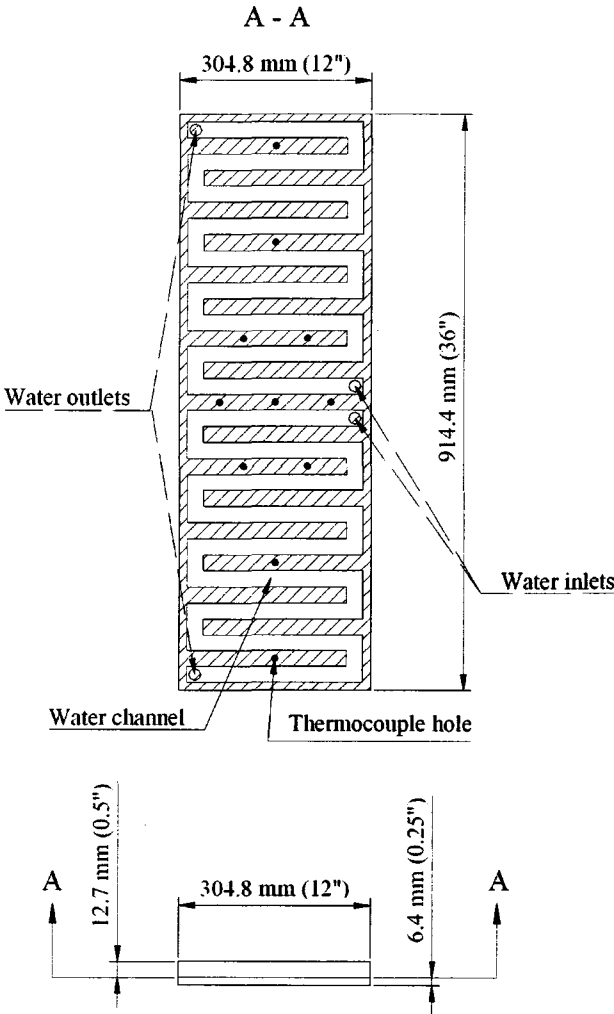


Figure 3.6: Schematic of the cooled vertical wall with cooling channels.

wall, estimated from the temperature measurements, were approximately $0.26^{\circ}\text{C}/\text{cm}$ and $0.31^{\circ}\text{C}/\text{cm}$ respectively. The heated vertical wall was isolated from the bottom wall by supporting its guard wall on four small Delrin blocks, which were $19.1\text{mm}(0.75'') \times 10.2\text{mm}(0.4'') \times 6.86\text{mm}(0.27'')$, so that an air gap of approximately 1mm high was present as shown in Figure 3.7. Since the cross sectional area of these blocks was small and the conductivity of them was low, the corner was approximately insulated.

An aluminium partition 914mm ($36''$) long and 6.35mm ($0.25''$) thick was attached at different locations to the heated vertical wall or the top wall of the cavity using a high thermal conductivity paste as shown in Figure 3.1(a) for the studies in the cavity with a partition. Two partitions of height, H_P , 19.05mm ($0.75''$) and 38.1mm ($1.5''$), corresponding to non-dimensional heights, H_P/H , of 0.0625 and 0.125 were used in this study. On the heated vertical wall, the partition was placed at y/H of 0.65 and 0.95 respectively; while on the top wall the partition was located at x/H of 0.1, 0.2, 0.4 and 0.6 respectively.

3.2 Experimental Techniques

The temperature distribution of the air in the cavity was measured using an in-house temperature measurement system including a T-type thermocouple probe unit, a two-dimensional traverse and a data acquisition facility. The thermocouple probe unit was mounted on a frame which passed through the slots on the bottom wall of the cavity and then was fixed on the two-dimensional traverse so that the thermocouple probe could be moved horizontally and vertically within the cavity. The two-dimensional traverse with a minimum step size of 0.0254mm was driven by two VEXTA step motors that was controlled using LabView.

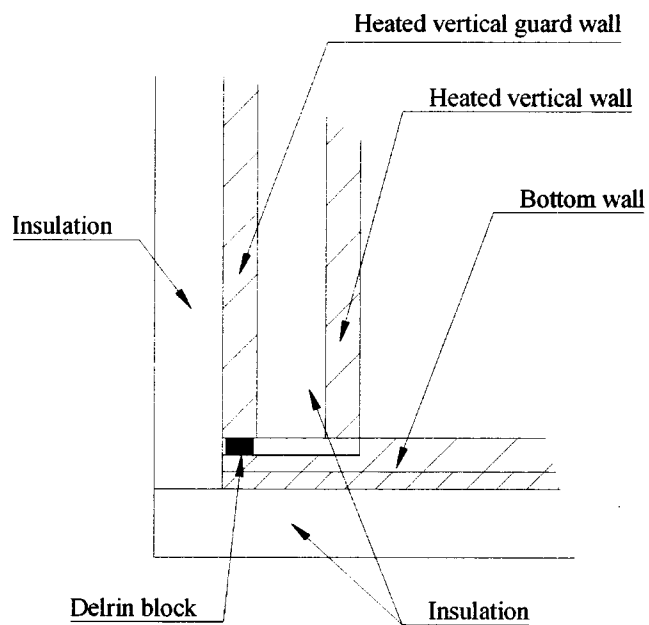


Figure 3.7: Detailed structure of the corner between the heated vertical wall, heated vertical guard wall and the bottom wall.

The construction and dimensions of the thermocouple probe unit are shown in Figures 3.8 and 3.9. A T-type thermocouple with diameter of 0.051mm ($0.002''$) was used in the probe. The bare wires of the thermocouple were passed through a thermocouple support that was constructed from two stainless steel tubes with diameters of 1.6mm ($0.0625''$). A 26 AWG Teflon tubing was inserted between the bare wire and the inner surface of the stainless steel tubes. The length of the stainless steel tubes was 57.2mm ($2.25''$) to keep the frame out of the thermal boundary layer. The distance between the two stainless steel tubes was 28.6mm ($1.125''$) so they would not block the flow near the measurement point. The support was mounted into a Teflon block which was mounted on the frame using a pair of steel pins. The leads from the bare thermocouple wire were connected to a 24 AWG T-type thermocouple wire inside the Teflon block. The entire junction was surrounded and anchored to the Teflon block using an electrically conductive epoxy. The 24 AWG T-type thermocouple wires were then connected to the data acquisition facility controlled by LabView through a noise rejecting, shielded I/O connector block. The data acquisition board was a 16-channel National Instruments data acquisition board with 16-bit resolution. The position of the thermocouple relative to the walls in the cavities was determined using two positioning rods installed in the probe holder, that closed an electrical circuit when they touched the wall. The distance between the thermocouple bead and the tip of the horizontal positioning rod was 0.7mm measured using a microscope combined to a vernier scale device with an accuracy of 0.02mm .

To ensure accuracy of the temperature measurement system, the thermocouple probe (diameter of 0.051mm or $0.002''$) and a typical thermocouple of the type embedded in the walls (diameter of 0.254mm or $0.010''$) were calibrated before the experiments by placing them in a container filled with heated water along with a platinum RTD with a reported accuracy of $\pm 0.01^\circ\text{C}$. The temperature of the water

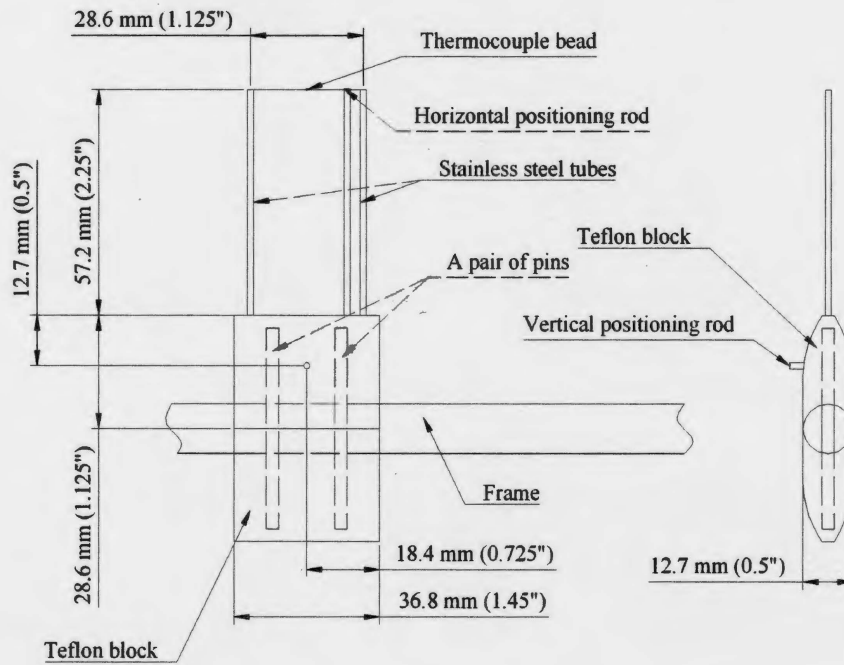


Figure 3.8: Structure and dimensions of the thermocouple probe unit.

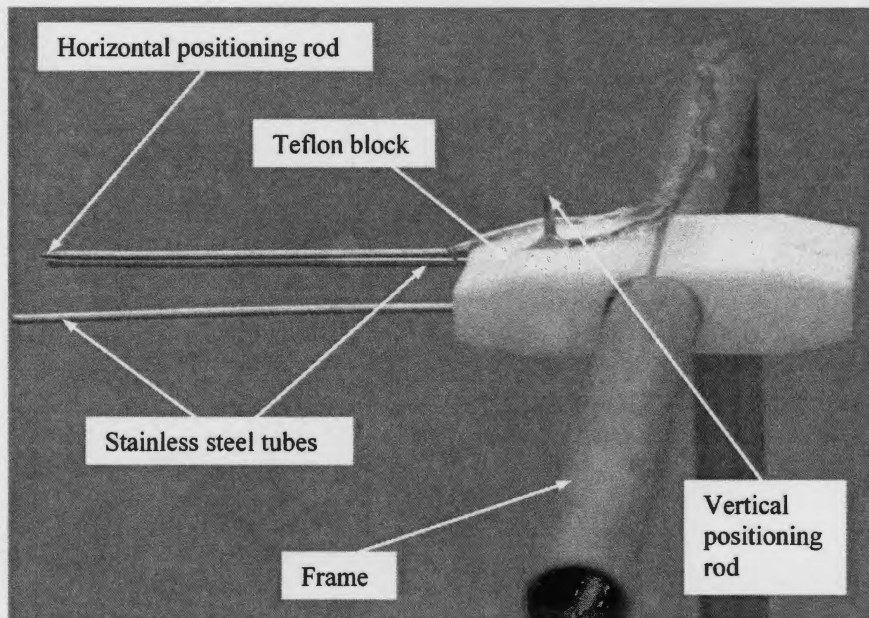


Figure 3.9: Photograph of the thermocouple probe unit.

was decreased gradually by adding ice into the container, until the temperature was close to 0°C . A comparison of temperature determined from the 0.002" thermocouple and the 0.010" thermocouple to the reading from the platinum RTD is shown in Figure 3.10. The results were curve fit to determine the calibration for the 0.002" thermocouple and 0.010" thermocouple as shown in Figure 3.10. These calibration equations were then used in the data analysis for all experiments.

Due to the relatively large change in temperature of the air near the heated vertical wall of the cavity, the temperature measurements were made at 0.254mm intervals for the first 3.81mm from the wall. The distance between consecutive measurement locations was subsequently increased from 0.508mm to 10.16mm as the distance from the wall was increased. The same method was also used in measuring temperature profiles along the rear surface of the partition which was attached on the top wall of the cavity.

In each experiment, the desired wall temperatures of the cavity were reached by adjusting the power to the heaters and the cooling water flow rates. Typical temperature distributions along the centreline of the heated vertical wall of the cavity for different aspect ratios are shown in Figure 3.11. In all cases, the maximum discrepancy, which occurred near the corner regions, between the local temperature and the average wall temperature was less than $\pm 4\%$. When the heaters on the top wall and its guard wall were turned off, only the two layers of insulation reduce the heat transfer from the top wall to the ambient. This thermal boundary condition is defined as "insulated" here. The typical top wall temperature distributions under this thermal boundary condition are shown in Figure 3.12, and the mean temperature of the top wall is used in the analysis for this case. Measurements were started after the wall temperatures fluctuated less than $\pm 0.5^{\circ}\text{C}$ for over 1 hour following Chinnakotla et al. [98]. The temperature distributions near the heated vertical wall of the cavity

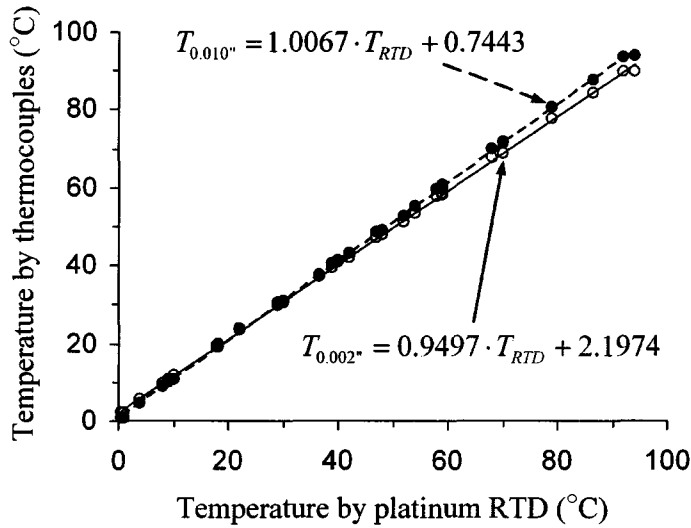


Figure 3.10: Comparison of temperatures measured with \circ : the 0.002” thermocouple and \bullet : the 0.010” thermocouple with the temperature measured by a platinum RTD.

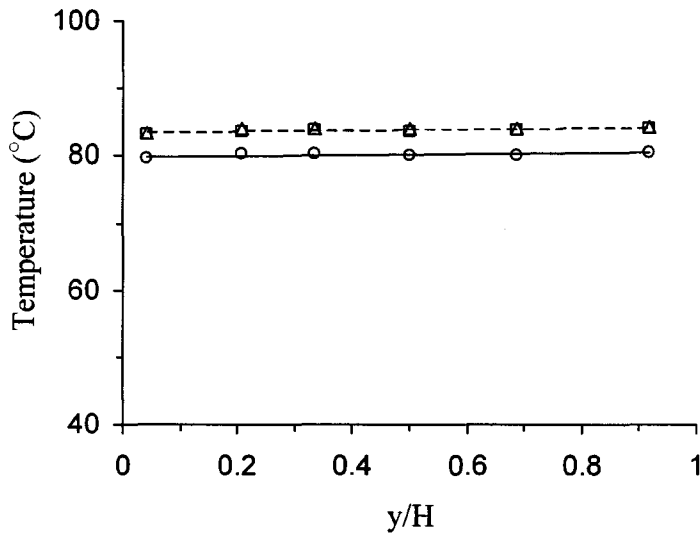


Figure 3.11: Typical temperature distributions along the centreline of the heated vertical wall of the rectangular cavities with aspect ratios of Δ : 0.5, \circ : 1.0 and \square : 2.0 for the top wall temperature of approximately $93^{\circ}C$ corresponding to the non-dimensional temperature of 1.14.

were measured at 11 heights that were 25mm (1") to 4.57mm (0.18") apart. The instantaneous temperature measurements from the thermocouple probe were averaged for approximately 20 seconds at each measurement location.

The flow in the cavity was visualized using incense smoke, similar to Sernas and Lee [41] and Tian and Karayiannis [6]. The incense smoke was illuminated by a laser light sheet that was projected into the cavity through one of the two slots machined in the bottom wall of the cavity for the thermocouple probe frame. The smoke was generated by slowly moving air over burning incense. The smoke was cooled to approximately room temperature before it was injected into the cavity through the other slot in the bottom wall for the thermocouple probe frame. Care was taken to ensure the injection of the smoke was slow enough with an average velocity less than 15cm/s , which was estimated from the cross sectional area of the outlet of the injection pipe and the flow rate of the smoke, to allow it to follow the flow streamlines in the cavity. The flow images were recorded using a digital camera positioned outside the window of the sidewall of the cavity. The resolution of these pictures is 2592×1944 pixels that covered an area of 595cm^2 , with an exposure time of 1 second.

3.3 Data Reduction and Uncertainty Analysis

The local heat flux from the heated vertical wall into the cavity was estimated from the slope of the temperature profile in the near-wall region of the boundary layer, where conduction is the dominant mode of heat transfer so the slope is approximately constant. The conduction layer is typically about one third of the thickness of the natural convection thermal boundary layer (Holman [99]). A best linear fit of the data over approximately the first third of the boundary layer thickness was then used

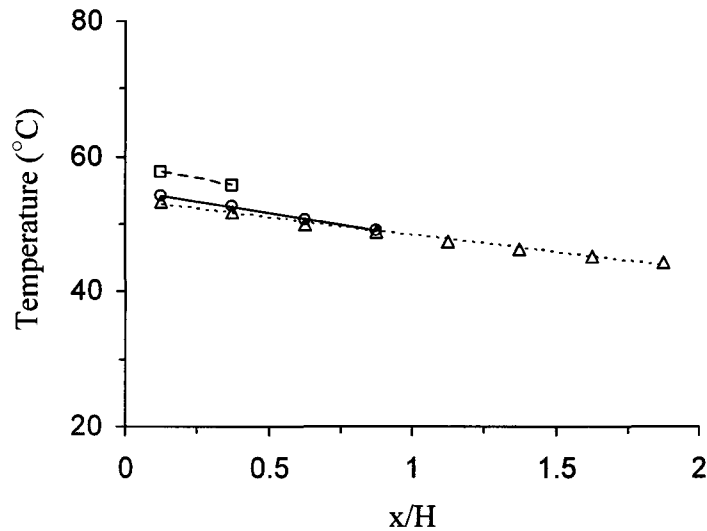


Figure 3.12: Temperature distributions on the insulated top wall of the rectangular cavities with aspect ratios of \triangle : 0.5, \circ : 1.0 and \square : 2.0.

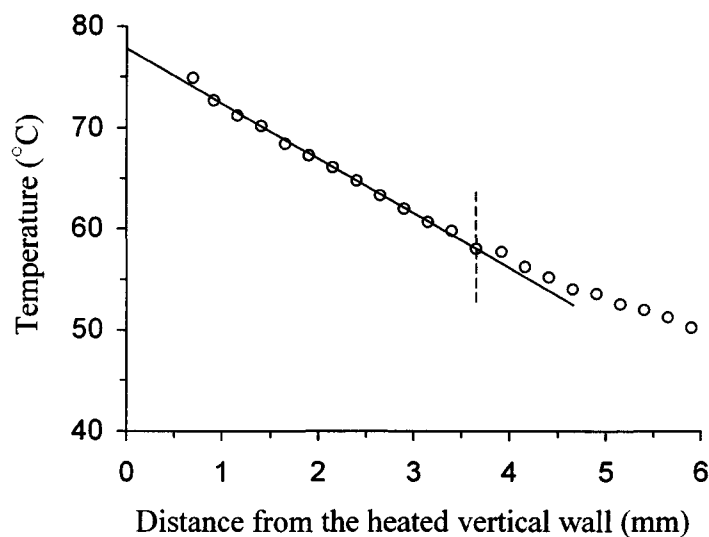


Figure 3.13: Best linear fit used to determine the slope of the temperature profile at the non-dimensional height $y/H = 0.6$ of the square cavity with the top wall temperature of 79°C corresponding to the non-dimensional temperature of 0.99.

to determine the slope of the temperature profile as shown in Figure 3.13. In all cases, at least seven measurement points existed in the near-wall region of the boundary layer. The local heat flux was estimated as

$$q'' = -k \frac{\partial T}{\partial x}, \quad (3.2)$$

where k is determined by the average air temperature in the conduction layer. The local heat flux was then used to determine the local heat transfer coefficient given by

$$h = \frac{q''}{T_H - T_\infty}. \quad (3.3)$$

The T_∞ is measured by the thermocouple probe, and the local temperature of the heated vertical wall T_H was determined by projecting the temperature profiles to the wall. It was found that there was a consistent discrepancy between the wall temperature determined from the temperature profile and that measured from the thermocouple embedded in the heated vertical wall. This is likely due to the small change in the position of the thermocouple probe frame in the x-direction when the horizontal positioning rod touched the heated vertical wall. The difference was typically less than 6% of the temperature difference across the thermal boundary layer, but in some cases was as large as 11%.

The local Nusselt number and Rayleigh number along the heated vertical wall were obtained by

$$Nu = \frac{h \cdot y}{k}, \quad (3.4)$$

$$Ra = \left(\frac{\beta}{\alpha \nu}\right) \cdot g \cdot (T_H - T_\infty) \cdot y^3. \quad (3.5)$$

Here β , α and ν are the properties of the air at the temperature of $\frac{(T_H + T_\infty)}{2}$.

The accuracy of the local heat flux computed from the temperature profiles were checked by applying an energy balance for the heated vertical wall following the procedure presented in [100]. This was done only in the central area of the heated vertical wall as shown in Figure 3.14 since it was difficult to estimate the heat losses at the edges of the wall. The equations to express the total energy into and leaving the area are given, respectively, by

$$Q_{in(a)} = Q_H + Q_T, \quad (3.6)$$

and

$$Q_{out(a)} = Q_C + Q_G + Q_B + Q_R + Q_L. \quad (3.7)$$

The subscripts represent the different sources of energy into or leaving the area. For example, Q_H is the energy input by the heater, which was estimated from the heater input parameters. Q_C is the energy into the thermal boundary layer along the heated vertical wall, that was calculated by integrating the heat convected to the boundary layer over the central area. The conduction heat transfer from the adjacent areas including the guard wall was considered in the energy balance as well. In this central area, the discrepancy in the energy balance was within 15% to 25% for all cases.

An energy balance was also performed for the entire system. A control volume was chosen as shown in Figure 3.15 to estimate the energy balance for the entire system. The control volume included the heated vertical wall, the cooled vertical wall, the top wall and the bottom wall. The total energy into and leaving the control volume are given, respectively, by

$$Q_{in(CV)} = Q_{h,V} + Q_{h,T} + Q_{G \rightarrow T} + Q_{G \rightarrow B}, \quad (3.8)$$

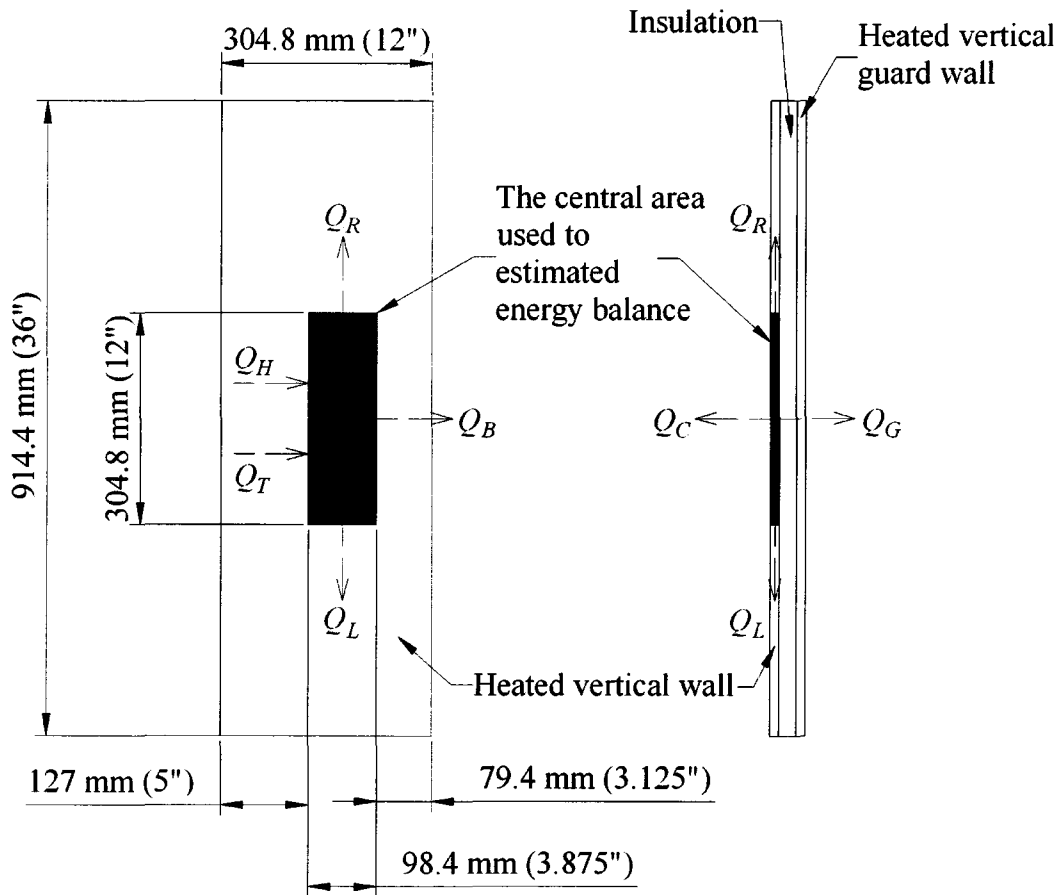


Figure 3.14: Schematic of the central area of the heated vertical wall used to estimate energy balance.

and

$$Q_{out(CV)} = Q_{V \rightarrow G} + Q_{T \rightarrow G} + Q_{T \rightarrow T} + Q_{w,C} + Q_{C \rightarrow O} + Q_{B \rightarrow B} + Q_{B \rightarrow O} + Q_{w,B}. \quad (3.9)$$

Here, the subscripts V , C , T and B respectively represent the heated vertical wall, the cooled vertical wall, the top wall and the bottom wall of the cavity. G indicates the guard walls of the heated vertical wall and the top wall. The subscript w means the cooling water, and O represents the ambient of the system. In the current investigation, the discrepancy in the energy balance was found to be within 5%–17%.

The uncertainties in the measurements reported here were evaluated using the approach outlined by Coleman and Steele [101]. The uncertainty of the local heat flux is given by

$$\frac{\Delta q''}{q''} = \sqrt{\left\{ \frac{\sqrt{\Delta T_H^2 + \Delta T_{edge}^2}}{(T_H + T_{edge})} \right\}^2 + \left\{ \frac{\Delta(\frac{\partial T}{\partial x})}{(\frac{\partial T}{\partial x})} \right\}^2}. \quad (3.10)$$

Here, the uncertainties of temperature at the edge of the conduction layer, ΔT_{edge} , and the projected heated vertical wall temperature, ΔT_H , were $\pm 1^\circ C$. The variation of the slope of the temperature profile ($\frac{\partial T}{\partial x}$) is less than 5%.

The uncertainty of the local heat transfer coefficient is given by

$$\frac{\Delta h}{h} = \sqrt{\left\{ \frac{\Delta q''}{q''} \right\}^2 + \left\{ \frac{\sqrt{\Delta T_H^2 + \Delta T_\infty^2}}{(T_H - T_\infty)} \right\}^2}, \quad (3.11)$$

where ΔT_∞ is the uncertainty of the ambient temperature outside of the thermal boundary layer T_∞ determined by the thermocouple probe and was $\pm 1^\circ C$.

The uncertainty of the local Nusselt number is given by

$$\frac{\Delta Nu}{Nu} = \sqrt{\left\{ \frac{\Delta h}{h} \right\}^2 + \left\{ \frac{\Delta y}{y} \right\}^2 + \left\{ \frac{\sqrt{\Delta T_H^2 + \Delta T_{edge}^2}}{(T_H + T_{edge})} \right\}^2}, \quad (3.12)$$

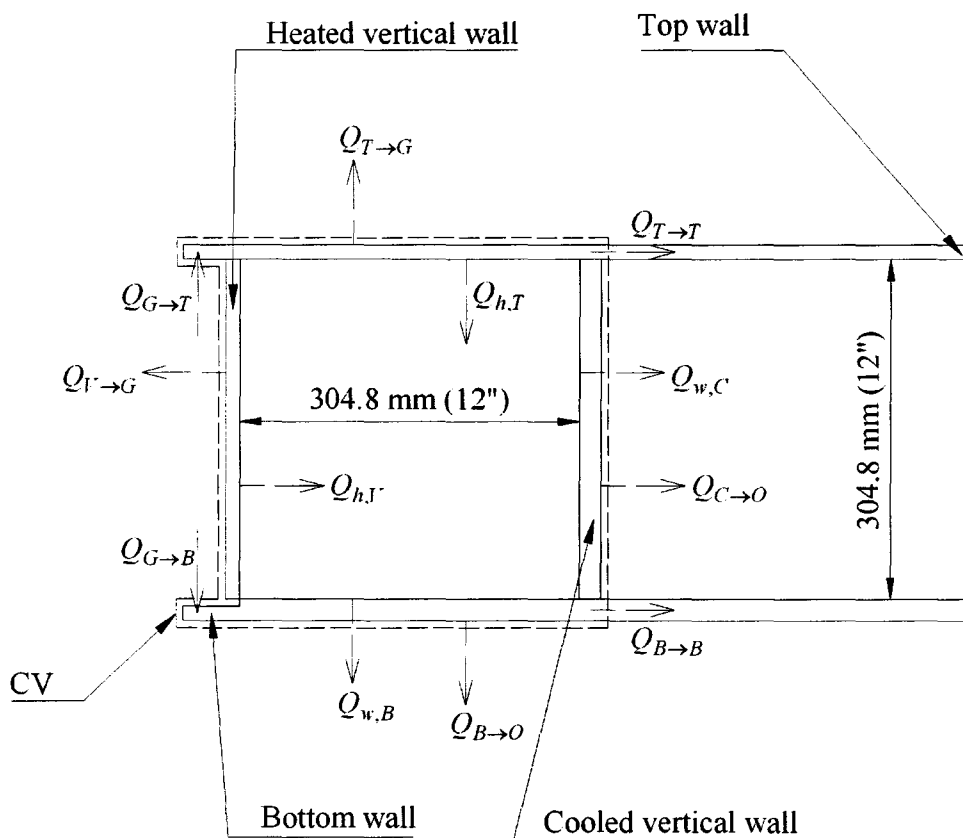


Figure 3.15: Schematic of the control volume used to estimate energy balance for the entire system.

and the uncertainty of the local Rayleigh number is given by

$$\frac{\Delta Ra}{Ra} = \sqrt{3\left\{\frac{\sqrt{\Delta T_H^2 + \Delta T_\infty^2}}{(T_H + T_\infty)}\right\}^2 + \left\{\frac{\sqrt{\Delta T_H^2 + \Delta T_\infty^2}}{(T_H - T_\infty)}\right\}^2 + 9\left\{\frac{\Delta y}{y}\right\}^2}. \quad (3.13)$$

Here, the uncertainty of the position of the measurement point in the y -direction, Δy , was $\pm 0.025\text{mm}$.

In the current investigation, variations of the non-dimensional ambient temperature outside of the thermal boundary layer with height for the different top wall temperatures were studied. The uncertainty in the temperature gradient $\frac{d\theta_\infty}{d(y/H)}$ is given by

$$\frac{\Delta\left[\frac{d\theta_\infty}{d(y/H)}\right]}{\frac{d\theta_\infty}{d(y/H)}} = \sqrt{\frac{(\Delta\theta_{\infty,2}^2 + \Delta\theta_{\infty,1}^2)}{(\theta_{\infty,2} - \theta_{\infty,1})^2} + \frac{(\Delta y_2^2 + \Delta y_1^2)}{(y_2 - y_1)^2}}. \quad (3.14)$$

Here the non-dimensional ambient temperature outside of the thermal boundary layer was defined as $\theta_\infty = (T_\infty - T_C)/(T_H - T_C)$. In all measured heights, the variation of θ_∞ is less than 3%, except for the region with the undulating flow.

The uncertainties in the local heat flux $\frac{\Delta q''}{q''}$, local heat transfer coefficient $\frac{\Delta h}{h}$, local Nusselt number $\frac{\Delta Nu}{Nu}$, local Rayleigh number $\frac{\Delta Ra}{Ra}$ and the temperature gradient $\frac{\Delta[d\theta_\infty/d(y/H)]}{d\theta_\infty/d(y/H)}$ are summarized in Table 3.1.

Table 3.1: Summary of the uncertainties in the local heat flux, local heat transfer coefficient, local Nusselt number, local Rayleigh number and temperature gradient.

Uncertainties of the	Range of uncertainties
local heat flux, $\frac{\Delta q''}{q''}$	$\pm 4\% - \pm 5\%$
local heat transfer coefficient, $\frac{\Delta h}{h}$	$\pm 6\% - \pm 10\%$
local Nusselt number, $\frac{\Delta Nu}{Nu}$	$\pm 6\% - \pm 10\%$
local Rayleigh number, $\frac{\Delta Ra}{Ra}$	$\pm 4\% - \pm 9\%$
temperature gradient, $\frac{\Delta[d\theta_\infty/d(y/H)]}{d\theta_\infty/d(y/H)}$	$\pm 3\% - \pm 8\%$

Chapter 4

The effect of the top wall temperature on the laminar natural convection in rectangular cavities with smooth walls

The laminar natural convection in air-filled rectangular cavities with smooth walls was examined for different top wall temperatures. The average non-dimensional top wall temperature, $\theta_T = (T_T - T_C)/(T_H - T_C)$, was in the range of approximately 0.52 to 2.3. In the current investigation, this temperature range can be divided into two regions: $\theta_T \lesssim 1.2$ defined as a modest top wall temperature here and $\theta_T \gtrsim 1.2$ defined as a large top wall temperature here. The average temperatures of the vertical walls on the two sides of the cavities were maintained at approximately uniform but different temperatures. The global Grashof number based on the height of the cavity, Gr_H , given by

$$Gr_H = \frac{g\beta(T_H - T_C)H^3}{\nu^2}, \quad (4.1)$$

was maintained approximately the same for all the different cases. Here T_H and T_C are the average temperatures of the vertical walls in the cavity, and β and ν are the volume expansion coefficient and thermal diffusivity of the air at $(T_H + T_C)/2$. The results for the modest top wall temperature are presented first, followed by those for a large top wall temperature. Finally, the effect of a large top wall temperature on the natural convection in rectangular cavities with aspect ratios of 0.5, 1.0 and 2.0 are presented and discussed.

4.1 The effect of a modest top wall temperature

The laminar natural convection in rectangular cavities with aspect ratios of 0.5, 1.0 and 2.0 was initially investigated by maintaining the vertical walls at approximately 82°C and 15°C , respectively, so the global Grashof number based on the height of the cavities, Gr_H , was approximately 1.8×10^8 . The bottom wall temperature for all three cavities was maintained at approximately 15°C and the top wall was insulated with an average temperature of approximately 52°C , corresponding to a non-dimensional top wall temperature of approximately 0.52. The non-dimensional temperature profiles at different heights along the heated vertical wall of the three cavities and the flow patterns in the upper left corner for the cavities are shown in Figure 4.1. There is a thin thermal boundary layer along the heated vertical wall that grows in thickness as the flow travels up the wall, as expected. The temperature profiles outside of the boundary layer region were approximately uniform indicating there was not a significant natural convection flow outside of this thermal boundary layer. The temperature in the region away from the heated vertical wall increases with height. Thus, most of the air in the cavity was stably stratified, reducing the local buoyancy force acting on the flow in the boundary layer as it travels up the heated vertical wall.

The temperature profiles between $y/H = 0.5$ and $y/H = 0.8$ had an undershoot in the region near the edge of the boundary layer, where the local temperature fell below the local ambient temperature in the region away from the heated vertical wall. A similar undershoot was observed by Tian and Karayiannis [6] in their temperature profiles measured for the natural convection air flow in a square cavity with a global Grashof number of 2.22×10^9 . Cheesewright [49] indicated that this occurred in natural convection boundary layers in non-isothermal surroundings since the heat flux to the fluid in the outer region of the boundary layer was not sufficient to change its temperature as quickly as the temperature outside the boundary layer.

For the three cavities with the insulated top wall, at a given height, the non-dimensional temperature distributions in the region away from the heated vertical wall generally increased with an increase in the aspect ratio, particularly in the region $y/H > 0.5$. Since the top wall of the cavities was insulated, the temperature of the convection flow moving along the top wall was larger than the top wall temperature, resulting in an energy transfer into the horizontal walls and the cooled vertical wall from the air flow. With an increase of the aspect ratio, the total area of these walls becomes smaller so less heat was transferred into the walls.

There is some evidence of secondary flow outside the boundary layers along the heated vertical wall and the top wall in the flow visualizations in the upper left corner of the three cavities (Figure 4.1). This was also reported by Tian and Karayiannis [6]. In this case, this evidence is not very apparent due to the inability of the laser sheet to properly illuminate this region but was visible to the naked eye. A schematic of the flow pattern of the secondary flow in the corner region of the square cavity is shown in Figure 4.2. The mixing caused by this secondary flow would likely be the cause for the temperature distributions just outside the boundary layer at $y/H = 0.8$ and 0.9 to be approximately constant. For the most part, however, the flow in the

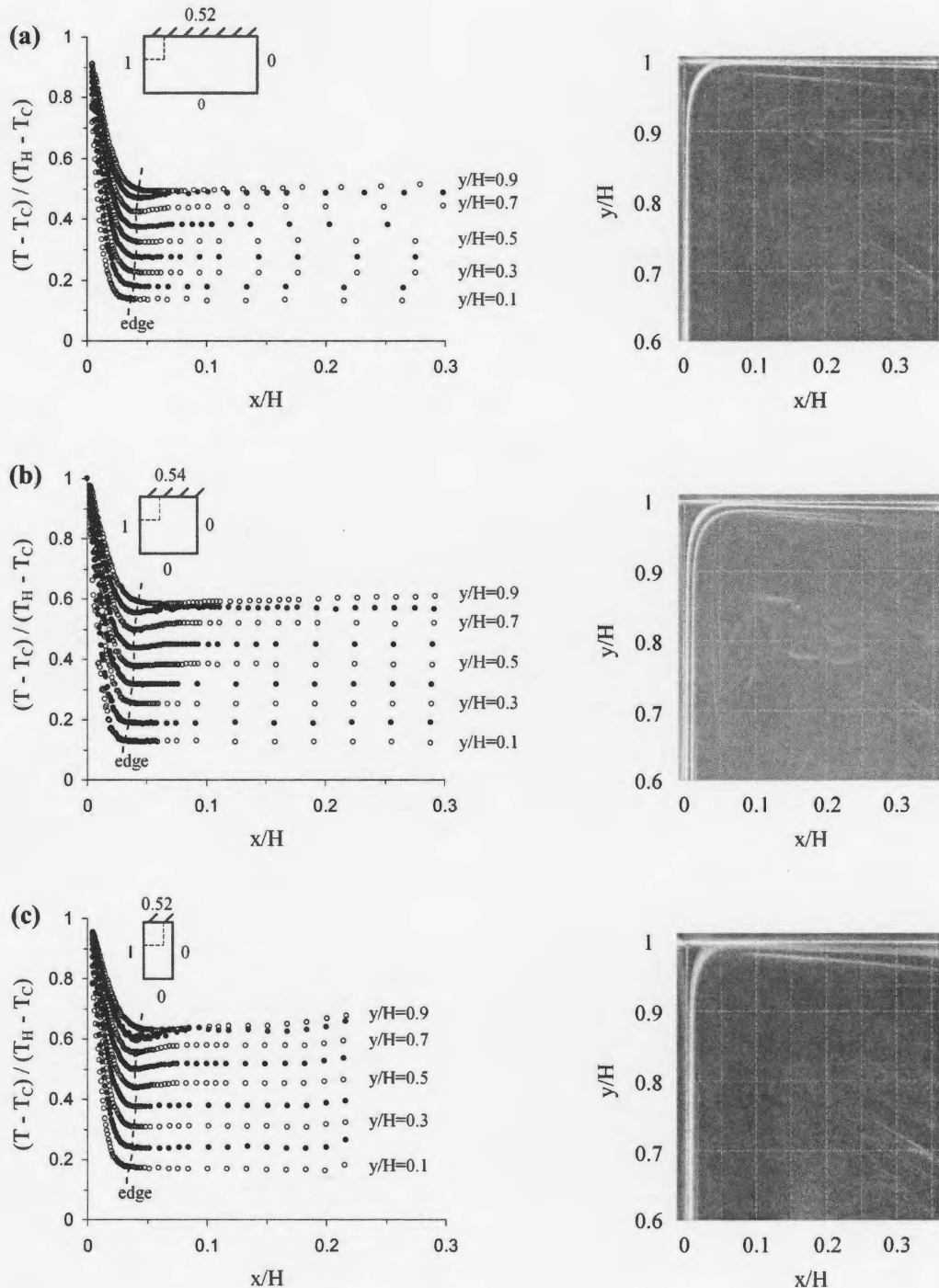


Figure 4.1: Non-dimensional temperature profiles in cavities (Left) and flow patterns in the upper left corner region (Right) for cases with aspect ratios of (a) 0.5, (b) 1.0 and (c) 2.0 for non-dimensional top wall temperatures of approximately 0.52 (insulated). Here, open and filled symbols were used to distinguish the temperature distributions at the different heights.

three cavities moves along the wall, and seems to travel around the corner without any evidence of separation. Ravi et al. [17] also noted that the air bounded by the boundary layer flow was stratified in a square cavity with an insulated top wall. However, they observed there was a thickening of the boundary layer on the top wall after the flow traveled around the corner, and this difference may be due to differences in the temperature of the 'insulated' top wall.

The effect that the top wall temperature had on the laminar natural convection flow in these cavities was investigated further by performing measurements for three additional cases with non-dimensional top wall temperatures of approximately 0.83, 1 and 1.14. The non-dimensional temperatures of the vertical walls and the bottom wall were maintained as for the previous case so that the global Grashof numbers Gr_H in these cases were approximately the same. Thus, the thermal boundary conditions of the vertical walls in the different cases were approximately the same. The experimental conditions are summarized in Table 4.1, and the temperature profiles along the heated vertical walls with the corresponding flow images in the top corners are presented in Figures 4.3, 4.4 and 4.5. A typical schematic of the flow pattern in the upper left corner region of the rectangular cavity with the aspect ratio of 0.5 and non-dimensional top wall temperature of approximately 1 is shown in Figure 4.6. In all cases, there is a thin thermal boundary layer along the heated vertical wall, but the temperature profiles near the top of the cavities and the natural convection flow patterns along the top wall changed as the temperature of the top wall was increased. When the top wall of the cavities were heated, the temperature of the air in the region far from the heated vertical wall near the top wall was not uniform and increased significantly. In these cases, the flow separated from the top wall near the corner due to the formation of a negatively buoyant plume as indicated by Ravi et al. [17]. This causes a secondary flow in the region between the separated flow

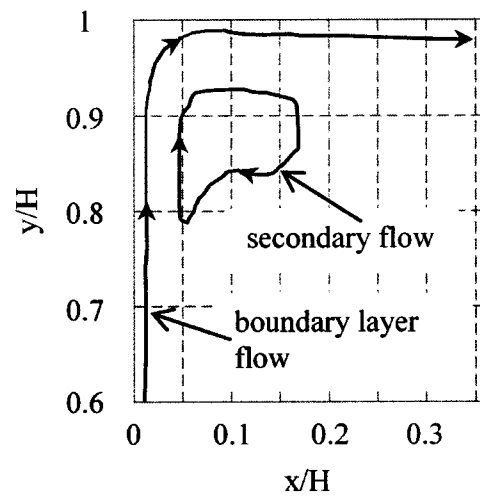


Figure 4.2: A schematic of the flow pattern in the upper left corner region of the square cavity with the non-dimensional top wall temperature of approximately 0.54 (insulated).

on the top wall and the boundary layer on the heated vertical wall, which is shown schematically in Figure 4.6. The secondary flow results in the temperature distributions in this region ($0.07 \lesssim x/H \lesssim 0.12$) to be relatively uniform, in particular for the case with a higher top wall temperature as shown in Figure 4.5. There was a good correspondence between the variation of the temperature profiles and the flow visualization near the top of the cavity. Thus, it suggests that the non-uniformity in the temperature profiles is a direct result of the flow field. When the non-dimensional top wall temperature was approximately 0.83, the temperature profiles at $y/H = 0.8$ and 0.9 became non-uniform beyond $x/L = 0.15$. This corresponded to the separated flow region observed near the top wall in this case. For a given cavity, the non-uniformity in the temperature profiles near the top of the cavity and the separated flow region on the top wall moved toward the heated vertical wall as the non-dimensional top wall temperature was increased from approximately 0.83 to 1.14. The secondary flow formed between the separated flow on the top wall and the boundary layer on the heated vertical wall was reduced in width as the temperature of the top wall increased. This change affected the temperature distributions in the secondary flow just outside of the boundary layer at $y/H = 0.8$ and 0.9. In particular, the temperature in this region increased slightly with height for the smaller top wall temperature, but was approximately constant for the larger temperature, most likely because the secondary flow is stronger when the separated flow is closer to the heated vertical wall. The location of the separated flow region changed with the top wall temperature, but was nearly independent of the aspect ratio of the cavities.

Variation of the non-dimensional local ambient temperature outside the boundary layer with height for the different top wall temperatures are shown in Figure 4.7. The temperature in the region far from the heated vertical wall, i.e. $x/H \gtrsim 0.1$, was used as the local ambient temperature outside the boundary layer. In all three cav-

Table 4.1: Summary of the wall temperatures, global Grashof numbers, and parameters in the correlation $Nu = C \cdot Ra^n$ for cases with modest top wall temperatures.

AR	Case	T_H (°C)	T_C (°C)	T_T (°C)	T_B (°C)	θ_H	θ_C	θ_T	θ_B	$Gr_H \times 10^{-8}$	n	C
0.5	1	81	14	49	14	1	0	0.52	0	1.86	0.36	0.071
				(insulated)								
	2	81	16	70	16	1	0	0.83	0	1.78	0.36	0.08
	3	81	16	81	16	1	0	1	0	1.78	0.36	0.082
	4	84	20	93	20	1	0	1.14	0	1.67	0.36	0.085
1.0	1	83	16	52	16	1	0	0.54	0	1.81	0.32	0.15
				(insulated)								
	2	83	13	71	12	1	0	0.83	0	1.93	0.32	0.16
	3	80	13	79	13	1	0	0.99	0	1.88	0.32	0.165
	4	80	13	89	13	1	0	1.13	0	1.88	0.32	0.185
2.0	1	90	21	57	21	1	0	0.52	0	1.71	0.37	0.072
				(insulated)								
	2	87	19	75	19	1	0	0.82	0	1.75	0.37	0.074
	3	83	17	83	17	1	0	1	0	1.77	0.37	0.076
	4	84	16	94	16	1	0	1.15	0	1.82	0.37	0.074

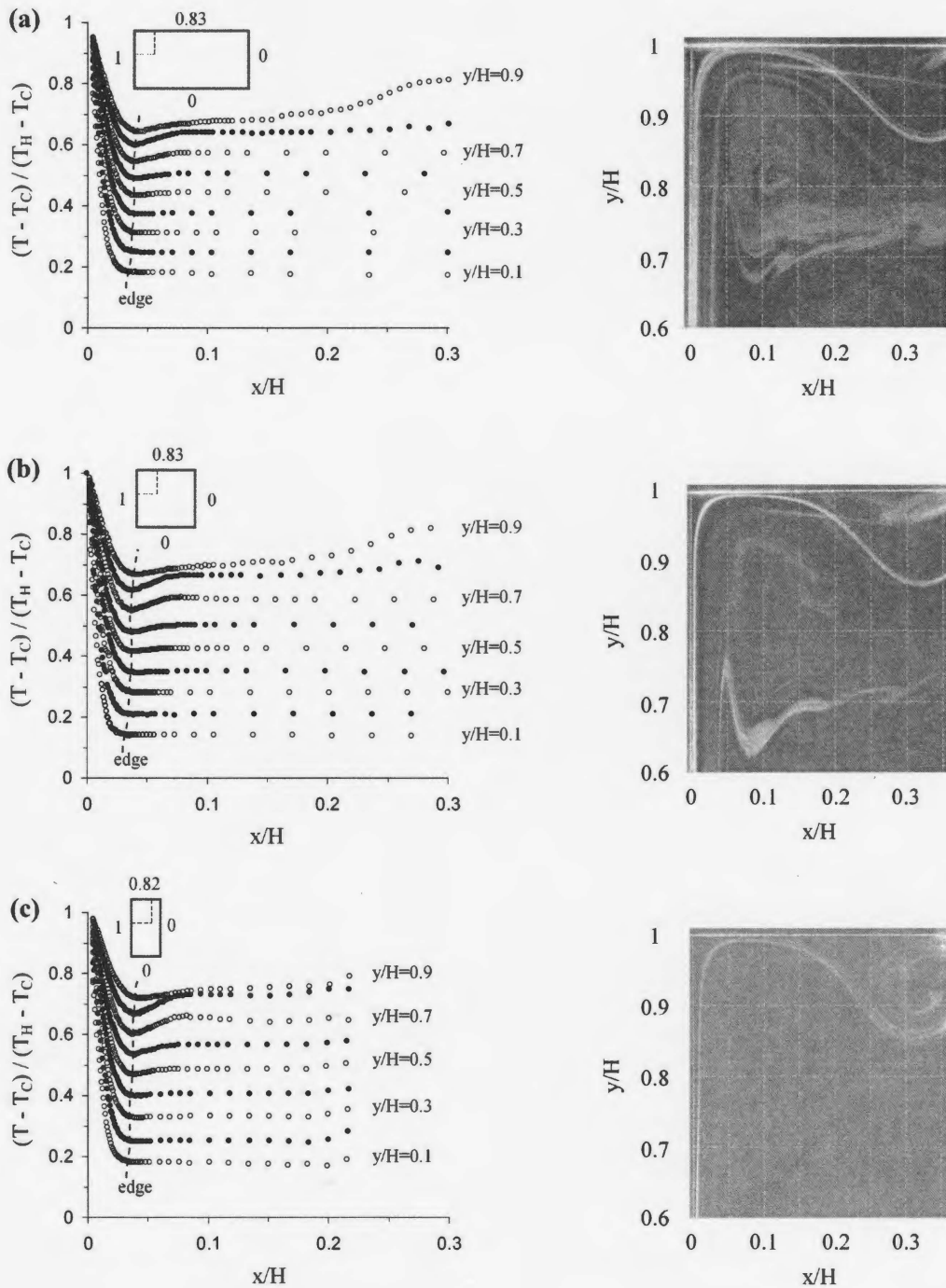


Figure 4.3: Non-dimensional temperature profiles in cavities (Left) and flow patterns in the upper left corner region (Right) for cases with aspect ratios of (a) 0.5, (b) 1.0 and (c) 2.0 for non-dimensional top wall temperatures of approximately 0.83. Here, open and filled symbols were used to distinguish the temperature distributions at the different heights.

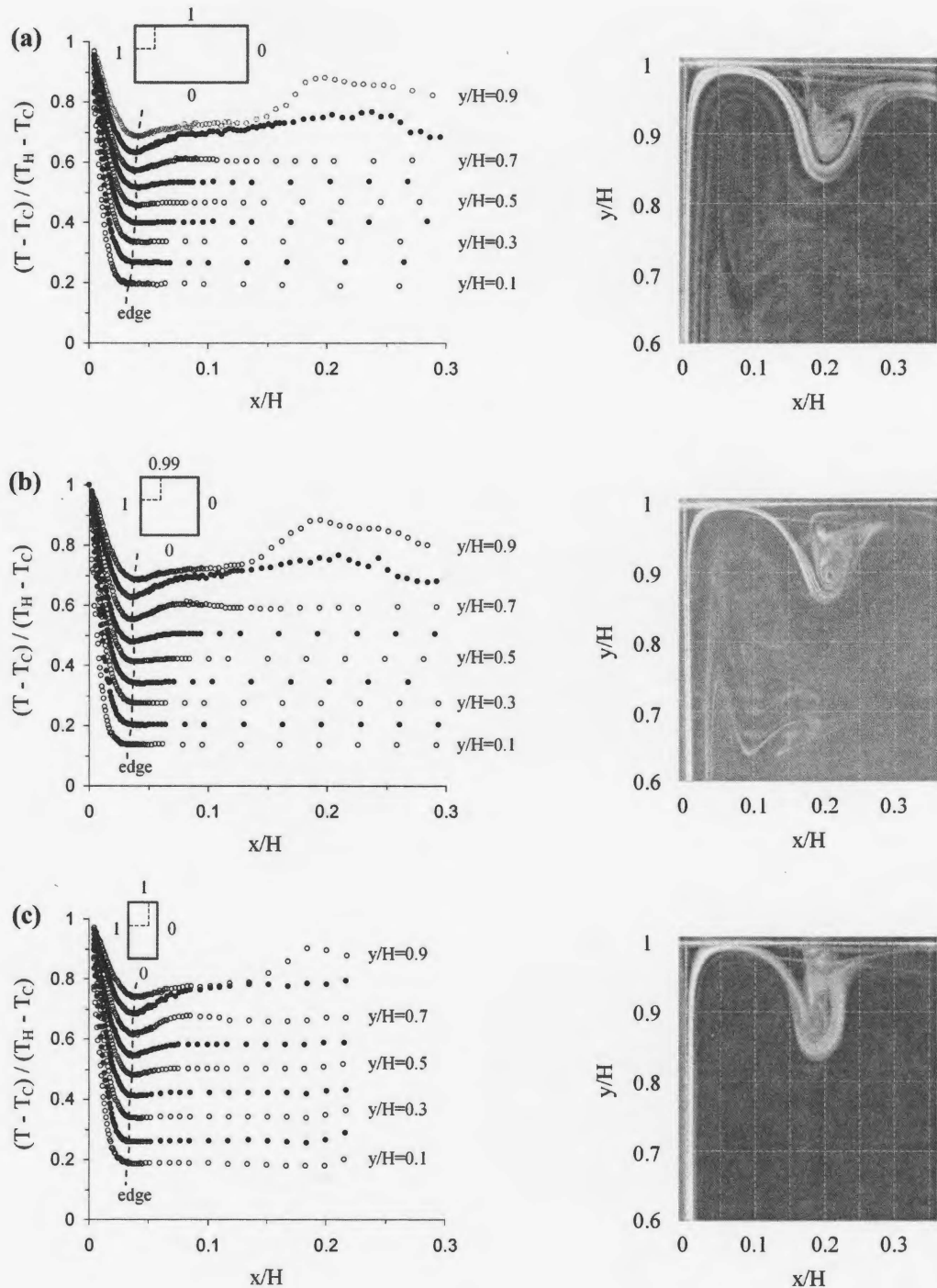


Figure 4.4: Non-dimensional temperature profiles in cavities (Left) and flow patterns in the upper left corner region (Right) for cases with aspect ratios of (a) 0.5, (b) 1.0 and (c) 2.0 for non-dimensional top wall temperatures of approximately 1. Here, open and filled symbols were used to distinguish the temperature distributions at the different heights.

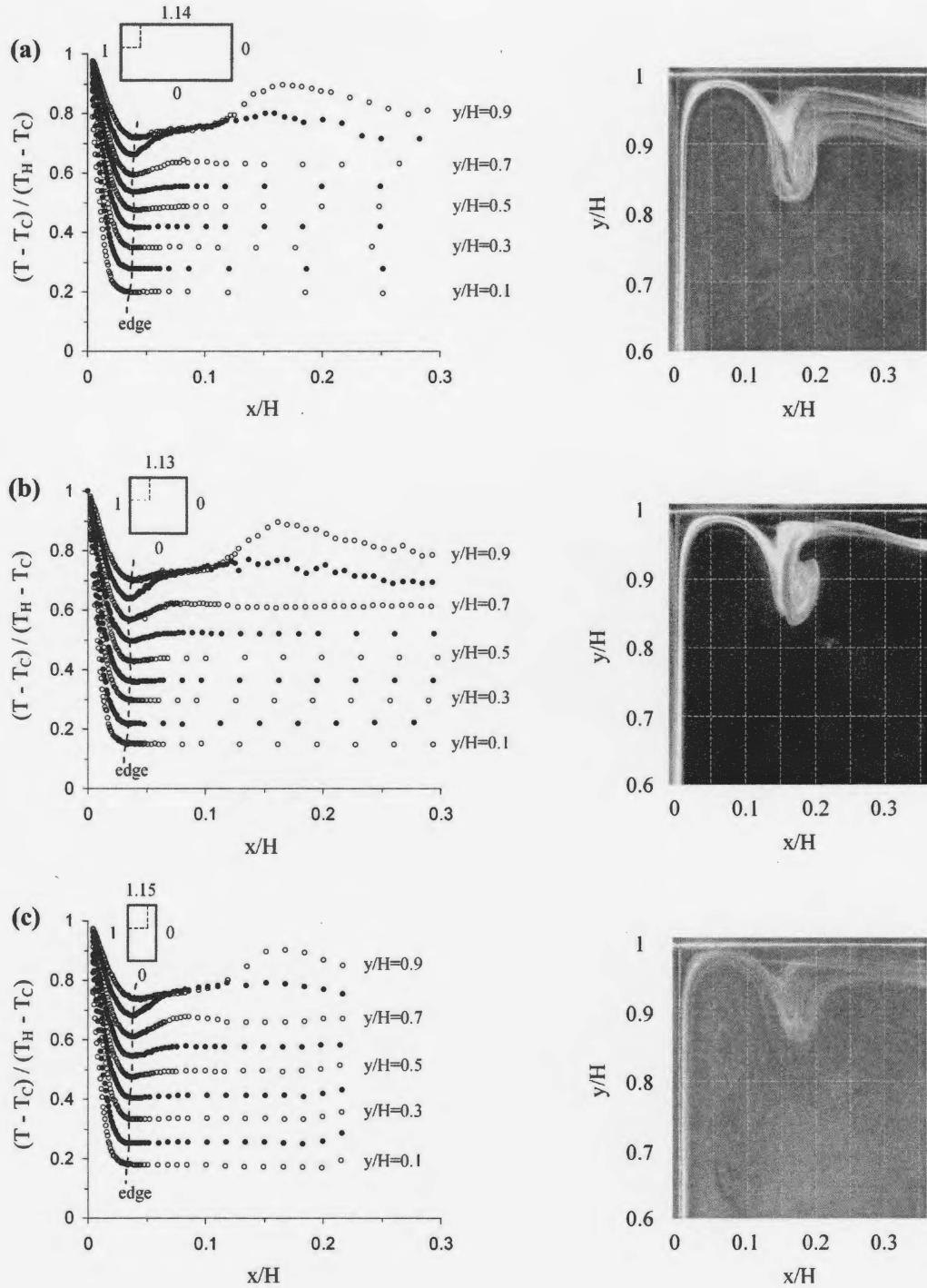


Figure 4.5: Non-dimensional temperature profiles in cavities (Left) and flow patterns in the upper left corner region (Right) for cases with aspect ratios of (a) 0.5, (b) 1.0 and (c) 2.0 for non-dimensional top wall temperatures of approximately 1.14. Here, open and filled symbols were used to distinguish the temperature distributions at the different heights.

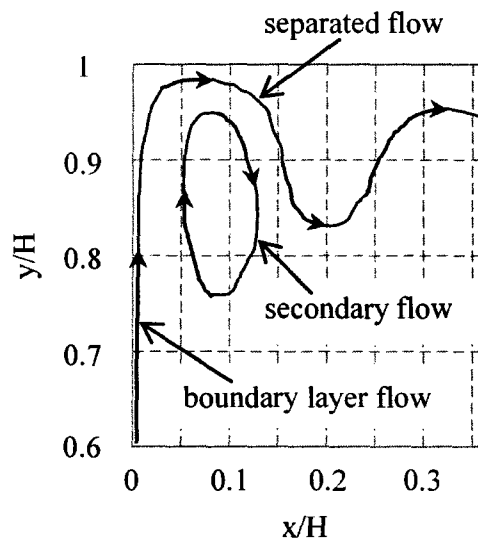


Figure 4.6: A typical schematic of the flow pattern in the upper left corner region of the rectangular cavity with the aspect ratio of 0.5 and non-dimensional top wall temperature of approximately 1.

ities, the ambient temperature outside the boundary layer increased approximately linearly with the height over most of the cavity. The exception was near the top wall ($y/H > 0.8$) when it was heated. Under these thermal boundary conditions, the separated flow near the top wall affected the temperature field in the region $y/H > 0.8$ as shown in the flow visualizations and temperature profiles. With an increase of the top wall temperature, the local ambient temperature outside the boundary layer increased as expected. For the cases with the heated top wall, the sensitivity of the local ambient temperature to the top wall temperature decreased with an increase of the aspect ratio. The local ambient temperature was determined by the temperature of the edge of the natural convection flow along the top and bottom walls. In the cases with the heated top wall, the energy was transferred from the top wall into the flow. The surface of the top wall, along which the natural convection flow moved, and the top wall temperature are two main parameters that affect the temperature of the edge of the natural convection flow along the top wall. For the cavity with aspect ratio of 2.0, the flow separation on the top wall resulted in the contact area between the top wall and the flow along the wall to be small, so less energy was transferred into the flow. As a result, the local ambient temperature was insensitive to the change in the top wall temperature. For the 1.0 aspect ratio cavity with non-dimensional top wall temperatures of 0.83 and 1, the temperature difference between the top wall and the edge of the natural convection flow along the wall was not significant, resulting in less heat transfer into the air flow. Thus, the difference of the local ambient temperatures under these two top wall temperatures was generally less than 3%.

The change in the temperature gradient $d\theta_\infty/d(y/H)$, from a linear fit to the data between $y/H = 0.1$ and 0.7, with the change in the top wall temperature is shown in Figure 4.8. For all three cavities, the temperature gradient increased with an increase of the top wall temperature. The increase in the temperature gradient

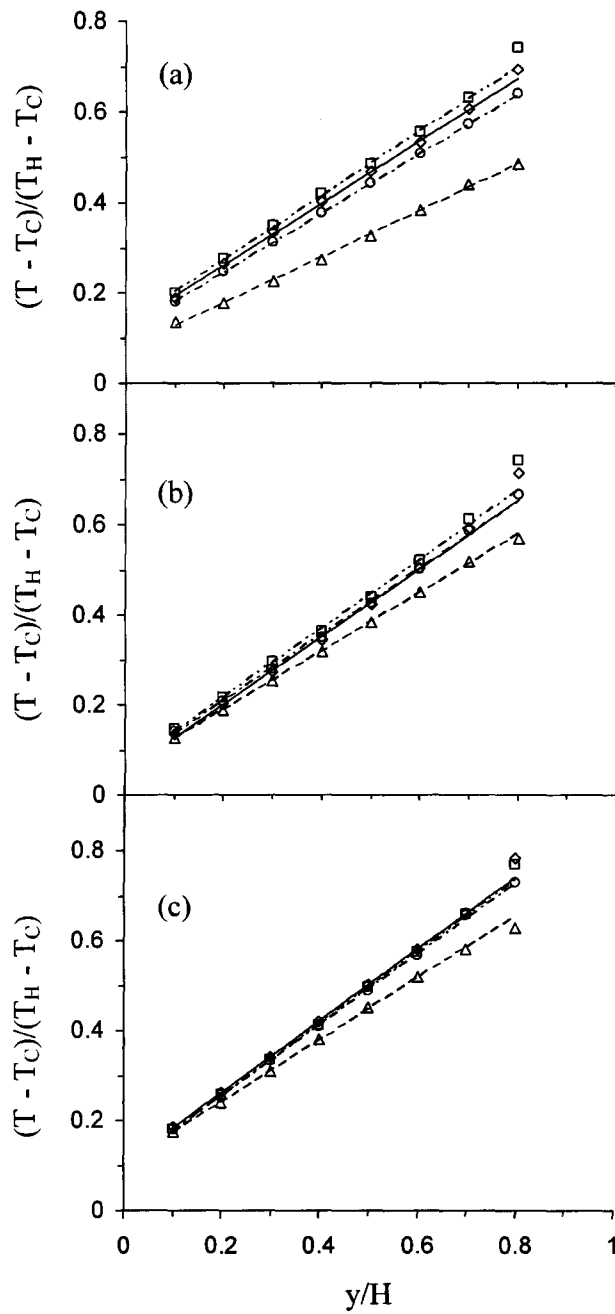


Figure 4.7: Comparison of the non-dimensional local ambient temperature outside the boundary layer for cases with aspect ratios of (a) 0.5, (b) 1.0 and (c) 2.0. Here the non-dimensional top wall temperatures were Δ :0.52 (insulated), \circ :0.83, \diamond :1 and \square :1.14.

$d\theta_{\infty}/d(y/H)$ was more significant for the smaller aspect ratio. This difference may be due to the change in the ratio of the size of the separated flow region to the cavity width for the different aspect ratios. For the 0.5 aspect ratio cavity, this ratio is approximately 0.1, so the local ambient temperature outside the boundary layer is significantly affected by the convection flow moving along the top wall, which is sensitive to the change in the top wall temperature. However, for the higher aspect ratio cavity, the ratio of the size of the separated flow region to the cavity width increased to around 0.4. In this case, the local ambient temperature outside the boundary layer is to a large extent determined by the temperature of the separated flow, which is more sensitive to the heated vertical wall temperature than the top wall temperature.

The local heat flux from the heated vertical wall, q'' (determined from the temperature gradient at the wall) for the three cavities under the different top wall temperatures is shown in Figure 4.9. As expected, the local heat flux into the cavity from the heated vertical wall decreased as the flow developed along the wall. The change in the top wall temperature had a greater effect on the local heat transfer near the top of the heated vertical wall, which was more significant for the cavity with the aspect ratio of 0.5. For example, when the non-dimensional top wall temperature was increased from approximately 0.52 to 1.14, the local heat flux near the top of the heated vertical wall decreased by approximately 43% in the 0.5 aspect ratio cavity, while it decreased by approximately 26% in the 2.0 aspect ratio cavity. As the top wall was heated, the local heat flux near the top of the heated vertical wall decreased due to the change in the flow pattern in this region. The change in the local heat flux with the temperature of the heated top wall was dependent on the aspect ratio. This can be attributed to the sensitivity of the local ambient temperatures to the top wall temperature, which decreased with an increase of the aspect ratio.

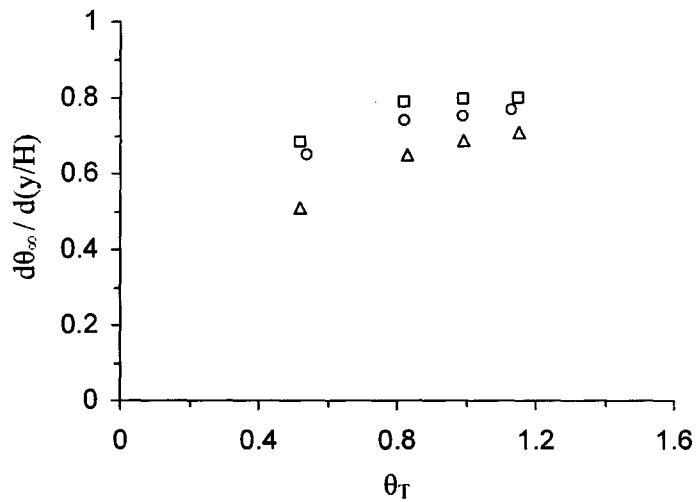


Figure 4.8: Change in the vertical gradient of the temperature outside the boundary layer on the heated vertical wall with the change in the top wall temperature for cases with aspect ratios of Δ :0.5, \circ :1.0 and \square :2.0.

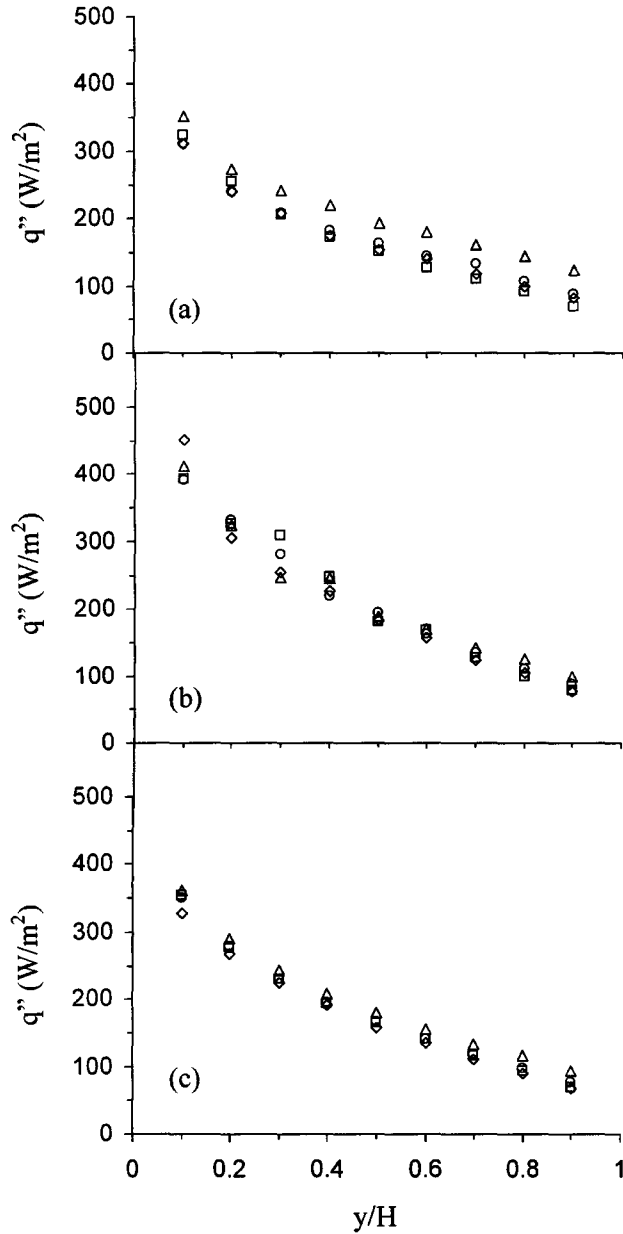


Figure 4.9: Comparison of the local heat flux along the heated vertical wall of cavities with aspect ratios of (a)0.5, (b) 1.0 and (c) 2.0. Here the non-dimensional top wall temperatures were \triangle : 0.52 (insulated), \circ : 0.83, \diamond : 1 and \square : 1.14.

The change in the local Nusselt number with the local Rayleigh number for the three cavities is shown in Figure 4.10. The local Rayleigh numbers along the heated vertical wall of the cavities for non-dimensional heights from $y/H = 0.1$ to 0.9 varied from 8.6×10^4 to 3.8×10^7 . These are well below the critical value for transition from laminar to turbulent flow, suggesting the flow is laminar. This was supported by the flow visualizations which clearly showed a laminar boundary layer along the heated vertical wall. It was found that the data over most of the heated vertical wall could be correlated by $Nu = C \cdot Ra^n$, except for $y/H \geq 0.8$ and $y/H \leq 0.1$. In the region $y/H = 0.2$ to 0.7 , the curve fit is well within the experimental uncertainty. Typical results with error bars for the case with a non-dimensional top wall temperature of approximately 1 are shown in Figure 4.11. When the top wall temperature was increased, there is a significant increase in the Nusselt number at $y/H = 0.8$. This is likely due to the secondary flow between the separated flow on the top wall and the boundary layer on the heated vertical wall. The values of the constant C and the index n were different for the different aspect ratios and are given in Table 4.1. For the cavities with aspect ratios of 0.5 and 1.0, the value of C increased with an increase of the top wall temperature, while there was no significant change in C with the top wall temperature for the 2.0 aspect ratio cavity. The values of the index n in the correlations for the three rectangular cavities are significantly different from that in the case with an isothermal vertical wall in either isothermal or non-isothermal surroundings. For example, Incropera and Dewitt [102] studied the natural convection from an isothermal vertical wall immersed in an isothermal quiescent medium and expressed the local Nusselt number of the air flow as

$$Nu = 0.386 \cdot Ra^{\frac{1}{4}}. \quad (4.2)$$

Cheesewright [49] and Chen and Eichhorn [2] investigated the steady natural convection from an isothermal vertical surface to a thermally stratified fluid and found that

$$Nu \sim Ra^{\frac{1}{4}} \cdot Pr^{-\frac{1}{4}}. \quad (4.3)$$

This discrepancy is due to the top and bottom walls of the cavity. The presence of these walls resulted in a change in the stratification rate of the fluid outside the boundary layer, that, in turn, caused the local buoyancy force and then the vertical momentum of the upward boundary layer flow along the heated vertical wall to be changed.

4.2 The effect of a large top wall temperature

Heretofore, the natural convection flow in rectangular cavities under large top wall temperatures has not been investigated experimentally. In this section, the results for a large top wall temperature are presented and discussed for the square cavity. The numerical study by Shiralkar and Tien [16] suggested that the vertical boundary layer flow along the heated vertical wall of a square cavity separated near the upper left corner before reaching the top wall when the temperature of the top wall was much larger than the heated vertical wall. In particular, the flow formed a recirculating region near the corner when the temperature difference in the vertical direction was five times that in the horizontal direction. These results were significantly different from those obtained in rectangular cavities with modest top wall temperatures. For this study, in order to obtain a larger non-dimensional top wall temperature, the average temperatures of the vertical walls on the two sides of the cavity were adjusted to approximately $46^{\circ}C$ and $9^{\circ}C$, respectively, corresponding to a global Grashof number

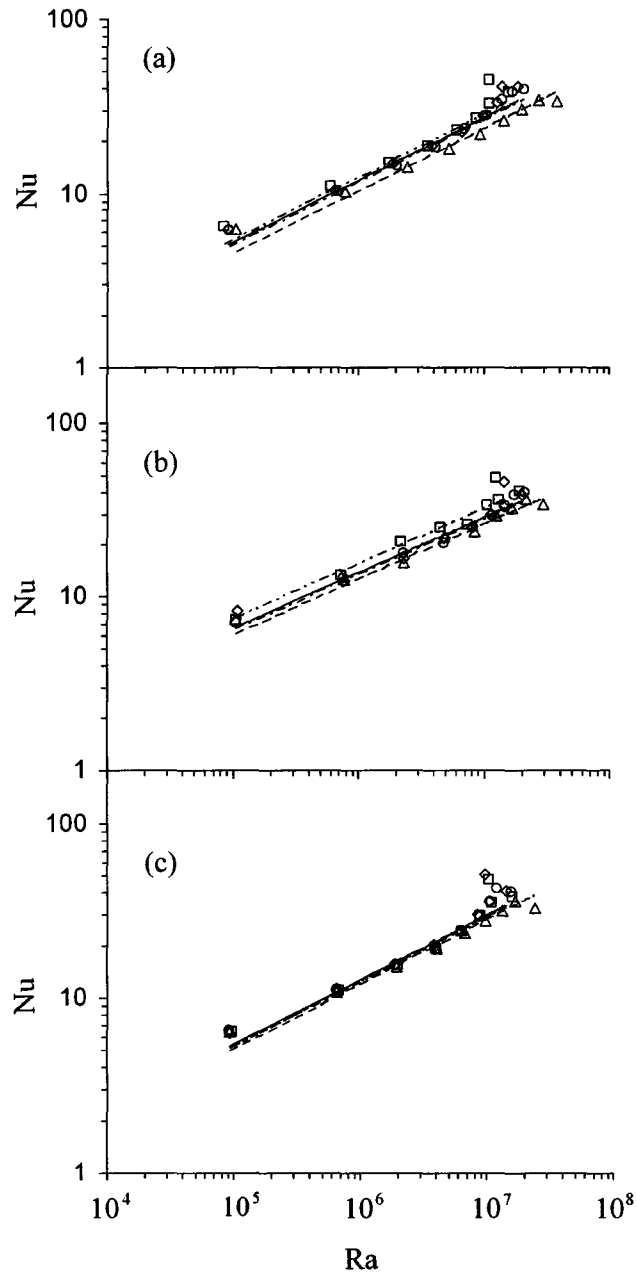


Figure 4.10: Change in the local Nusselt number with the local Rayleigh number for cases with aspect ratios of (a) 0.5, (b) 1.0 and (c) 2.0. Here the non-dimensional top wall temperatures were \triangle : 0.52 (insulated), \circ : 0.83, \diamond : 1 and \square : 1.14.

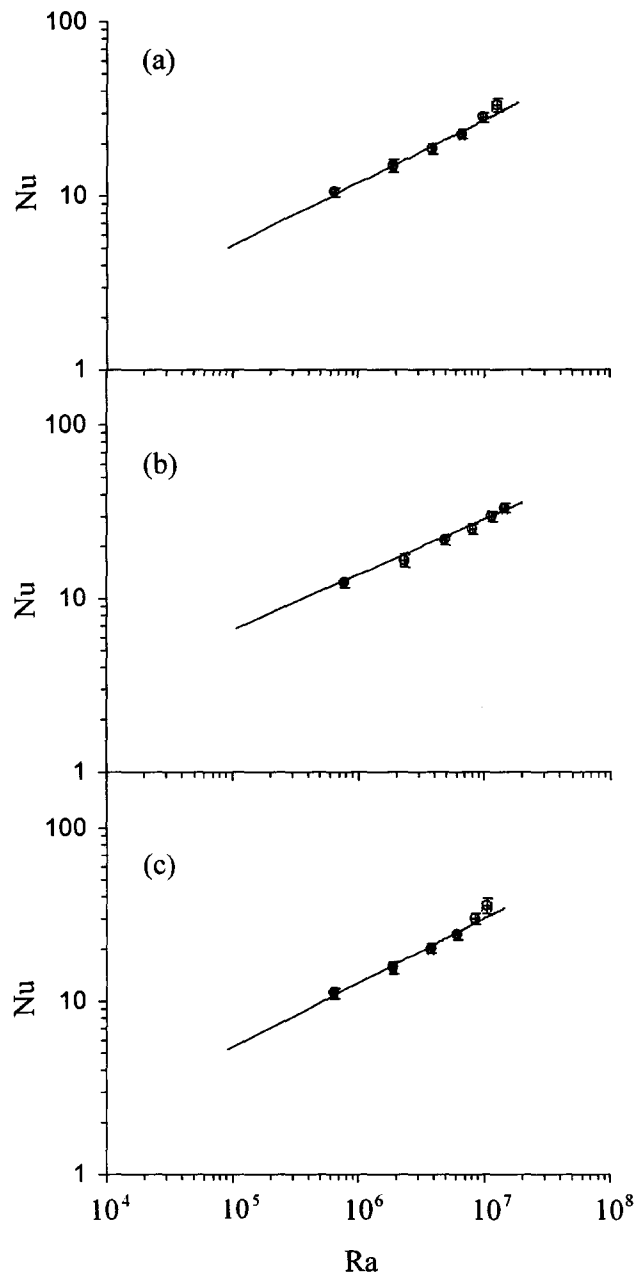


Figure 4.11: Change in the local Nusselt number with the local Rayleigh number for the case with a non-dimensional top wall temperature of approximately 1. Here the error bars for local Nusselt numbers and local Rayleigh numbers are, respectively, set to (a) $\pm 6 - 9\%$ and $\pm 4 - 8\%$ for aspect ratio of 0.5, (b) $\pm 6 - 9\%$ and $\pm 4 - 6\%$ for aspect ratio of 1.0 and (c) $\pm 6 - 10\%$ and $\pm 4 - 9\%$ for aspect ratio of 2.0.

Gr_H of approximately 1.4×10^8 . The bottom wall temperature was maintained at approximately $9^\circ C$ while the average top wall temperature was varied from $63^\circ C$ to $102^\circ C$, corresponding to non-dimensional top wall temperatures of 1.4 to 2.3. The detailed experimental conditions are given in Table 4.2.

The flow patterns and the temperature contours in the upper left quarter of the square cavity for non-dimensional top wall temperatures of approximately 1.4, 1.9 and 2.3 are shown in Figure 4.12. A typical schematic of the flow pattern is shown in Figure 4.13. The temperature contours were generated from the measured temperature profiles using a commercial software package. The results show that the natural convection boundary layer flow travelling along the heated vertical wall separates from the wall before reaching the top wall. It is difficult to accurately determine the separation point without quantitative velocity measurements in the near-wall region. However, for this study, it was estimated from the flow visualizations as the point where the upward flow first leaves the vertical wall. The temperature contours provide similar flow field information as the flow visualization, since once the flow separates the convective effects will dominate the diffusive effects. As a result of the flow separation, there is a recirculating flow region between the separated flow and the heated vertical wall, similar to the numerical results of Shiralkar and Tien [16]. Here, the flow attaches to the top wall at approximately $x/H = 0.3$ for all the three cases. In Shiralkar and Tien [16], they did not report the location where the natural convection flow reattached to the wall. Two images for the non-dimensional top wall temperature of 2.3 taken approximately 4 hours apart are shown in Figure 4.14. This figure shows that the flow is steady and there is no significant temporal variability in the flow. The temperature contours show that the core region of the cavity is moderately stratified. There is, however, a highly stratified region above the natural convection boundary layer flow after it separates from the vertical wall. In this highly

Table 4.2: Summary of the wall temperatures, global Grashof numbers, and parameters in the correlation $Nu = C \cdot Ra^n$ for cases with large top wall temperatures.

AR	Case	T_H (°C)	T_C (°C)	T_T (°C)	T_B (°C)	θ_H	θ_C	θ_T	θ_B	$Gr_H \times 10^{-8}$	n	C
	1	43	9	57	9	1	0	1.41	0	1.29	0.37	0.088
0.5	2	44	10	75	10	1	0	1.91	0	1.27	0.38	0.085
	3	52	12	103	12	1	0	2.28	0	1.39	0.40	0.067
	1	48	10	63	10	1	0	1.39	0	1.38	0.36	0.1
1.0	2	42	9	72	9	1	0	1.91	0	1.26	0.40	0.058
	3	49	8	102	8	1	0	2.29	0	1.50	0.40	0.061
	1	41	8	54	8	1	0	1.39	0	1.28	0.36	0.099
2.0	2	38	8	65	8	1	0	1.90	0	1.20	0.37	0.087
	3	47	9	97	9	1	0	2.32	0	1.40	0.39	0.068

stratified region, there is a downward flow moving along the heated vertical wall due to the recirculating flow in this region. With an increase of the top wall temperature, the region above the natural convection boundary layer after it separates from the vertical wall becomes more stratified, likely resulting in the reduction of the strength of the recirculating flow in this region. The vertical size of the highly stratified region increased with an increase of the top wall temperature. These results are significantly different from those in the cavity with modest top wall temperatures where there was evidence of a natural convection flow separating from the top wall but not a highly stratified region. The results show that the flow undulates in the vertical direction after turning in the horizontal direction, similar to the results in rectangular cavities with the modest top wall temperatures. For the larger top wall temperature examined here, the boundary layer flow passes through its neutral buoyancy point and separates from the vertical wall before reaching the top wall so the undulations occur lower in the cavity. The magnitude of the undulations in the flow after the flow separation becomes smaller when the top wall temperature increases, indicating the flow becomes more stable with an increase of the top wall temperature. This differed from the numerical results of Shiralkar and Tien [16], where there was no evidence of undulations in the flow. In that case, the non-dimensional top wall temperature was three times larger than studied here, likely resulting in a larger stratification above the separated boundary layer flow which suppressed the undulations.

The characteristics of the boundary layer flow along the heated vertical wall of the square cavity are mainly determined by the buoyancy force and the initial vertical momentum in the flow, as well as the shear stress on the vertical wall. The local buoyancy force in the flow can be estimated by analyzing the temperature distributions in the square cavity. The change of the local buoyancy force in the flow

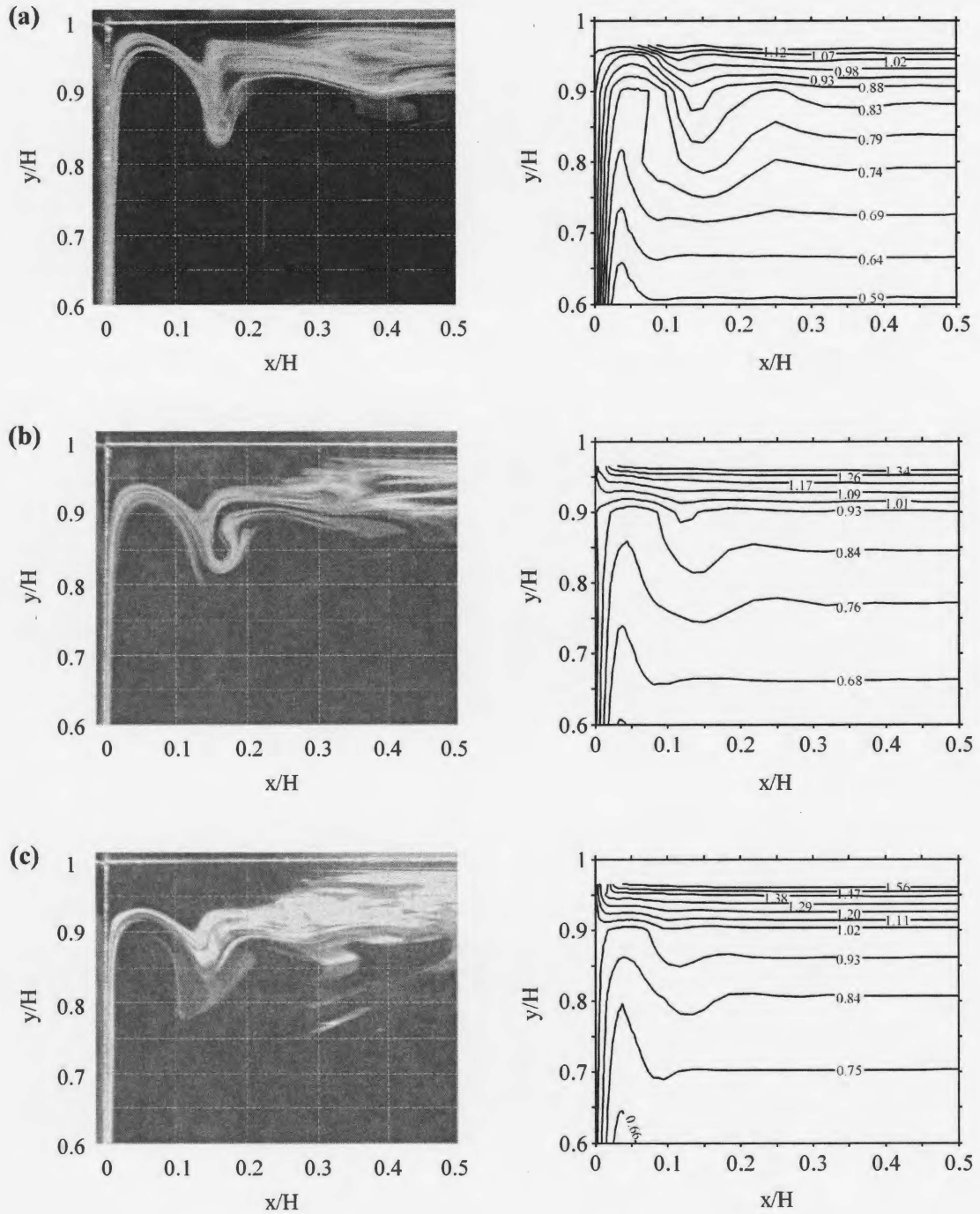


Figure 4.12: Flow patterns (Left) and temperature contours (Right) in the upper left region of the square cavity with non-dimensional top wall temperatures of (a) 1.4, (b) 1.9 and (c) 2.3.

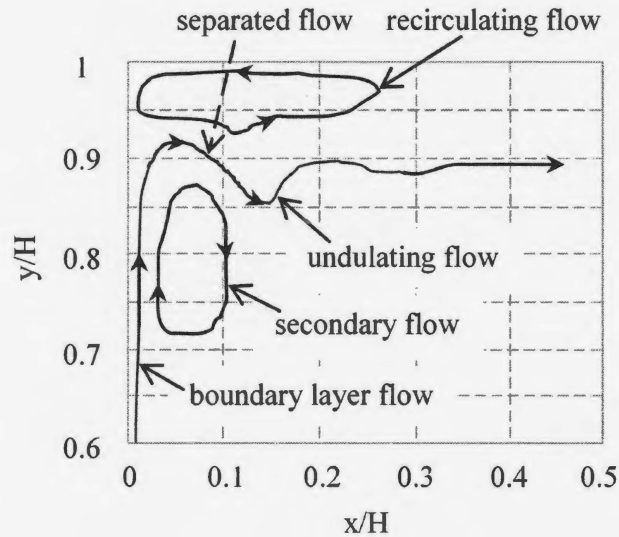


Figure 4.13: A typical schematic of the flow pattern in the upper left corner region of the square cavity with the non-dimensional top wall temperature of 2.3.

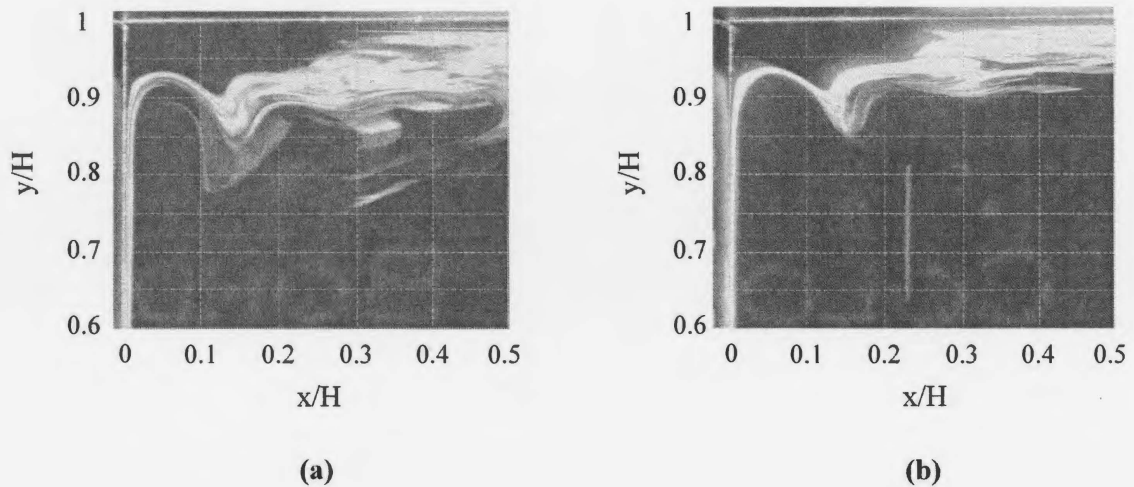


Figure 4.14: Typical flow patterns in the upper left region of the square cavity with non-dimensional top wall temperature of 2.3. The images (a) and (b) were taken approximately 4 hours apart.

along the heated vertical wall given by

$$F_B(y) = \rho_\infty(y) \cdot g \cdot \beta(y) \cdot [T(x, y) - T_\infty(y)] \quad (4.4)$$

for the different cases are shown in Figure 4.15. For clarity, an enlarged view in the region $y/H \geq 0.6$ is shown on the right in this figure. Here, $\rho_\infty(y)$ and $T_\infty(y)$ are the density and temperature of air in the cavity far from the heated vertical wall, and $\beta(y)$ is determined from $T_\infty(y)$. The results show that the local buoyancy force decreases with height due to the increase of T_∞ as expected. There are negative local buoyancy forces above $y/H \approx 0.5$ due to the undershoots in the temperature profiles. The negative buoyancy force became larger near the upper corner suggesting that the boundary layer flow along the vertical wall had passed its neutral buoyancy point. The region of negative buoyancy becomes larger near the top wall, where the upward natural convection boundary layer flow separates from the heated vertical wall, indicating the negative buoyancy force does play a significant role in affecting the upward motion of the boundary layer flow. For the three cases, at $y/H \geq 0.95$, the negative buoyancy force dominated the region. When the non-dimensional top wall temperatures were 1.9 and 2.3, the local buoyancy profiles in this region changed significantly compared to the case with the non-dimensional top wall temperature of 1.4, since the recirculating flow region became larger with the increase of the top wall temperature.

Heretofore, a number of theoretical models have been developed for the natural convection flows on isothermal vertical walls in stratified environments. However, there does not appear to have been any attempts to compare these solutions to experimental results for natural convection of air flows in cavities where there is a stratified core region. In order to examine if these models can accurately predict

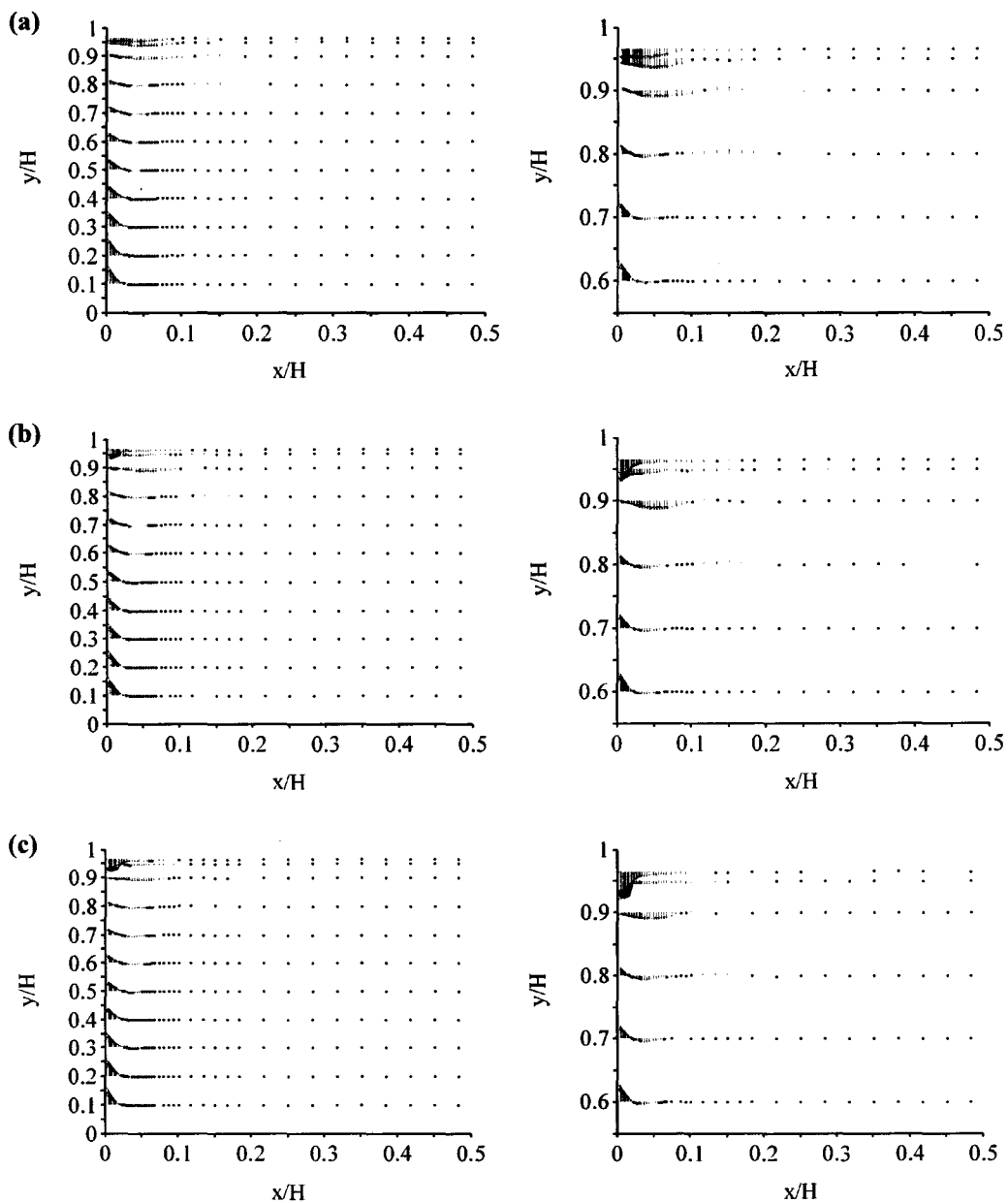


Figure 4.15: Changes in the local buoyancy force distributions along the heated vertical wall (Left) with an enlarged view in the corner region (Right) for non-dimensional top wall temperatures of (a) 1.4, (b) 1.9 and (c) 2.3.

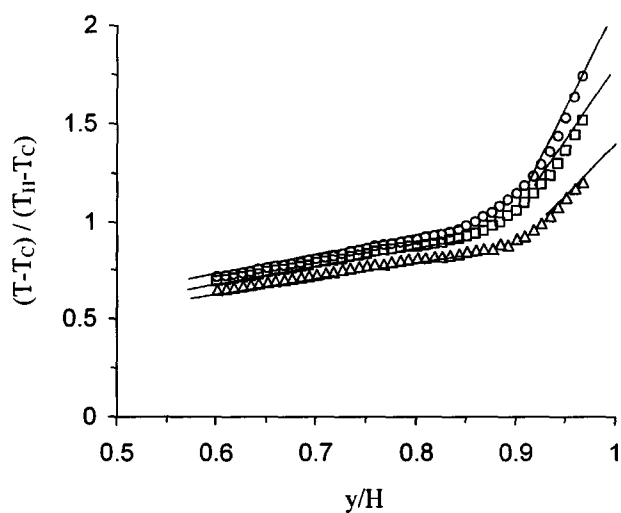


Figure 4.16: Comparison of the non-dimensional temperature distributions at $x/H = 0.25$ for the square cavity with non-dimensional top wall temperatures of Δ : 1.4, \square : 1.9 and \circ : 2.3.

the characteristics of the natural convection air flow in a square cavity, the current measurements along the heated vertical wall were compared to the similarity solution proposed by Kulkarni et al.[1] and the non-similarity solution proposed by Chen and Eichhorn [2]. One limitation of these models is that the stratification of the ambient air (in the core region here) must be known *a priori* to solve the partial differential equations. In the case of the cavity flow examined here, the stratification rate was determined from the experimental data. The change in temperature at $x/H = 0.25$ with height is shown in Figure 4.16. The temperature gradient in the moderately stratified core region is largely unaffected by the change in the temperature of the top wall. However, the distance from the top wall to the location where the natural convection boundary layer flow separates from the heated vertical wall increases with the top wall temperature, thereby increasing the size of the highly stratified region near the top of the cavity as noted above.

The non-dimensional temperature profiles in the square cavity determined using the similarity solution of Kulkarni et al. [1] for the three different top wall temperatures are shown in Figure 4.17 with the corresponding experimental profiles. Here, $\theta_1 = (T - T_\infty)/(T_H - T_\infty)$ is the non-dimensional temperature, and $\eta_1 = (g\beta/4\nu^2)^{1/4}a^{1/4}x$ is the non-dimensional distance from the heated vertical wall, where a is the stratification rate of the ambient temperature. The results show that the similarity solution presented by Kulkarni et al. [1] does not describe the current investigated cases. For the three cases, at $y/H = 0.1$ to 0.8 , the experimental temperature distributions approached the profile predicted by the similarity solution [1] but did not reach this profile. At $y/H \geq 0.95$, the experimental temperature profiles were significantly different from that predicted by the similarity solution, since the similarity solution can not predict the temperature field in the highly stratified region above the natural convection boundary layer flow after it separates from the

vertical wall. For the cases with the non-dimensional top wall temperatures of 1.9 and 2.3, the temperature profiles at $y/H = 0.9$ significantly overshoot the similarity profile since it is not valid in the separated natural convection flow. The integral of the buoyancy force for the thermal boundary layer determined from the similarity solution was negative for air flow. Thus, the similarity solution can at most describe a decelerating boundary layer flow after it has passed through the neutral buoyancy point. However, in the current three cases, the local integral of the buoyancy for the thermal boundary layer was positive along the most part of the heated vertical wall. It should be noted this is different from the results for higher Prandtl number fluids where the integral of the buoyancy for the boundary layer flow determined from the similarity solution [1] is positive. The similarity solution may better describe the flows in those cases.

The non-similarity model profiles outlined in Chen and Eichhorn [2] are compared to the experimental temperature profiles along the heated vertical wall for the three different top wall temperatures in Figure 4.18. Here, $\theta_2 = (T - T_\infty)/(T_H - T_{\infty,0})$ is a non-dimensional temperature where $T_{\infty,0}$ is the temperature of the ambient air at the height of 0 extrapolated from the measured temperature gradient dT_∞/dy , and $\eta_2 = (g\beta/4\nu^2)^{1/4}(a/\xi)^{1/4}x$ is a non-dimensional distance from the heated vertical wall. This model includes a parameter ξ given by $\xi = ay/(T_H - T_{\infty,0})$ that accounts for changes in the streamwise direction. The temperature profiles from the non-similarity model [2] in the region $y/H < 0.5$ are in good agreement with the measurements. However, in the upper part of the heated vertical wall, there are some discrepancies between the experimental data and the profiles from the model. At $y/H = 0.8$ and 0.9, the non-uniformity in the experimental temperature profiles due in part to the undulation in the flow after it separates from the heated vertical wall was not considered in the model. For the cases with the non-dimensional top wall temperatures of

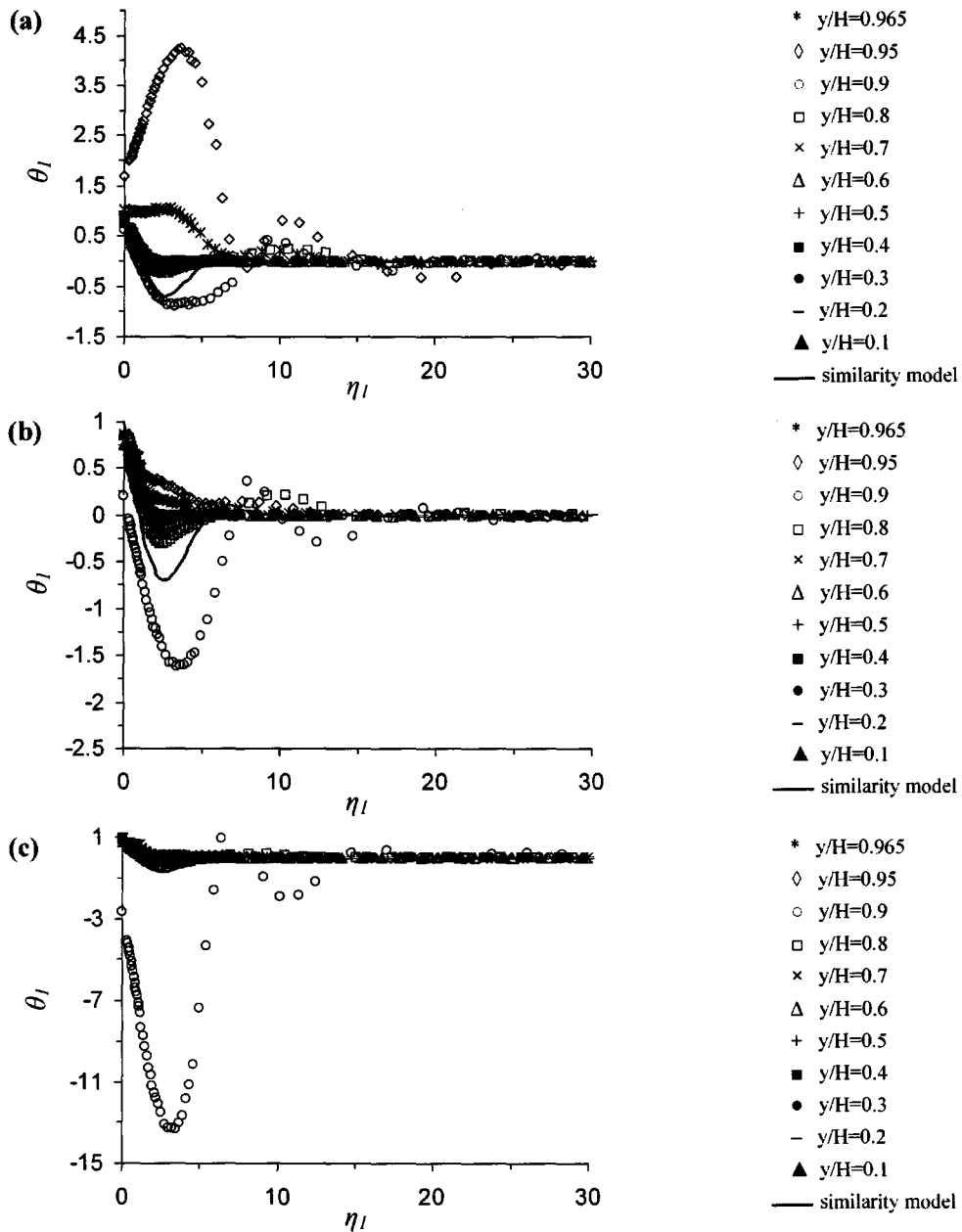


Figure 4.17: Comparison of the non-dimensional temperature distributions, θ_1 , predicted by the similarity model [1] with the measurements in the square cavity for non-dimensional top wall temperatures of (a) 1.4, (b) 1.9, and (c) 2.3 at the different heights.

1.9 and 2.3, at $y/H \geq 0.95$, the experimental results are significantly different from the predictions of the model [2]. This would be expected since this region is highly stratified, where the air temperature far from the heated vertical wall is larger than the heated vertical wall temperature and there is a recirculating flow near the corner region.

One question of interest is whether the temperature profiles for the non-similarity model [2] can predict the heat transfer from the heated vertical wall. This was examined by comparing the non-dimensional temperature gradient on the surface of the wall from the non-similarity solution given by

$$-\theta'_2|_{\eta_2=0} = Nu(y) \cdot Gr(y)^{-1/4} \cdot \left(\frac{T_H - T_\infty}{T_H - T_{\infty,0}} \right)^{5/4} \cdot \sqrt{2}, \quad (4.5)$$

where $Nu(y)$ is the local Nusselt number and $Gr(y)$ is the local Grashof number. The results in Figure 4.19 show that the predictions from the non-similarity solution in the region $y/H \lesssim 0.8$ were slightly larger than the measurements. For $y/H \gtrsim 0.8$, this discrepancy increased significantly, again likely due to the undulation in the boundary layer flow after it separates from the vertical wall that is not considered in the model. For the cases with the non-dimensional top wall temperatures of 1.9 and 2.3, at $y/H = 0.95$, the non-dimensional temperature gradient, obtained from the measurements, $-\theta'_2(0, y/H)$, is negative, indicating the heat was transferred from the flow to the heated vertical wall.

The change in the non-dimensional integral of the buoyancy force along the

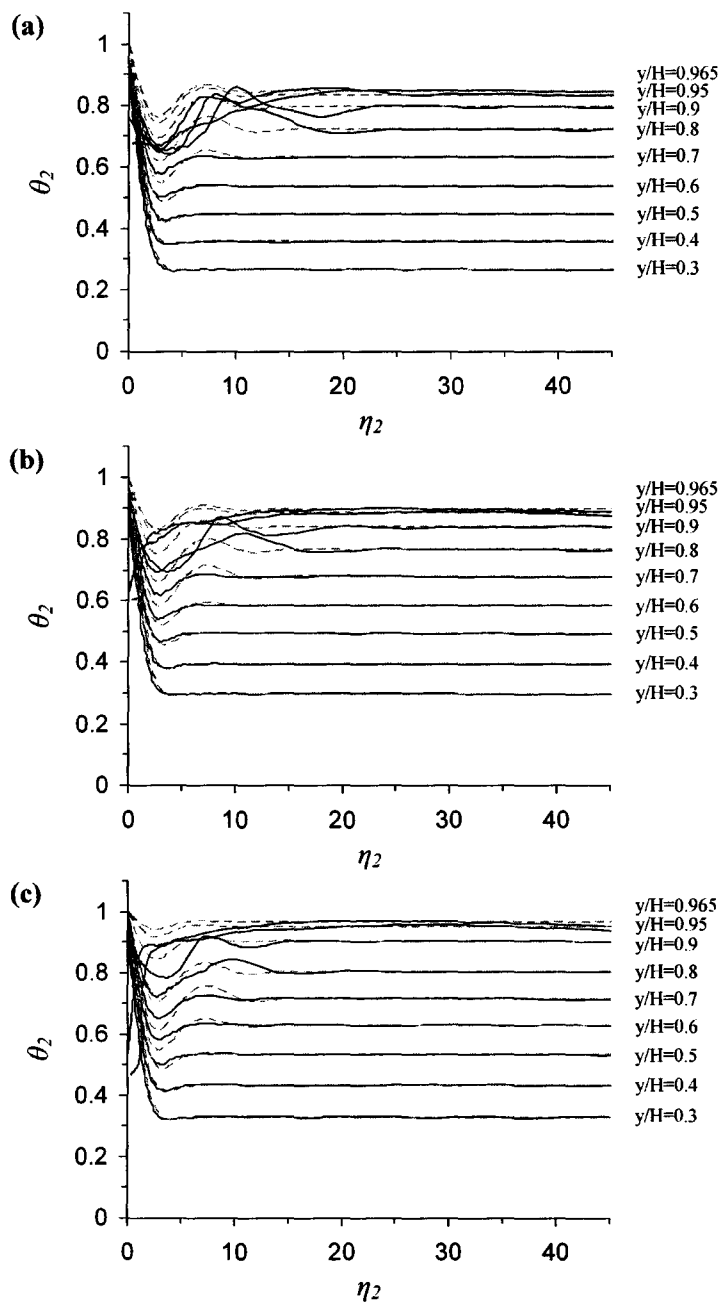


Figure 4.18: Comparison of the non-dimensional temperature profiles — — —: predicted by the non-similarity solution [2] and ———: from the measurements in the square cavity for non-dimensional top wall temperatures of (a) 1.4, (b) 1.9, and (c) 2.3.

heated vertical wall given by

$$B(y) = \frac{\int_0^\delta \rho_\infty(y)g\beta(y) \cdot [T(x, y) - T_\infty(y)] \cdot dx}{(T_H - T_{\infty,0})\rho_\infty(y)\beta(y)g} \cdot \left(\frac{g\beta(y)a}{4\nu^2\xi}\right)^{1/4} = \int_0^\delta \frac{(T - T_\infty)}{(T_H - T_{\infty,0})} \cdot d\eta_2 \quad (4.6)$$

for the model [2] and measurements are shown in Figure 4.20. The non-dimensional integral of the buoyancy force, $B(y)$, decreased along the heated vertical wall due to the increase in T_∞ with height. At $y/H \lesssim 0.8$, the model predictions and measurements were in reasonable agreement and the model seemed to capture some trends in the data. In particular, the model seemed to reasonably predict the change in buoyancy when the temperature of the top wall increased. The buoyancy for the non-similarity model decreased more rapidly with height than the experimental data, suggesting the model does not capture all of the features from the measurements. It is not clear if this was from differences in the initial thermal boundary layer. At $y/H \gtrsim 0.8$, as expected, there were significant discrepancies between the experimental data and the model predictions due to the flow separation in this region.

The change in the non-dimensional momentum flux of the boundary layer flow along the heated vertical wall from the non-similarity model [2] given by

$$M(y) = \frac{\int_0^\delta V \rho_\infty(y) V \cdot dx}{\rho_\infty(y) \cdot 2^{5/2} \cdot \nu^{1/2} \cdot [g\beta(y)]^{3/4} \cdot (T_H - T_{\infty,0})^{3/4} \cdot y^{5/4}} \quad (4.7)$$

for the three different cases is shown in Figure 4.21. Here, the momentum flux can be expressed in terms of a dimensionless stream function that can be solved to estimate the momentum flux without the velocity distributions [2]. The momentum flux decreased with the height, approaching zero at a location near the top wall. This occurred more rapidly with the larger top wall temperature as expected. The model

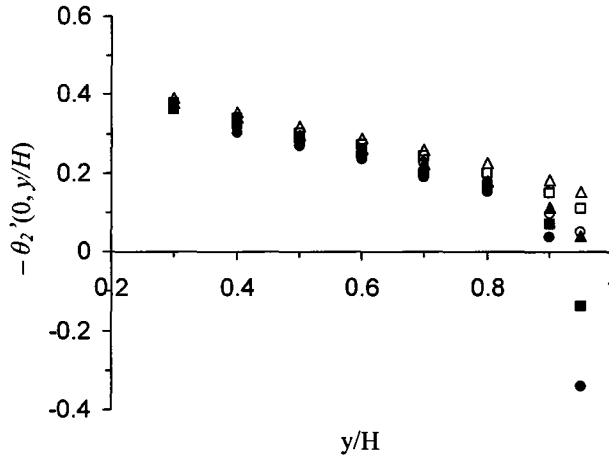


Figure 4.19: Comparison of the non-dimensional temperature gradient at the surface of the heated vertical wall, $-\theta_2'(0, y/H)$, from the non-similarity model [2] (open) and the experimental data (solid) with the non-dimensional top wall temperatures of Δ : 1.4, \square : 1.9, and \circ : 2.3.

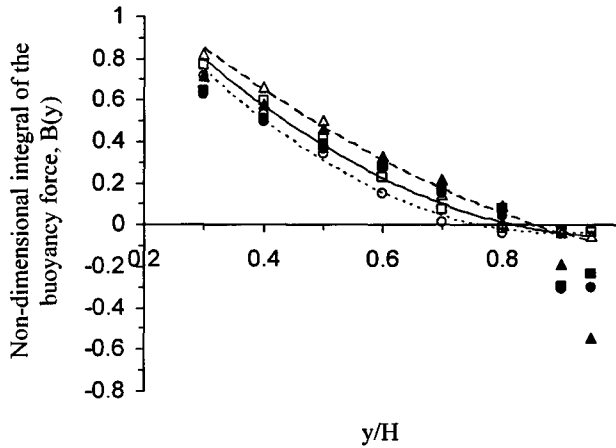


Figure 4.20: Comparison of the non-dimensional integral of the buoyancy force across the boundary layer flow along the heated vertical wall, $B(y)$, from the non-similarity model [2] (open) and the experimental data (solid) with the non-dimensional top wall temperatures of Δ : 1.4, \square : 1.9, and \circ : 2.3.

can not predict the location where the flow separates from the vertical wall but it can be inferred from the location where the momentum approached zero. This location is similar to that observed in the measurements, at least for the largest top wall temperature. For the lower top wall temperatures, the pressure gradient induced by the recirculating flow in the corner region should be affecting the flow in the corner.

4.3 The effect of the large top wall temperature on the natural convection in rectangular cavities with different aspect ratios

The investigation of the effect of the large top wall temperature on the laminar natural convection was extended to the rectangular cavities with aspect ratios of 0.5 and 2.0. The experiments were performed with non-dimensional top wall temperatures of approximately 1.4, 1.9 and 2.3. The temperatures of the walls in the rectangular cavities were maintained to approximately the same as in the square cavity so the global Grashof numbers Gr_H were approximately the same. The experimental conditions are summarized in Table 4.2.

The temperature profiles along the heated vertical walls of the rectangular cavities with aspect ratios of 0.5 and 2.0 for a non-dimensional top wall temperature of approximately 2.3, as well as the corresponding flow images in the upper left corner regions are compared to those in the square cavity in Figure 4.22. Similar to the results in the square cavity, the upward boundary layer flow along the heated vertical wall of the rectangular cavities separated from the wall before reaching the top wall, resulting in a recirculating flow region between the separated flow and the heated vertical wall. The location of the flow re-attachment to the top wall after

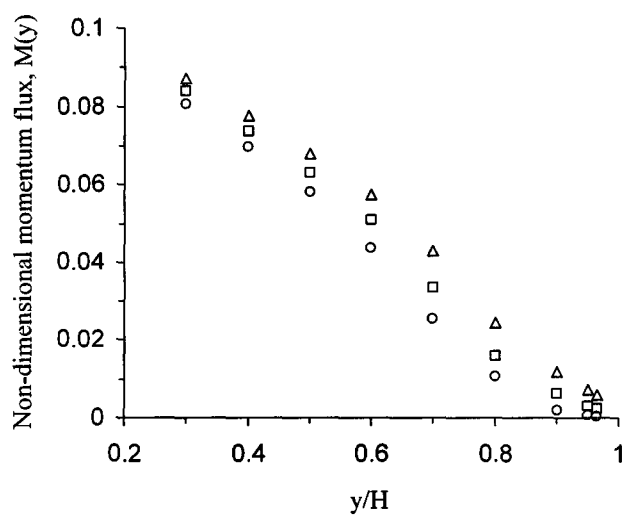


Figure 4.21: Comparison of the non-dimensional momentum flux of the boundary layer flow along the heated vertical wall, $M(y)$, predicted from the non-similarity model [2] for non-dimensional top wall temperatures of \triangle : 1.4, \square : 1.9, and \circ : 2.3.

turning over changed from approximately $x/H = 0.4$ to 0.2 when the aspect ratio increased from 0.5 to 2.0 , indicating the region of the recirculating flow increased in the horizontal direction with a decrease of the aspect ratio. The distance from the top wall to the location where the upward natural convection flow along the heated vertical wall turned over decreased from $y/H \approx 0.13$ to $y/H \approx 0.06$ as the aspect ratio was increased from 0.5 to 2.0 , since the increased contact area between the top and bottom walls and the natural convection flow along the walls resulted in more momentum of the natural convection flow to be consumed by shear stress. Thus, the recirculating flow region decreased in the vertical direction with an increase of the aspect ratio. The x -location of the trough of the undulating flow was approximately the same for the three cavities.

The non-dimensional temperature profiles along the heated vertical walls show that there is a thin thermal boundary layer along the heated vertical wall. The ambient temperature in the region far from the heated vertical wall increases with height for all the three cavities, so most of the air in the cavity was stably stratified. The undulating flow caused the temperature of the air in the undulation region at $x/H \approx 0.12$ to be non-uniform. The vertical location where the non-uniformity in the temperature profiles occurred changed with the aspect ratio, since the distance from the top wall to the location where the upward flow along the heated vertical wall turned over decreased with an increase of the aspect ratio. For example, the non-uniformity in the temperature profiles occurred at $y/H = 0.8$ for the aspect ratio of 0.5 , while it appeared at $y/H = 0.9$ for the aspect ratio of 2.0 . The mixing caused by the secondary flow between the undulating flow and the boundary layer on the heated vertical wall resulted in the temperature of the air to be approximately constant in the region $0.06 \lesssim x/H \lesssim 0.08$. With an increase of the aspect ratio, the y -location of the mixing region increased due to the increase in the y -location where the upward

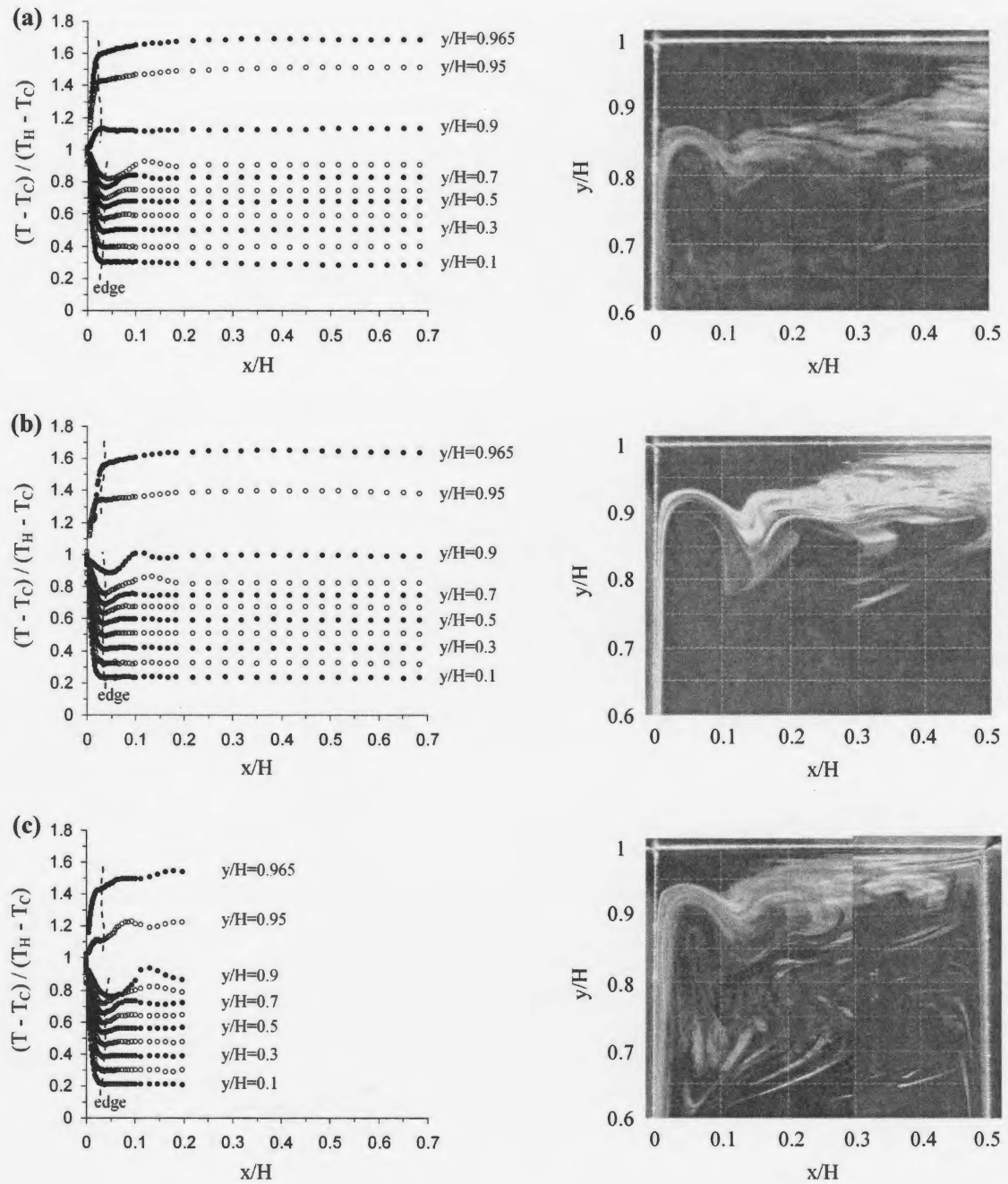


Figure 4.22: Non-dimensional temperature profiles in cavities (Left) and flow patterns in the upper left corner region (Right) for cases with aspect ratios of (a) 0.5, (b) 1.0 and (c) 2.0 for non-dimensional top wall temperature of approximately 2.3.

flow separated from the heated vertical wall. For example, in the cavity with the aspect ratio of 0.5, the mixing occurred at heights of $y/H = 0.7$ and 0.8 resulting in the air temperatures just outside of the boundary layer at these heights to be similar. This region moved to $y/H = 0.8$ and 0.9 for the cavity with aspect ratio of 2.0.

The recirculating flow region between the separated flow and the heated vertical wall caused the temperature profiles in this region to be significantly different from those in the region below the separated flow. The temperature profiles in this region indicate a boundary layer flow moving downward along the heated vertical wall, suggesting the recirculating flow between the separated flow and the heated vertical wall was anti-clockwise, similar to the numerical result of Shiralkar and Tien [16]. With an increase of the aspect ratio, the anti-clockwise recirculating flow region decreased as shown in the flow visualizations. This is reflected in the cavity with the aspect ratio of 2.0, where the downward boundary layer along the heated vertical wall was observed only at $y/H \gtrsim 0.95$.

The temperature profiles along the heated vertical walls and the flow visualizations in the upper left corner regions in the three cavities for the non-dimensional top wall temperatures of approximately 1.9 and 1.4 are shown in Figures 4.23 and 4.24. For a given aspect ratio, as expected, a decrease of the non-dimensional top wall temperature results in the distance from the top wall to the location where the upward flow turned over to decrease. Consequently, the recirculating flow region between the separated flow and the heated vertical wall becomes smaller. It was shown that for the square cavity (Figure 4.12) the highly stratified region above the separated boundary layer flow became more stable with an increase of the top wall temperature. Thus, with a decrease of the top wall temperature the magnitude of the undulation in the flow became larger, resulting in a wider region where the temperature profiles are non-uniform. For example, when the non-dimensional top wall temperature of

the cavity with aspect ratio of 0.5 decreased to 1.4, the temperature non-uniformity occurred at heights $y/H = 0.7$ to 0.9 , compared to at $y/H = 0.8$ for the case with the non-dimensional top wall temperature of 2.3.

The x-location of the trough of the undulating flow is nearly insensitive to the change in the top wall temperature and the aspect ratio of the cavities. This is different from the cases with non-dimensional top wall temperatures of 0.83 to 1.14. This discrepancy is likely due to the presence of the recirculating flow region between the separated flow and the heated vertical wall in the cases with the large top wall temperatures. Hence, the top wall does not directly block the upward boundary layer flow along the heated vertical wall and forces it to separate from the wall in the cases with large top wall temperatures.

The change in the non-dimensional ambient temperature outside the boundary layer with height in the three cavities is shown in Figures 4.25. Similar to that with the modest top wall temperatures, the ambient temperature outside the boundary layer increased approximately linearly with the height over most of the cavity. With an increase of the top wall temperature, the local ambient temperature outside the boundary layer was affected down to $y/H \approx 0.1$. At modest top wall temperatures, the ambient temperature outside the boundary layer near the bottom wall was essentially independent of the top wall temperature as shown in Figure 4.7. The change in the ambient temperature outside the boundary layer was more sensitive to the change in the top wall temperature with a decrease of the aspect ratio. This is because the contact area between the top wall and the natural convection flow along the top wall was increased with a decrease of the aspect ratio. For the 0.5 aspect ratio cavity, the ratio of the size of the recirculating flow region in the upper left corner to the cavity width is approximately 0.2, so the convection flow moves along approximately 80% of the width of the top wall corresponding to a non-dimensional contact

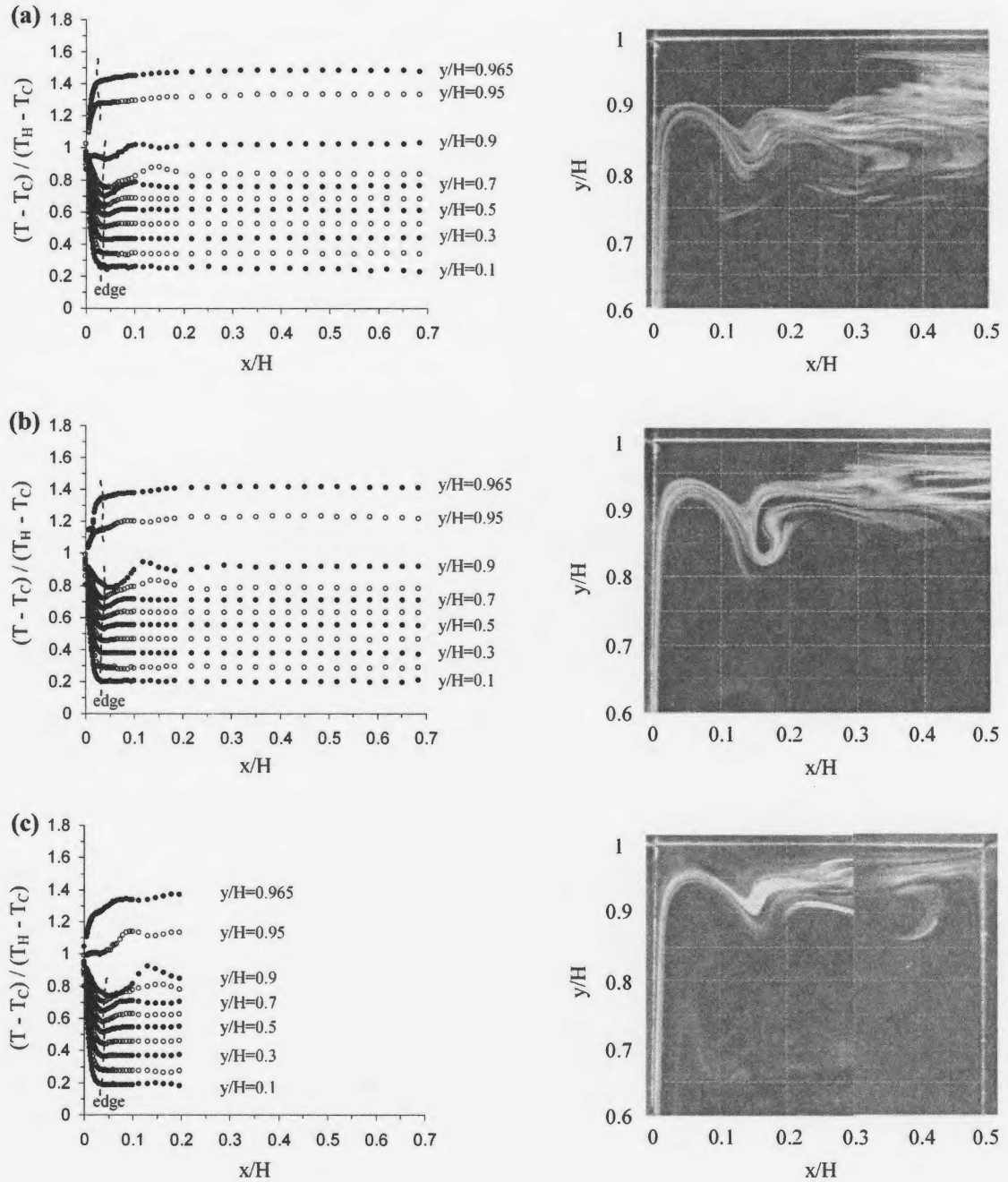


Figure 4.23: Non-dimensional temperature profiles in cavities (Left) and flow patterns in the upper left corner region (Right) for cases with aspect ratios of (a) 0.5, (b) 1.0 and (c) 2.0 for non-dimensional top wall temperature of approximately 1.9.

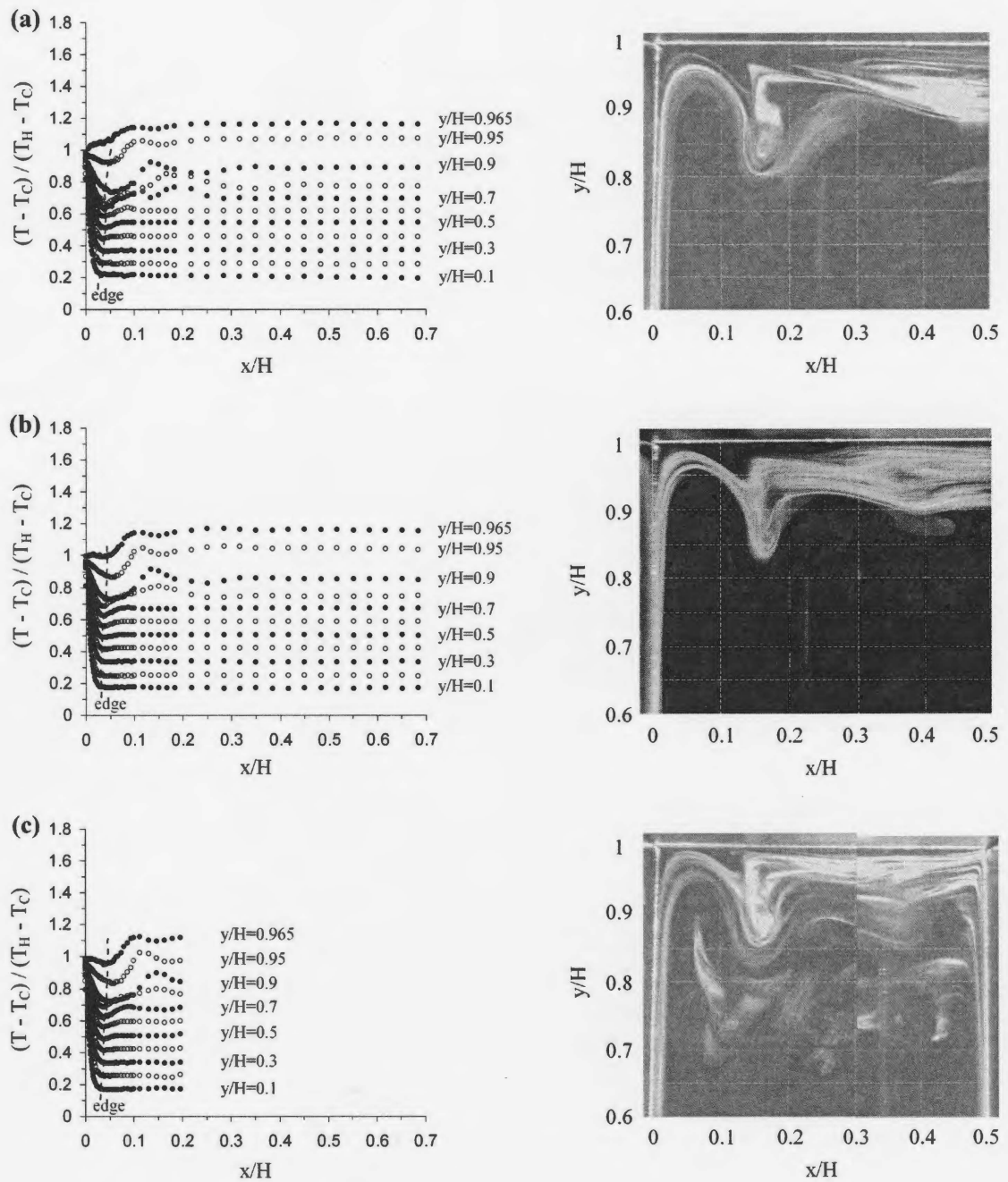


Figure 4.24: Non-dimensional temperature profiles in cavities (Left) and flow patterns in the upper left corner region (Right) for cases with aspect ratios of (a) 0.5, (b) 1.0 and (c) 2.0 for non-dimensional top wall temperature of approximately 1.4.

length of $x/H \approx 1.6$. For the 2.0 aspect ratio cavity, however, the ratio of the size of the recirculating flow region to the cavity width is around 0.4. Hence, the contact area between the top wall and the convection flow only occupied approximately 60% of the width of the top wall, corresponding to a non-dimensional contact length of $x/H \approx 0.3$ in this case. Therefore, more energy could be transferred into the natural convection flow along the top wall in the cavity with the aspect ratio of 0.5 compared to that in the cavity with the aspect ratio of 2.0. As a result, the change in the temperature gradient $d\theta_\infty/d(y/H)$ with the change in the top wall temperature, shown in Figure 4.26, was relatively more significant for the smaller aspect ratio. Here, the temperature gradient $d\theta_\infty/d(y/H)$ was obtained from a linear fit to the data between $y/H = 0.1$ and 0.7. For all three cavities, in general, the temperature gradient increased linearly with an increase of the top wall temperature. The rate of increase in the temperature gradient became smaller when the aspect ratio was changed from 0.5 to 2.0. This is due to the change in the contact area between the top wall and the natural convection flow along the wall. This area decreased with an increase of the aspect ratio, resulting in less energy transfer from the top wall into the cavity. For a given aspect ratio, $d\theta_\infty/d(y/H)$ changes more rapidly with the change in the top wall temperature at modest top wall temperatures (shown in Figure 4.8) compared to the case with larger top wall temperatures. This is due to the presence of the recirculating flow in the upper left corner region of the cavity with large top wall temperatures, which reduced the energy transfer from the top wall into the cavity.

The change in the local Nusselt number along the heated vertical wall with the change in the top wall temperature for the three cavities under the larger top wall temperatures is shown in Figure 4.27. As expected, the local Nusselt number increased along the heated vertical wall. At $y/H \geq 0.7$, the Nusselt number increased significantly due to the effect of the secondary flow between the undulating flow

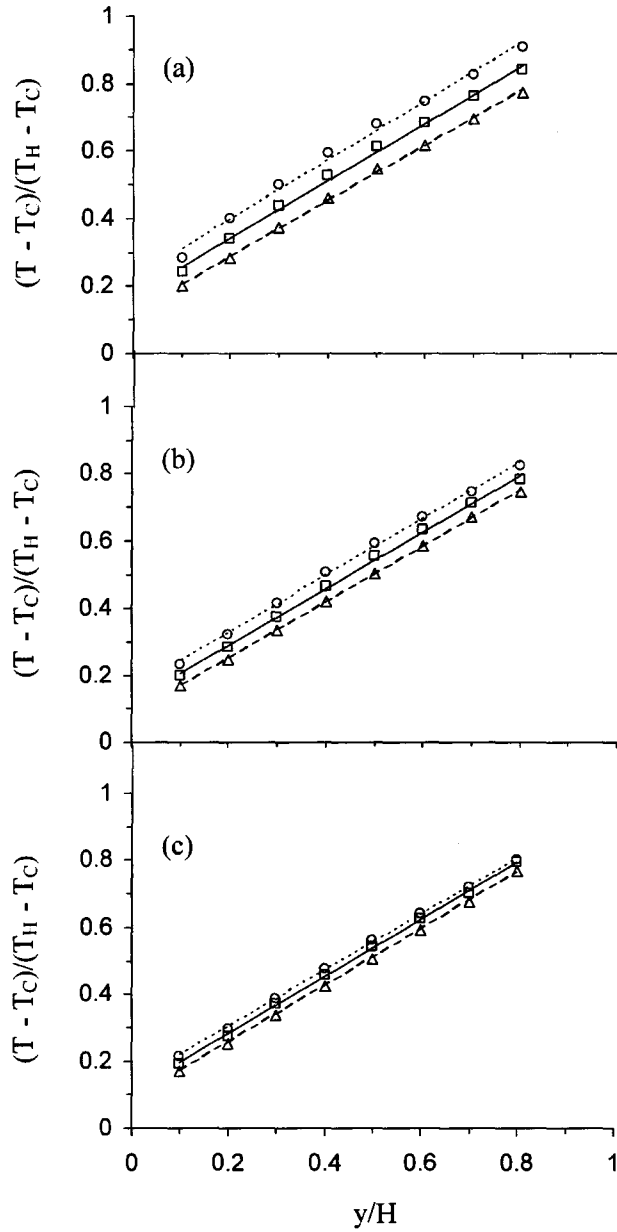


Figure 4.25: Comparison of the non-dimensional local ambient temperature outside of the boundary layer for cases with aspect ratios of (a) 0.5, (b) 1.0 and (c) 2.0. Here the non-dimensional top wall temperatures were Δ : 1.4, \square : 1.9 and \circ : 2.3.

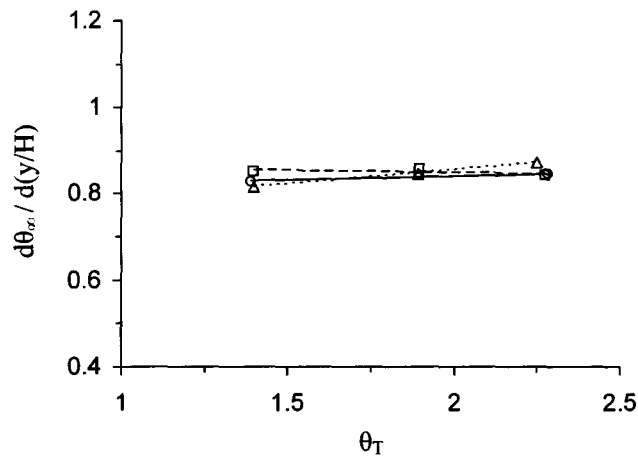


Figure 4.26: Change in the vertical gradient of the temperature outside the boundary layer on the heated vertical wall with the change in the top wall temperature for cases with aspect ratios of \triangle : 0.5, \circ : 1.0 and \square : 2.0.

and the boundary layer flow on the heated vertical wall. The increased top wall temperature increased the local ambient temperature outside of the boundary layer, resulting in the vertical momentum of the upward boundary layer flow along the heated vertical wall and the temperature gradient at the surface of the wall to be decreased which are corroborated by Figures 4.21 and 4.19 respectively. At $y/H < 0.6$, there is no significant change in the Nusselt number with an increase of the top wall temperature indicating the changes in the vertical momentum of the upward boundary layer flow and the temperature gradient at the heated vertical wall surface are similar. However, at $y/H \geq 0.7$, the local Nusselt number increased significantly with an increase of the top wall temperature, suggesting that the change in the top wall temperature has a larger effect on the vertical momentum of the boundary layer flow along the heated vertical wall than that on the temperature gradient at the surface of the heated vertical wall in this region. The increased top wall temperature will likely cause a reduction in the velocity of the recirculating flow downward along the heated vertical wall, as indicated by Shiralkar and Tien [16]. This would affect the vertical momentum of the upward boundary layer flow along the heated vertical wall. At $y/H > 0.7$, the increase of the local Nusselt number with the increase of the top wall temperature became larger with the decrease of the aspect ratio, since the region affected by the recirculating flow became larger with a decreased of the aspect ratio as shown in the flow visualizations (Figures 4.22 to 4.24).

The change in the local Nusselt number with the local Rayleigh number for the three cavities with larger top wall temperatures is shown in Figure 4.28. The data over most of the heated vertical wall could be correlated by $Nu = C \cdot Ra^n$, except for $y/H > 0.7$ due to the presence of the secondary flow. The form of the correlation here is the same as that obtained with the modest top wall temperatures. However, in the current cases, the value of the index n in a given cavity changed with the top

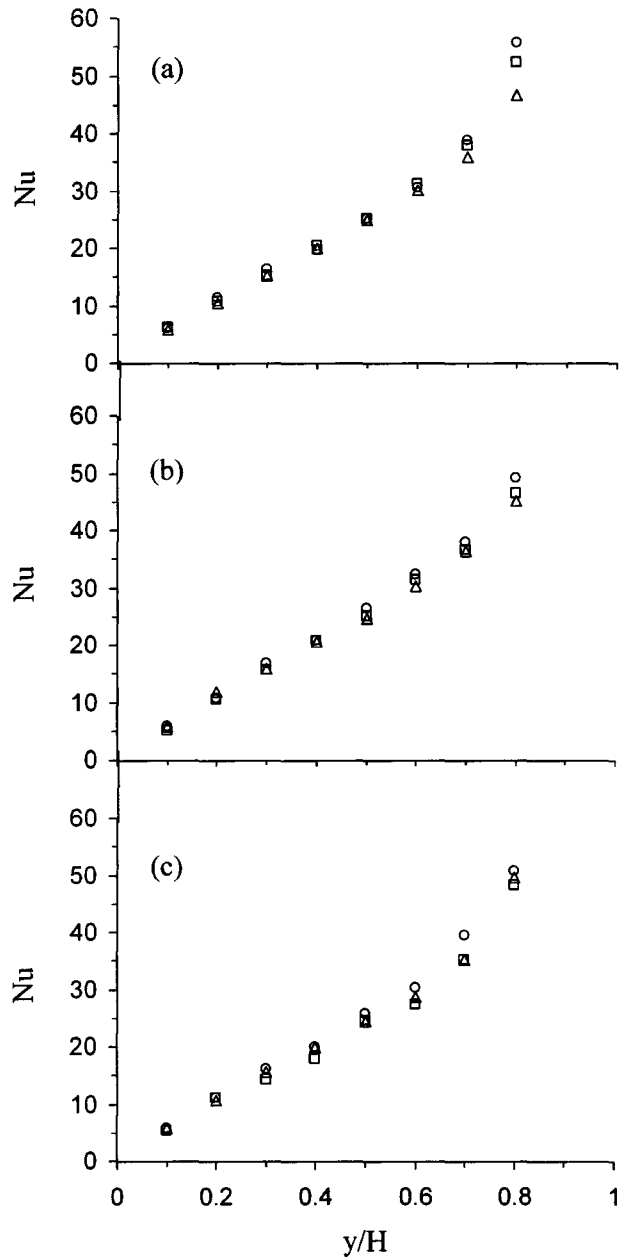


Figure 4.27: Comparison of the local Nusselt number along the heated vertical wall for cases with aspect ratios of (a) 0.5, (b) 1.0 and (c) 2.0. Here the non-dimensional top wall temperatures were \triangle : 1.4, \square : 1.9 and \circ : 2.3.

wall temperature as shown in Table 4.2.

The local Nusselt numbers are plotted against the local Rayleigh numbers along the heated vertical wall from $y/H = 0.2$ to 0.7 for all the present cases in Figure 4.29. The data were correlated by

$$Nu = 0.1031 \cdot Ra^{0.3534} \quad (4.8)$$

with a coefficient of determination of 0.86 for local Rayleigh number in the range 4×10^5 to 2×10^7 . The change in the average Nusselt number for the heated vertical walls \overline{Nu}_H with the vertical Rayleigh numbers Ra_V is shown in Figure 4.30. The average Nusselt number is given by

$$\overline{Nu}_H = \frac{\overline{h}H}{k}, \quad (4.9)$$

where \overline{h} is the average heat transfer coefficient for the heated vertical wall. The vertical Rayleigh number, based on the temperature difference between the top and bottom walls, is defined as

$$Ra_V = \frac{g\beta(T_T - T_B)H^3}{\alpha\nu}. \quad (4.10)$$

The average Nusselt number increases with the vertical Rayleigh number, as found by Shiralkar and Tien [16], and can be correlated by

$$\overline{Nu}_H = 1.0113 \cdot Ra_V^{0.2117} \quad (4.11)$$

with a coefficient of determination of 0.52 for global Grashof number Gr_H in the range 1.2×10^8 to 1.9×10^8 and Ra_V in the range 8×10^7 to 1.7×10^8 for the cases

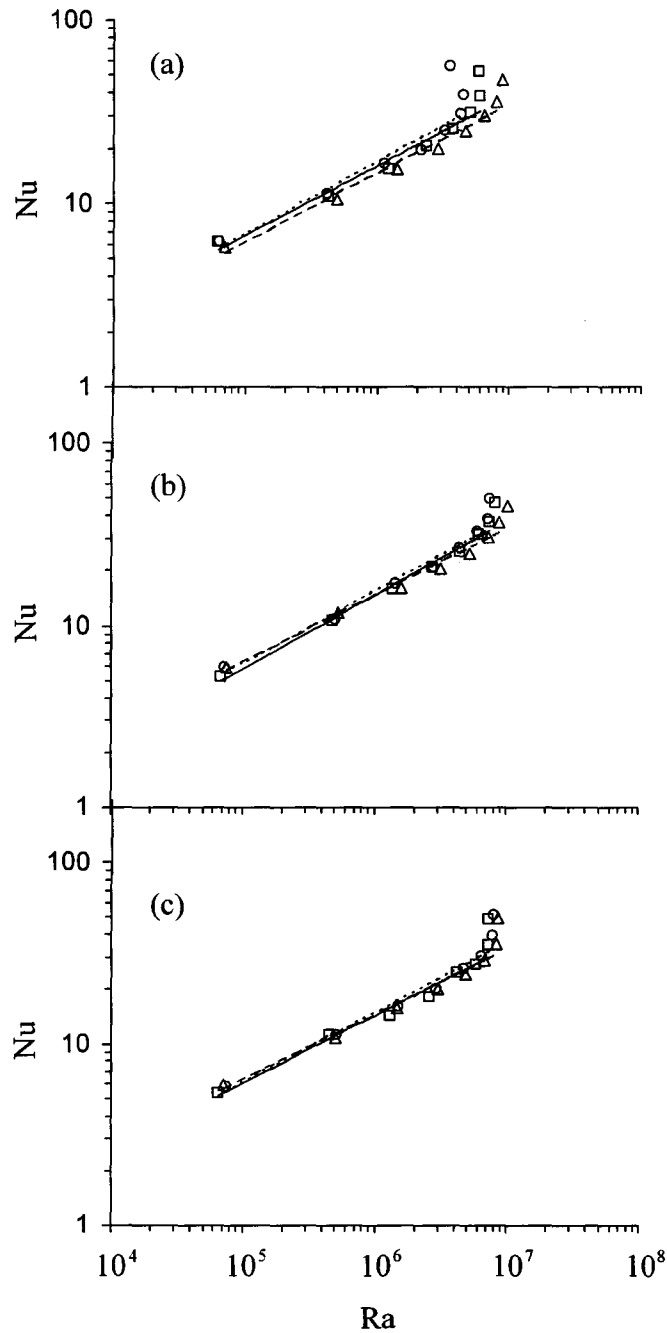


Figure 4.28: Change in the local Nusselt number with the local Rayleigh number for cases with aspect ratios of (a) 0.5, (b) 1.0 and (c) 2.0. Here the non-dimensional top wall temperatures were Δ : 1.4, \square : 1.9 and \circ : 2.3.

examined here. There are currently, to the author's best knowledge, no correlations in the literature for the average Nusselt number for the heated vertical wall and the vertical Rayleigh number for rectangular cavities with aspect ratios of 0.5 to 2.0.

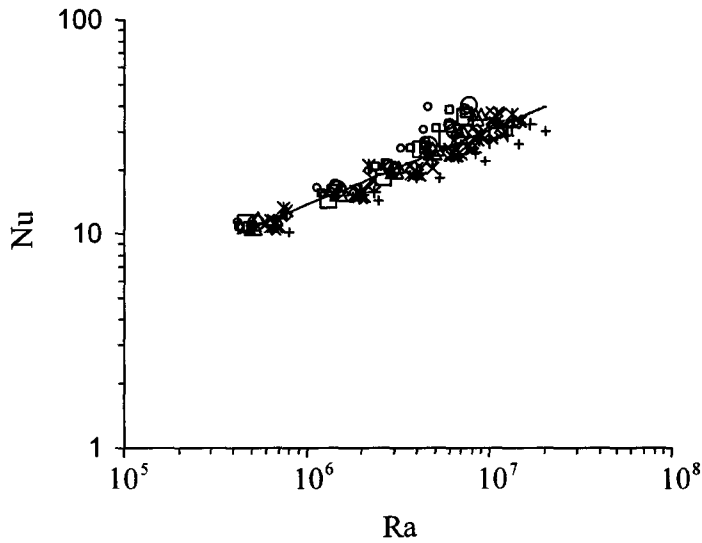


Figure 4.29: Change in the local Nusselt number with the local Rayleigh number along the heated vertical wall from $y/H = 0.2$ to 0.7 for cases with aspect ratios of 0.5 (small size symbols), 1.0 (mid size symbols) and 2.0 (large size symbols) under the non-dimensional top wall temperatures of $+$: 0.52 (insulated), \times : 0.83 , \diamond : 1 , $*$: 1.14 , \triangle : 1.4 , \square : 1.9 and \circ : 2.3 .

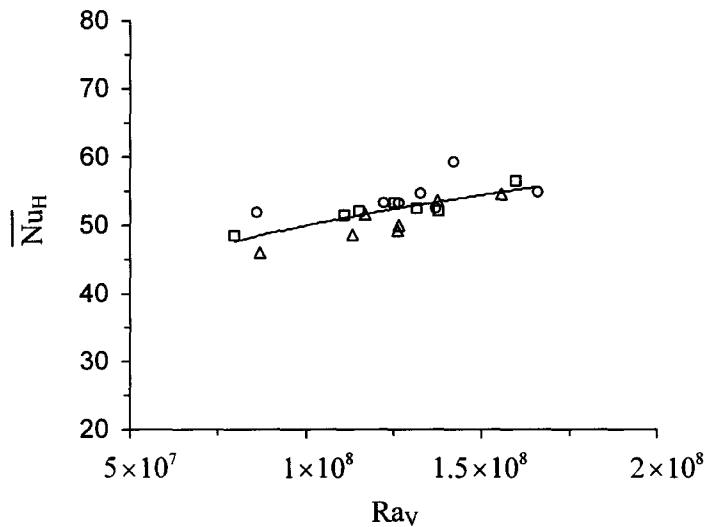


Figure 4.30: Change in the average Nusselt number for the heated vertical wall with the vertical Rayleigh number for cases with aspect ratios of \triangle : 0.5 , \circ : 1.0 and \square : 2.0 .

Chapter 5

Effect of a partition on the laminar natural convection in a square cavity with different top wall temperatures

The effect of a partition on the laminar natural convection air flow in a square cavity was investigated by maintaining the vertical walls at approximately 48°C and 9°C , respectively, so the global Grashof number based on the height of the cavity Gr_H was approximately 1.4×10^8 , similar to that in the square cavity with smooth walls reported in Chapter 4. The bottom wall temperature was maintained at approximately 9°C and the top wall temperature was changed. An aluminium partition was attached to the heated vertical wall at either $y/H = 0.65$ or 0.95 and to the top wall at either $x/H = 0.1, 0.2, 0.4$ or 0.6 . Partition heights of $0.75''$ and $1.5''$, corresponding to non-dimensional partition heights H_P/H of 0.0625 and 0.125 , were used in this study. The results for the partition on the heated vertical wall are discussed first,

followed by the partition on the top wall.

5.1 Effect of a partition on the heated vertical wall

The flow patterns in the upper left corner of the square cavity with the partition ($H_P/H = 0.0625$) on the heated vertical wall at $y/H = 0.65$ with non-dimensional top wall temperatures of approximately 0.57 (insulated), 1.4 and 2.3 are shown in Figure 5.1. Corresponding schematics of the flow adapted from the flow visualizations showing the key features of the flow are also presented in this figure. For these cases, the partition blocked the upward boundary layer flow along the heated vertical wall, resulting in flow separation and the formation of a recirculating flow behind the partition. A similar result was observed by Shi and Khodadadi [28] in their numerical simulations of the laminar natural convection in a similar partitioned square cavity with adiabatic horizontal walls. They noted that the changes in the flow patterns affected the temperature field in the region close to the partition. The flow along the heated vertical wall reattached to the wall at $y/H \approx 0.85$ after separating from the lip of the partition.

With an increase of the top wall temperature ($\theta_T = 1.4$ and 2.3), similar to the cases without the partition (Figures 4.12 (a) and (c)), the flow then separated from the heated vertical wall before reaching the top wall (Figures 5.1 (b) and (c)) due to the increased negative buoyancy force. There was a recirculating flow bounded by the heated vertical wall, the top wall and the separated flow. For a given top wall temperature, the distance from the top wall to the location where the upward boundary layer flow turned over was larger than that in the cavity without the partition (Figures 4.12 (a) and (c)) by approximately 30%. This is because the vertical momentum of the upward boundary layer flow along the heated vertical wall after

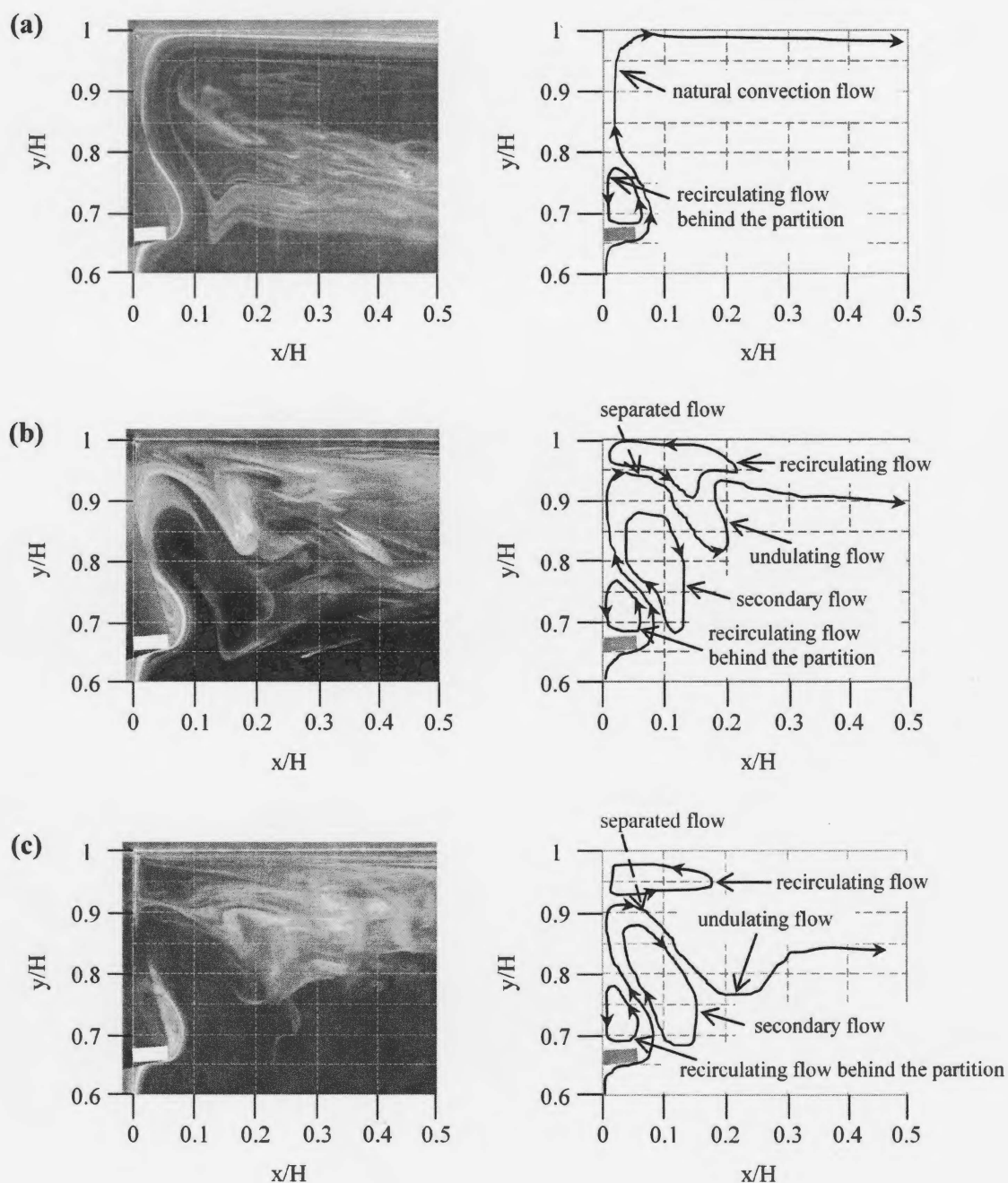


Figure 5.1: Flow patterns (Left) and the corresponding schematics (Right) in the upper left region of the square cavity with a partition on the heated vertical wall at $y/H = 0.65$ for the non-dimensional top wall temperatures of approximately (a) 0.57 (insulated), (b) 1.4 and (c) 2.3. The non-dimensional height of the partition here was 0.0625.

reattachment was decreased due to the blockage effect of the partition on the upward flow. The secondary flow between the recirculating flow behind the partition and the undulating flow near the top wall interacts with both the recirculating flow and the undulating flow, resulting in the undulating flow near the top wall to be more disorganized compared to that in the cavity without the partition (Figures 4.12 (a) and (c)). The recirculating flow behind the partition would cause the temperature distributions in this region to be relatively uniform due to the mixing of the recirculating flow and would be similar to the results presented by Shi and Khodadadi [28]. Thus, the temperature field measurements were not repeated for this case.

The flow visualizations in the upper left corner region of the cavity and the temperature distributions along the heated vertical wall were obtained for the cases with the partition at $y/H = 0.95$. Two partition heights were used and the experimental conditions are summarized in Table 5.1. The results for $H_P/H = 0.0625$ with non-dimensional top wall temperatures of approximately 0.59 (insulated), 1.4 and 2.3 are presented in Figures 5.2, 5.3 and 5.4. When the top wall of the cavity was insulated ($\theta_T \approx 0.59$), the flow and temperature field along most of the heated vertical wall are approximately the same as those in the cavity without the partition. In the region with $0.1 \lesssim y/H \lesssim 0.9$, the maximum discrepancy in the temperature distributions between the two cavities is less than 4%. At $y/H \gtrsim 0.9$, the temperature distributions in the region away from the heated vertical wall ($x/H \gtrsim 0.5$) is more uniform, indicating there is a secondary flow just outside the boundary layer along the top wall as also reported by Tian and Karayiannis [6]. This secondary flow is not very apparent in Figure 5.2 due to the limitation of the view of the field by the camera. The upward boundary layer flow along the heated vertical wall was blocked by the partition, resulting in a recirculating flow between the lip of the partition and the separated flow ($0.07 \lesssim x/H \lesssim 0.15$). As a result, the temperature distribu-

tion changed dramatically in this region compared to that in the cavity without the partition.

When the non-dimensional top wall temperature was increased to approximately 1.4, the partition at $y/H = 0.95$ slightly blocked the upward boundary layer along the heated vertical wall and forced it to separate from the heated vertical wall as shown in Figure 5.3 (b). As a result, the location of the trough of the undulating flow was moved away from the heated vertical wall compared to that in the cavity without the partition. This is reflected in the horizontal location of the temperature non-uniformity at $y/H = 0.8$ being moved from $x/H \approx 0.15$ to 0.2. Due to the blockage and thermal effects of the partition, the distance from the top wall to the location where the upward boundary layer flow along the heated vertical wall turned over was at $y/H \approx 0.95$ compared to $y/H \approx 0.98$ in the cavity without the partition. Hence, the secondary flow between the upward boundary layer flow along the heated vertical wall and the undulating flow moved down slightly, resulting in the temperature just outside of the boundary layer at $y/H = 0.9$ to be slightly larger than that at $y/H = 0.8$. The temperature profiles at $y/H \geq 0.95$ indicate a flow moving downward at the lip of the partition, suggesting that the recirculating flow between the partition and the separated flow is anti-clockwise.

For the top wall temperature of approximately 2.3 (Figure 5.4), the partition had little effect on the flow since the upward boundary layer flow separated from the heated vertical wall before reaching the partition. So, there were no significant differences in the flow patterns and temperature profiles with those in the cavity without the partition, except in the vicinity of the partition. This indicates that the thermal effect of the small partition is limited.

To investigate the effect of the partition height, the non-dimensional height of the aluminium partition was increased to 0.125, while maintaining the partition at

Table 5.1: Summary of the wall temperatures, global Grashof numbers, and parameters in the correlation $Nu = C \cdot Ra^n$ for the square cavity with a partition attached to the heated vertical wall at $y/H = 0.95$.

Partition		T_H	T_C	T_T	T_B	θ_H	θ_C	θ_T	θ_B	$Gr_H \times 10^{-8}$	n	C
Location	Length	(°C)	(°C)	(°C)	(°C)							
y/H=0.95		41	7	27	7	1	0	0.59	0	1.33	0.32	0.15
				(insulated)								
	<u>0.0625</u>	44	8	59	8	1	0	1.42	0	1.37	0.36	0.1
		51	8	106	8	1	0	2.28	0	1.55	0.40	0.061
	<u>0.125</u>	47	9	62	9	1	0	1.39	0	1.40	0.36	0.094
		55	12	110	12	1	0	2.28	0	1.46	0.40	0.06

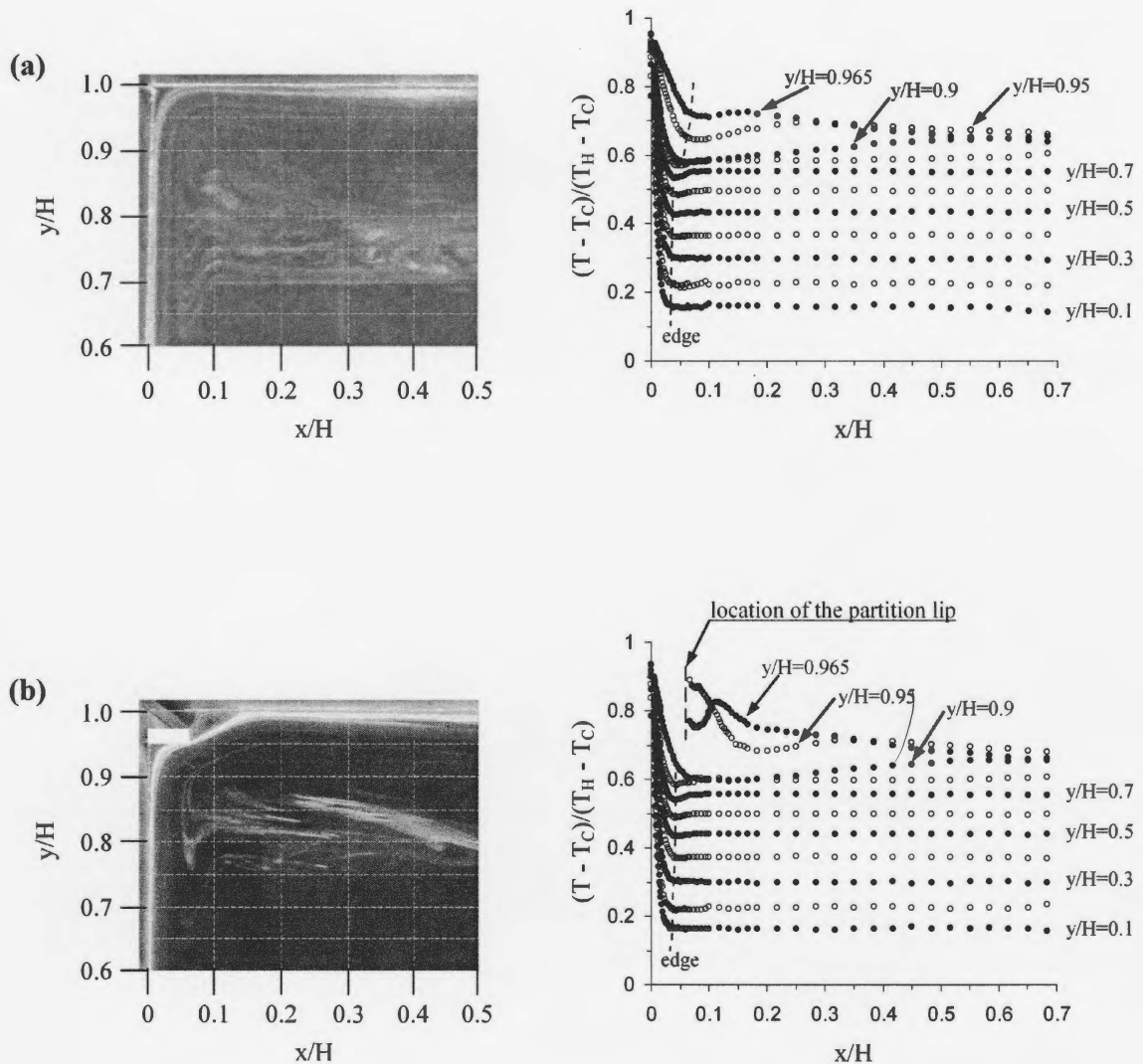


Figure 5.2: Flow patterns in the upper left region of the square cavity (Left) and non-dimensional temperature profiles in the square cavity for cases (a) without a partition and (b) with a partition on the heated vertical wall at $y/H = 0.95$ for non-dimensional top wall temperatures of approximately 0.59 (insulated). The non-dimensional height of the partition was 0.0625.

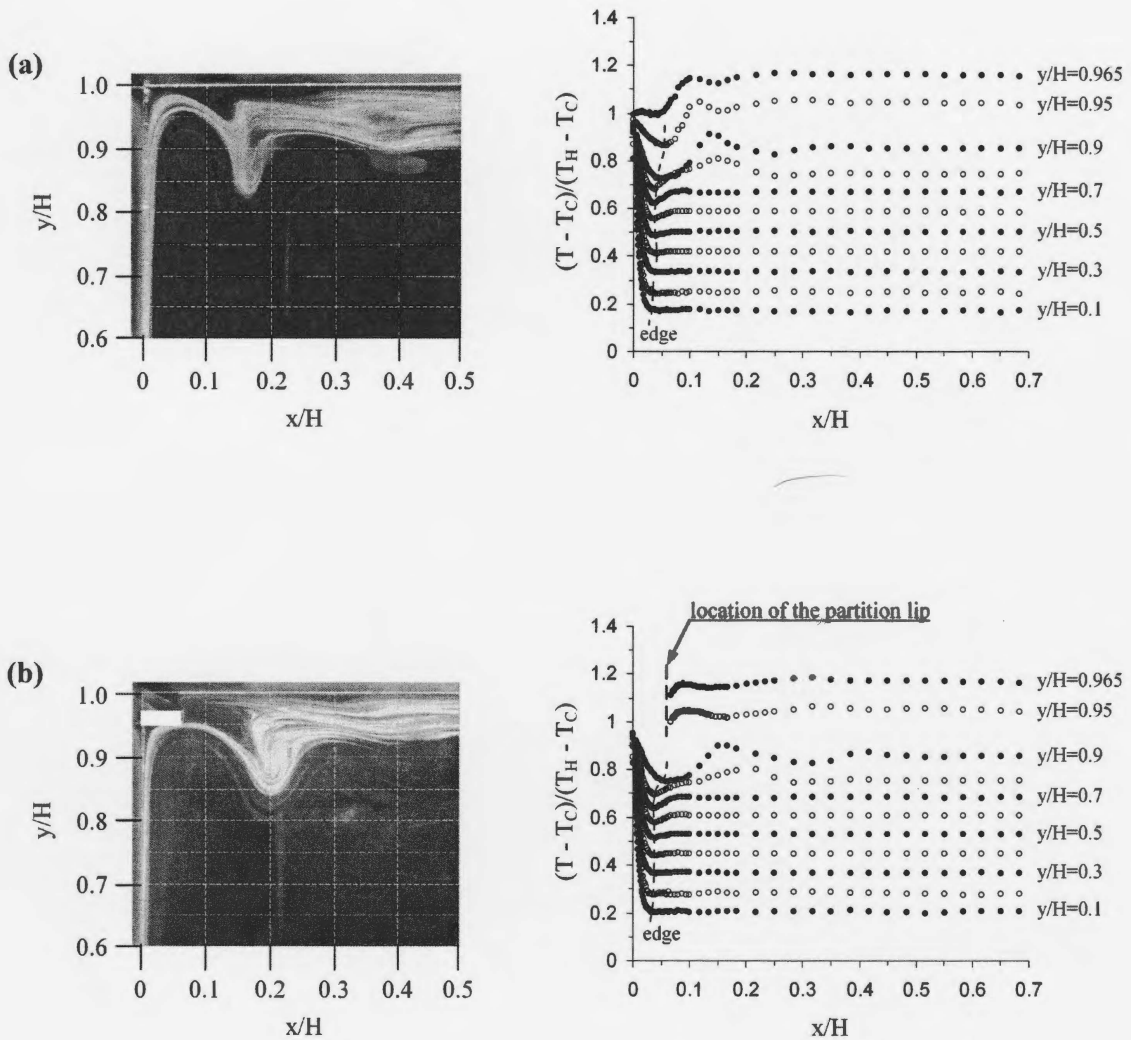


Figure 5.3: Flow patterns in the upper left region of the square cavity (Left) and non-dimensional temperature profiles in the square cavity for cases (a) without a partition and (b) with a partition on the heated vertical wall at $y/H = 0.95$ for non-dimensional top wall temperatures of approximately 1.4. The non-dimensional height of the partition was 0.0625.

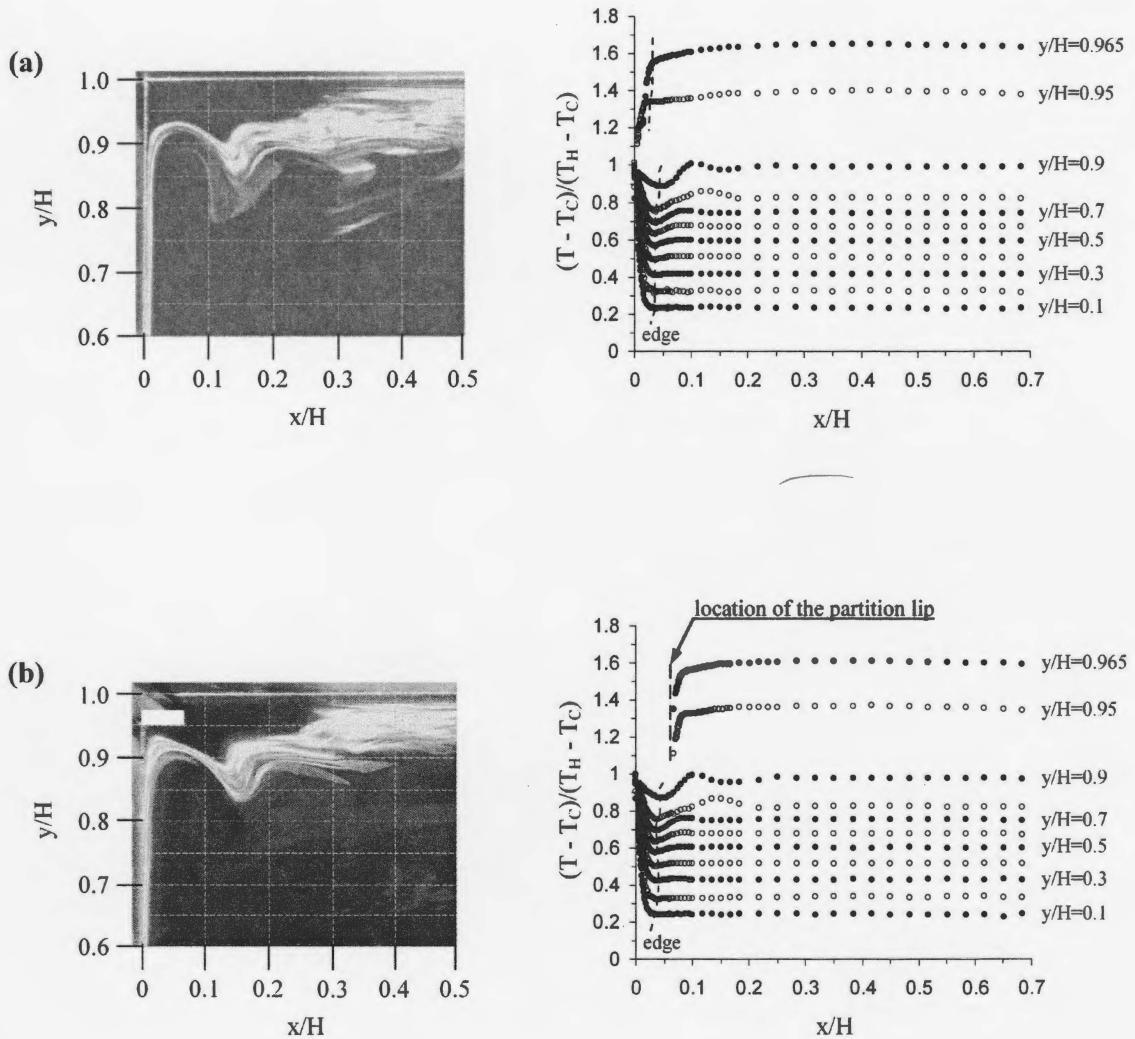


Figure 5.4: Flow patterns in the upper left region of the square cavity (Left) and non-dimensional temperature profiles in the square cavity for cases (a) without a partition and (b) with a partition on the heated vertical wall at $y/H = 0.95$ for non-dimensional top wall temperatures of approximately 2.3. The non-dimensional height of the partition was 0.0625.

$y/H = 0.95$. Shi and Khodadadi [28] studied the effect of a partition with different heights ($0.2 \leq H_P/H \leq 0.5$) attached close to the top of the heated vertical wall (at $y/H = 0.875$) in a cavity with an insulated top wall. The thermal effect of the partition increased with an increase of the partition height, resulting in the flow and temperature field in the region near the partition to be changed. They observed that the natural convection flow moved along the larger partition ($H_P/H = 0.35$ and 0.5) first, and then separated from the partition, since the partition temperature was close to the temperature of the heated vertical wall. This result is similar to the flow separation on the top wall of the current study without the partition and with modest top wall temperatures (Figures 4.3, 4.4 and 4.5). For the case with the non-dimensional partition height H_P/H of 0.2, the natural convection flow passed by the partition and then reattached to the top wall, similar to the results shown in Figure 5.2 (b).

The flow visualizations and temperature profiles for the cases with non-dimensional top wall temperatures of approximately 1.4 and 2.3 are presented in Figures 5.5 and 5.6. For the case with the non-dimensional top wall temperature of 1.4, the flow pattern and temperature profiles were nearly unchanged with an increase of the partition height, except in the region near the upper left corner of the cavity. Outside of the region $y/H \gtrsim 0.95$ and $x/H \lesssim 0.15$, the maximum discrepancy in the temperature distributions for the two cases with the different partitions is less than 6%. In the corner region, the size of the recirculating flow between the lip of the partition and the separated flow was reduced in the horizontal direction with an increase of the partition height. Therefore, the temperature distributions in this region were changed as shown in Figure 5.5 compared to those in the case with the small partition shown in Figure 5.3 (b). For example, the temperature gradients in the region close to the lip of the partition ($0.13 \lesssim x/H \lesssim 0.14$) decreased by approximately 29% and 46%

at heights $y/H = 0.965$ and 0.95 , when the non-dimensional partition height was increased from 0.0625 to 0.125 . When the non-dimensional top wall temperature was increased to approximately 2.3 , the thermal effect of the partition became stronger, resulting in the location where the upward boundary layer flow along the heated vertical wall turned over to be at $y/H \approx 0.95$ compared to $y/H \approx 0.93$ in the cavities with the smaller partition (Figure 5.4 (b)) or without the partition (Figure 5.4 (a)). In this case, the non-dimensional temperature of the partition, estimated as a fin with uniform cross section [102], was close to the heated vertical wall (≈ 1), which is significantly less than the non-dimensional top wall temperature of 2.3 . Hence, the local temperature gradient along the upward direction in this region was significantly decreased by the partition, resulting in an increase of the local buoyancy force in the upward boundary layer flow along the heated vertical wall, which would cause an increase in the vertical momentum of the boundary layer flow.

Variation of the non-dimensional ambient temperature outside of the boundary layer with height for cases with and without the partition at $y/H = 0.95$ is shown in Figure 5.7. In the partitioned cavity, similar to the results in the cavity without the partition, the ambient temperature outside of the boundary layer increased approximately linearly with the height over most of the cavity. With an increase of the top wall temperature, the local ambient temperature outside the boundary layer increased. For the case with the insulated top wall, the local ambient temperature outside the boundary layer in the partitioned cavity was approximately the same as that in the cavity without the partition. In the partitioned cavity with the insulated top wall (Figure 5.2), the partition with the non-dimensional partition height of 0.0625 only affected the flow and temperature fields in the vicinity of the partition, while the most part of the cavity was not affected by the presence of the partition.

The non-dimensional ambient temperature distributions outside of the bound-

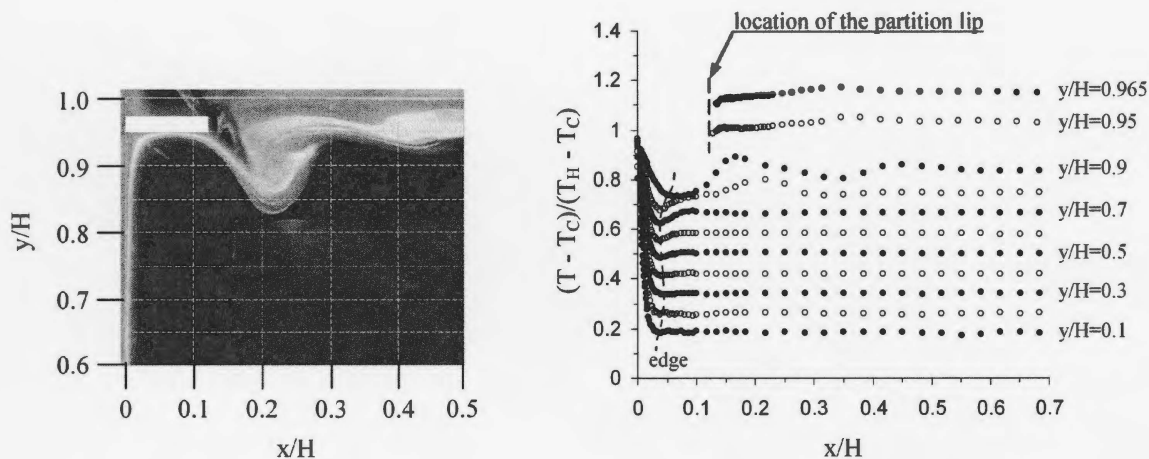


Figure 5.5: Flow pattern in the upper left region of the square cavity (Left) and non-dimensional temperature profiles in the square cavity with a partition attached on the heated vertical wall at $y/H = 0.95$ for the non-dimensional top wall temperature of approximately 1.4. The non-dimensional height of the partition was 0.125.

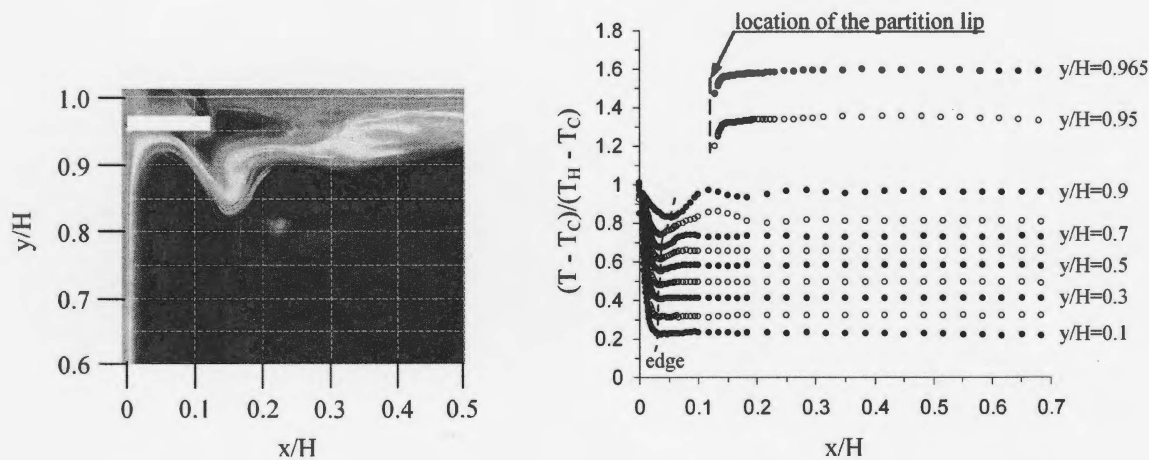


Figure 5.6: Flow pattern in the upper left region of the square cavity (Left) and non-dimensional temperature profiles in the square cavity with a partition attached on the heated vertical wall at $y/H = 0.95$ for the non-dimensional top wall temperature of approximately 2.3. The non-dimensional height of the partition was 0.125.

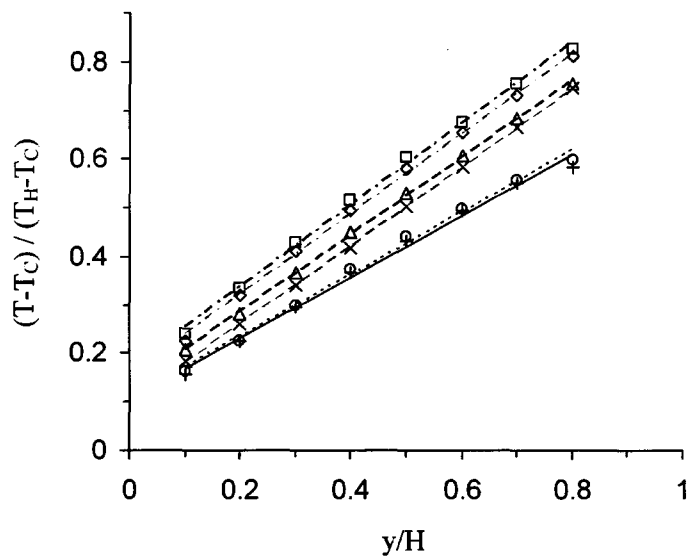


Figure 5.7: Comparison of the non-dimensional ambient temperature outside of the boundary layer for cases with or without a partition on the heated vertical wall at $y/H = 0.95$. Smooth wall cavity with θ_T of +: 0.54 (insulated). Partition with the non-dimensional height of 0.0625 and θ_T of \circ : 0.59 (insulated), \triangle : 1.4, and \square : 2.3. Partition with the non-dimensional height of 0.125 and θ_T of \times : 1.4 and \diamond : 2.3.

ary layer for cases with different partition height are compared to the smooth wall case in Figure 5.8. In general, there were only minor changes in the non-dimensional ambient temperature distributions outside of the boundary layer due to the presence of the partition for both partition heights. For the case with $\theta_T \approx 1.4$ and non-dimensional partition height of 0.0625, the non-dimensional ambient temperature outside of the boundary layer was slightly larger than in the other two cases. Once the upward boundary layer flow along the heated vertical wall separated from the wall, there would be a heat transfer between the top wall and the flow moving along the surface of the top wall. In addition, there could be some secondary energy transfer by the recirculating flow in the corner region. In the cavity with the 0.0625 high partition, the separated flow reattached to the top wall at $x/H \approx 0.2$ compared to $x/H \approx 0.3$ in the cavity without the partition. As a result, there could be more heat transfer into the flow along the top wall in the cavity with the smaller partition compared to that without the partition. When the height of the partition was increased to 0.125, the size of the recirculating flow between the partition and the separated flow decreased, while the location of the flow reattachment on the top wall was approximately the same (at $x/H \approx 0.2$) as for the smaller partition. Hence, with an increase of the partition height, the heat transfer from the top wall to the separated flow decreased slightly.

As θ_T was increased to 2.3, the non-dimensional ambient temperature outside the boundary layer in the cavity with the non-dimensional partition height of 0.125 was slightly lower than that in the other two cases. The larger partition caused the recirculating flow between the partition and the separated flow to be smaller than in the other two cases, so that less energy was transferred from the top wall to the separated flow. The smaller partition did not cause too much change in the recirculating flow compared to that in the cavity without the partition, thus the

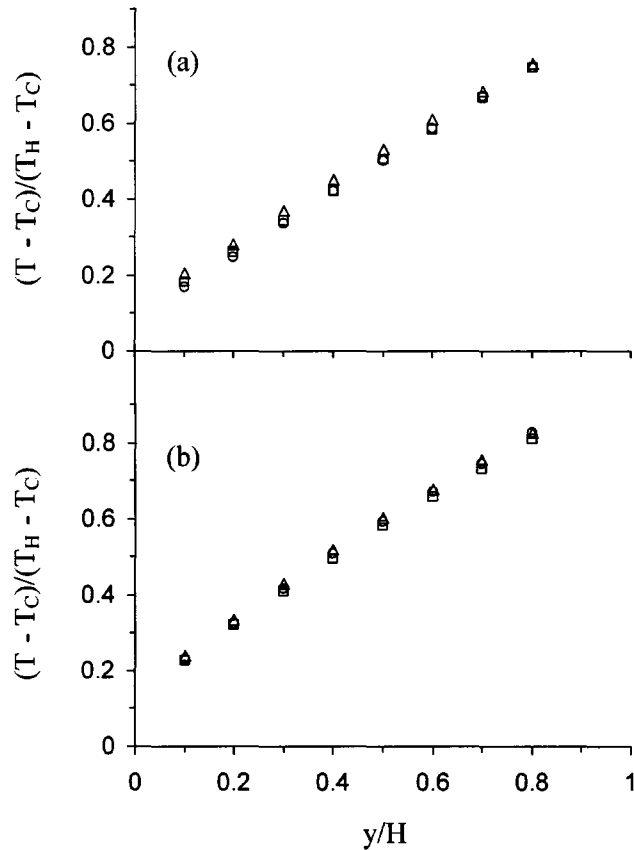


Figure 5.8: Comparison of the non-dimensional ambient temperature outside of the boundary layer for cases with the non-dimensional top wall temperatures of (a) 1.4 and (b) 2.3. ○: without partition, △: the partition with the non-dimensional height of 0.0625 on the heated vertical wall at $y/H = 0.95$, □: the partition with the non-dimensional height of 0.125 on the heated vertical wall at $y/H = 0.95$.

energy from the top wall into the separated flow should be similar in these two cases. Hence, there is no obvious difference in the non-dimensional ambient temperature outside the boundary layer in the cases with the smaller partition and without the partition.

The variation in the local Nusselt number along the heated vertical wall without and with the partition at $y/H = 0.95$ for the different top wall temperatures are shown in Figure 5.9. There were no discernable changes in the variation of the local Nusselt number in the cavities without and with the 0.0625 high partition for an insulated top wall. This is consistent with the flow visualizations and temperature distributions which showed nearly no changes in the flow pattern and temperature field in most of the cavity due to the partition, except in the vicinity of the partition.

When the top wall of the partitioned cavity was heated ($\theta_T \approx 1.4$ and 2.3), the Nusselt number at $y/H \gtrsim 0.7$ significantly increased due to the secondary flow between the undulating flow and the upward boundary layer flow on the heated vertical wall. At $y/H \lesssim 0.4$, there is no significant change in the Nusselt number with an increase of the top wall temperature of the partitioned cavities. However, at $y/H \gtrsim 0.5$, the local Nusselt number increased with an increase of the top wall temperature. This is due to the reduction of the blockage effect of the partition. With an increase of the non-dimensional top wall temperature, the y -location where the upward boundary layer flow separated from the heated vertical wall and turned over decreased, until it was lower than the location of the partition. Thus the blockage effect of the partition on the vertical momentum of the upward flow decreased until it was no longer present. The local Nusselt numbers along the heated vertical wall for partitioned cases with $\theta_T \approx 1.4$ and 2.3 and with different partition heights were also compared to those in the corresponding cases without the partition in Figure 5.9. At $y/H \lesssim 0.5$, the presence of the partition for both partition heights did not

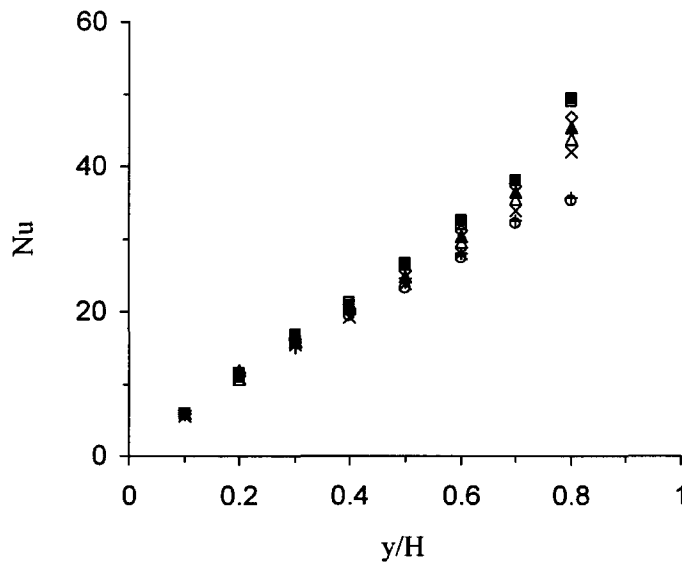


Figure 5.9: Comparison of the local Nusselt number along the heated vertical wall of the square cavity with or without a partition on the heated vertical wall at $y/H = 0.95$. Smooth wall cavity with θ_T of +: 0.54 (insulated), \blacktriangle : 1.4 and \blacksquare : 2.3. Partition with the non-dimensional height of 0.0625 and θ_T of \circ : 0.59 (insulated), \triangle : 1.4, and \square : 2.3. Partition with the non-dimensional height of 0.125 and θ_T of \times : 1.4 and \diamond : 2.3.

result in significant changes in the local Nusselt number compared to that in the cases without the partition. At $y/H \gtrsim 0.6$, there were changes in the local Nusselt number due to the partition and its height. For the case with the non-dimensional top wall temperature of 1.4, the local Nusselt number in the cavity without the partition was larger than that in the partitioned cavities. The Nusselt number decreased with an increase of the partition height due to the blockage effect of the partition on the upward boundary layer flow along the heated vertical wall. With an increase of the top wall temperature, the blockage effect of the partition on the vertical momentum of the upward boundary layer flow decreased, and thus the change in the local Nusselt number with the partition and its height became less significant. For the case with the non-dimensional top wall temperature of 2.3, the partition with the non-dimensional partition height of 0.0625 did not contact the upward boundary layer flow, therefore the Nusselt number in the partitioned cavity was approximately the same as in the cavity without the partition. As the non-dimensional partition height was increased to 0.125, the upward boundary layer flow made some contact with the partition, so the Nusselt number in the region close to the partition was slightly less than in the cases with the smaller partition and without the partition.

The change in the local Nusselt number with the local Rayleigh number for the partitioned cavities with different top wall temperatures is shown in Figure 5.10. The data over most of the heated vertical wall could be correlated by $Nu = C \cdot Ra^n$, except for $y/H \gtrsim 0.7$ due to the secondary flow region. For a given non-dimensional top wall temperature, the values of constant C and index n in the partitioned cavities (shown in Table 5.1) were approximately the same as those in the cavity without the partition (reported in Chapter 4), since the flow and temperature field in most of the partitioned cavity were similar to those in the corresponding cavity without the partition, and the discrepancies mainly appeared in the region close to the partition.

In summary, the results show that the effect of the partition at $y/H = 0.95$ on the laminar natural convection heat transfer characteristics is limited to the region close to the partition ($y/H \gtrsim 0.9$).

5.2 Effect of a partition on the top wall

The flow visualizations of the natural convection flow across the top half of the square cavity with the aluminium partition of $H_P/H = 0.0625$ on the top wall at different locations for non-dimensional top wall temperatures of 0.56 (insulated), 1.4 and 2.3 are presented in Figures 5.11 to 5.13. The detailed experimental conditions are summarized in Table 5.2. For the insulated top wall ($\theta_T \approx 0.56$), the primary effect of the partition was to block the flow, forcing the boundary layer flow along the top wall to separate from the wall. There is a resultant recirculating flow behind the partition as shown in Figure 5.11, similar to that presented by Ciofalo and Karayiannis [81]. The extent of the recirculating flow region decreased as the partition was located away from the heated vertical wall, except for the case with the partition at $x/H = 0.1$, since the momentum of the boundary layer flow approaching the partition is reduced by the shear stress on the top wall. For the case with the partition at $x/H = 0.1$, the flow in the narrow corner region between the partition and the heated vertical wall resulted in the upward boundary layer flow along the heated vertical wall to turn over and pass by the lip of the partition before reaching the top wall. Hence, the recirculating flow region behind the partition at $x/H = 0.1$ was smaller compared to that in the case with the partition at $x/H = 0.2$.

When the top wall was heated, the flow pattern changed significantly, especially in the region near the top wall. For these thermal boundary conditions ($\theta_T \approx 1.4$ and 2.3), the upward natural convection boundary layer flow along the heated vertical

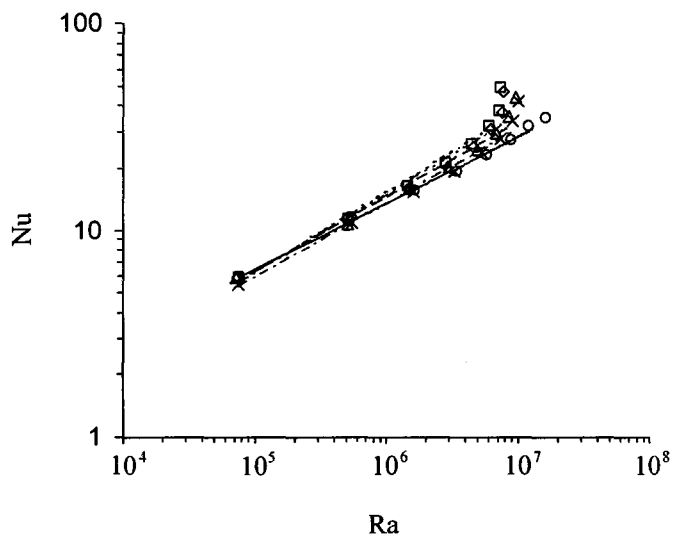


Figure 5.10: Change in the local Nusselt number with the local Rayleigh number for cases with a partition on the heated vertical wall at $y/H = 0.95$. Partition with the non-dimensional height of 0.0625 and θ_T of \circ : 0.59 (insulated), \triangle : 1.4 and \square : 2.3. Partition with the non-dimensional height of 0.125 and θ_T of \times : 1.4 and \diamond : 2.3.

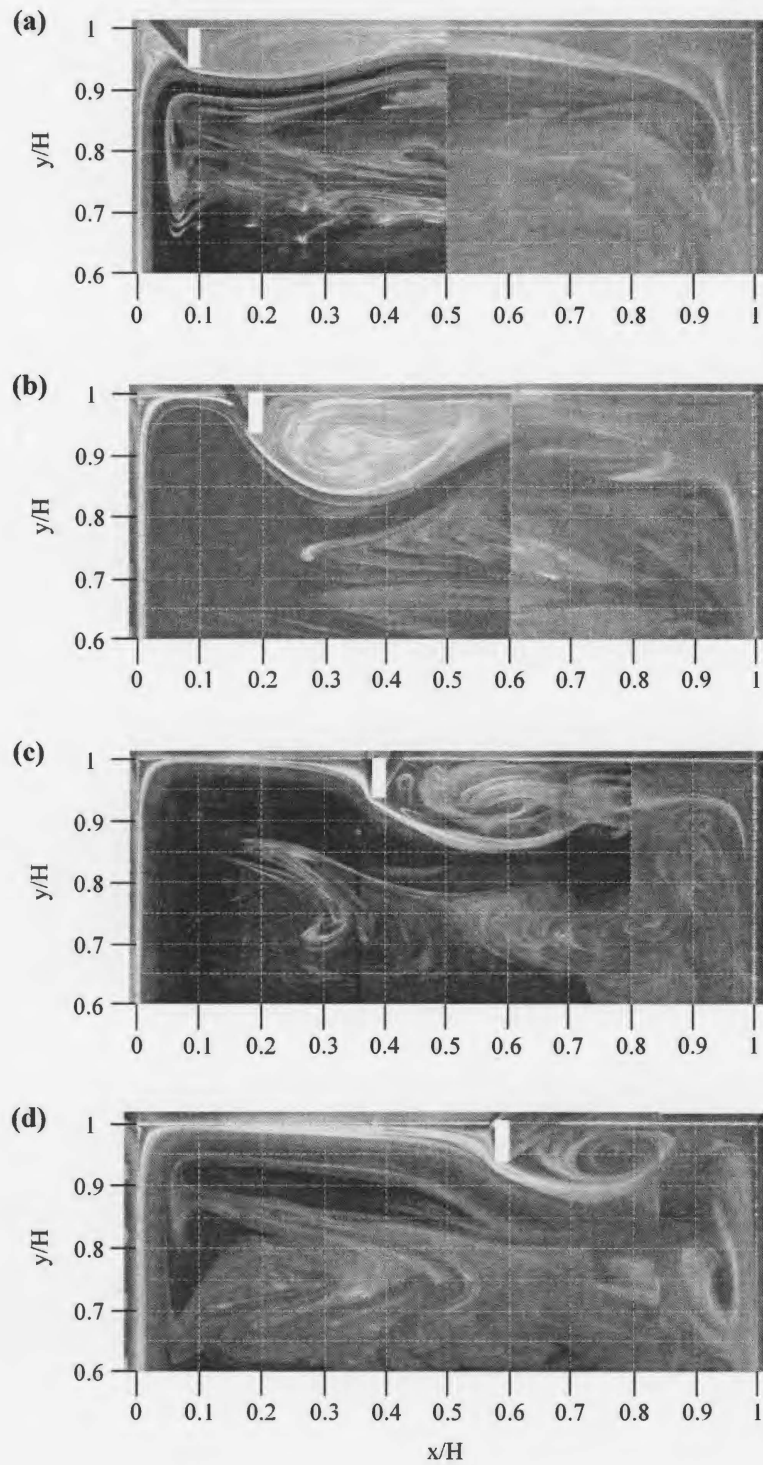


Figure 5.11: Flow patterns across the entire width of the partitioned square cavity for non-dimensional top wall temperature of approximately 0.56 (insulated) with the partition ($H_P/H = 0.0625$) attached at (a) $x/H = 0.1$, (b) $x/H = 0.2$, (c) $x/H = 0.4$ and (d) $x/H = 0.6$.

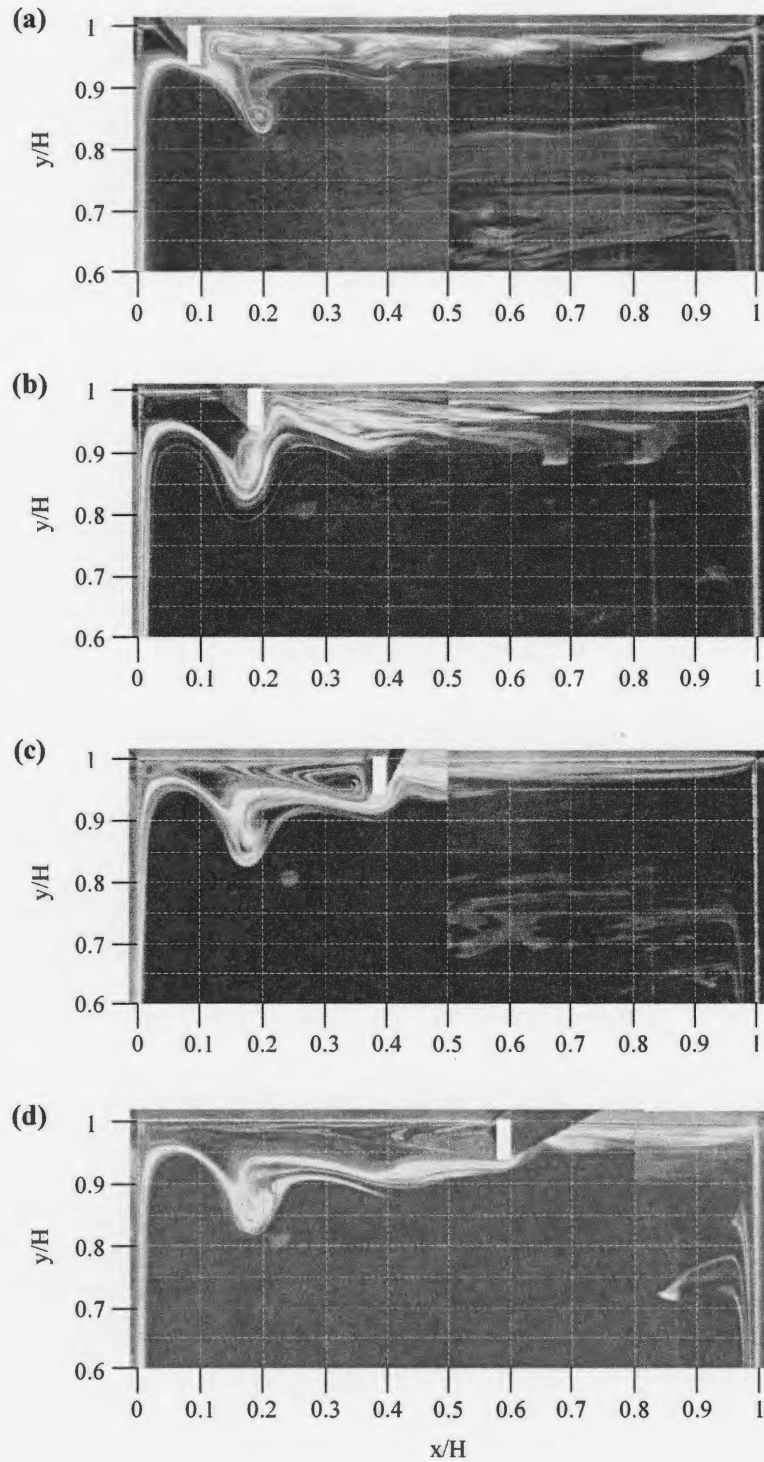


Figure 5.12: Flow patterns across the entire width of the partitioned square cavity for non-dimensional top wall temperature of approximately 1.4 with the partition ($H_P/H = 0.0625$) attached at (a) $x/H = 0.1$, (b) $x/H = 0.2$, (c) $x/H = 0.4$ and (d) $x/H = 0.6$.

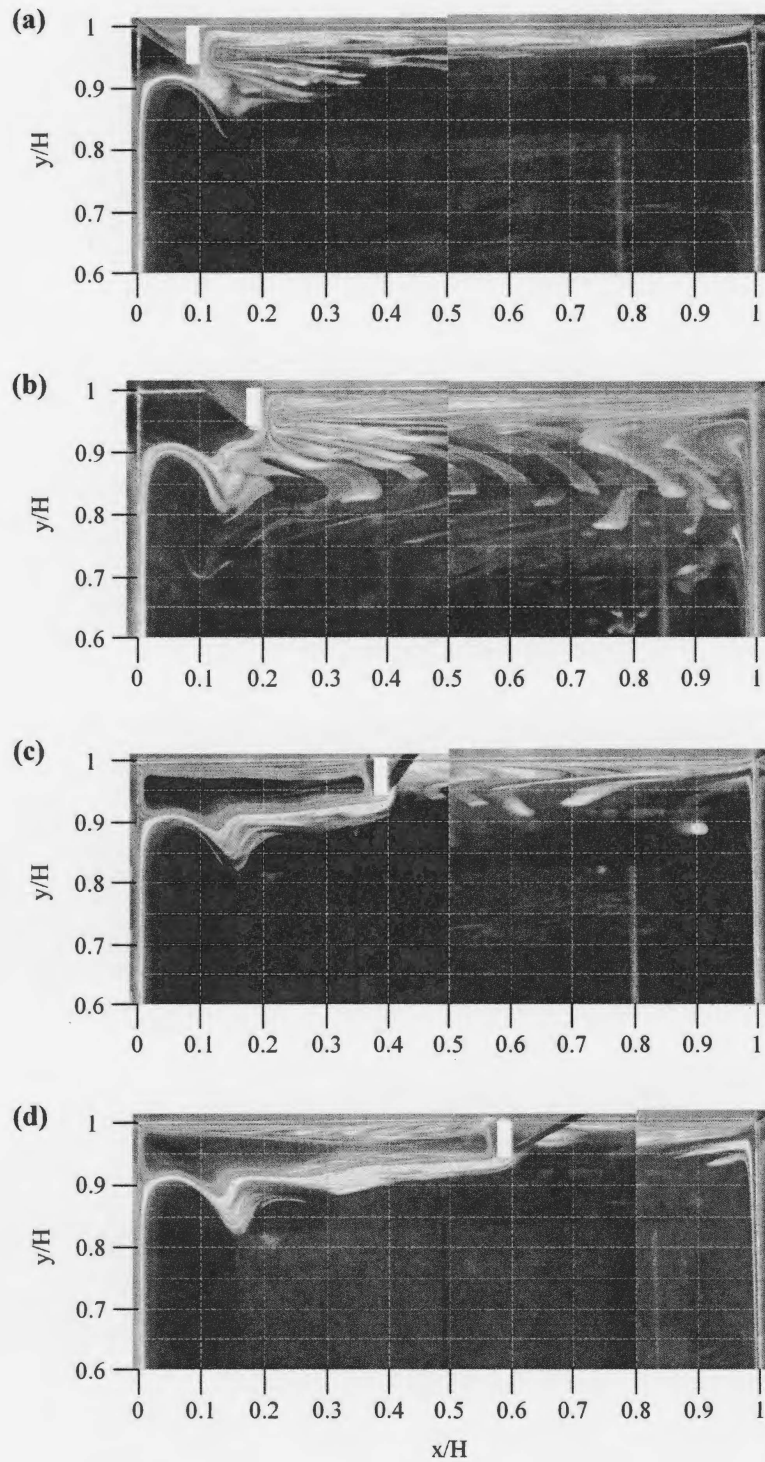


Figure 5.13: Flow patterns across the entire width of the partitioned square cavity for non-dimensional top wall temperature of approximately 2.3 with the partition ($H_P/H = 0.0625$) attached at (a) $x/H = 0.1$, (b) $x/H = 0.2$, (c) $x/H = 0.4$ and (d) $x/H = 0.6$.

Table 5.2: Summary of the wall temperatures, global Grashof numbers, and parameters in the correlation $Nu = C \cdot Ra^n$ for the square cavity with a partition attached to the top wall at different locations.

Partition		T_H	T_C	T_T	T_B	θ_H	θ_C	θ_T	θ_B	$Gr_H \times 10^{-8}$	n	C
Location	Length	(°C)	(°C)	(°C)	(°C)							
$x/H=0.2$		44	12	30	12	1	0	0.56	0	1.18	0.32	0.16
				(insulated)								
	0.0625	44	9	58	9	1	0	1.40	0	1.32	0.36	0.1
		52	10	105	10	1	0	2.26	0	1.48	0.40	0.06
	0.125	47	10	62	10	1	0	1.41	0	1.35	0.37	0.084
		53	10	107	10	1	0	2.26	0	1.50	0.41	0.053
$x/H=0.6$		42	7	27	7	1	0	0.57	0	1.36	0.32	0.15
				(insulated)								
	0.0625	43	7	57	7	1	0	1.39	0	1.39	0.36	0.1
		51	8	105	8	1	0	2.26	0	1.55	0.40	0.062
	0.125	49	10	63	10	1	0	1.36	0	1.41	0.37	0.085
		57	13	113	13	1	0	2.27	0	1.46	0.41	0.048
$x/H=0.1$		52	16	36	16	1	0	0.56	0	1.21	—	—
				(insulated)								
	0.0625	51	16	65	16	1	0	1.40	0	1.19	—	—
		53	17	99	17	1	0	2.28	0	1.20	—	—
	0.125	49	15	62	15	1	0	1.38	0	1.18	—	—
		53	16	100	16	1	0	2.27	0	1.24	—	—
$x/H=0.4$		51	14	35	14	1	0	0.57	0	1.28	—	—
				(insulated)								
	0.0625	53	17	67	17	1	0	1.39	0	1.20	—	—
		53	17	99	17	1	0	2.28	0	1.20	—	—
	0.125	49	15	62	15	1	0	1.38	0	1.18	—	—
		52	16	98	16	1	0	2.28	0	1.21	—	—
$x/H=0.2$	0.125 (Wooden)	48	12	62	12	1	0	1.39	0	1.29	—	—

wall separated from the wall before reaching the top wall as in the cavity without the partition. For a given top wall temperature, the distance from the top wall to the location where the upward boundary layer flow along the heated vertical wall turned over was slightly larger compared to that in the cases without the partition (Figures 5.3 and 5.4). There was a recirculating flow above the natural convection flow after it separated from the heated vertical wall and bounded by the partition, the top wall and the heated vertical wall. This recirculating flow is likely a secondary natural convection flow driven by the temperature difference between the partition and the heated vertical wall. The structure of this secondary natural convection flow is mainly determined by three factors: (1) the temperature difference between the partition and the heated vertical wall, which is the driving force of the flow; (2) the height of the partition, along which the flow could be accelerated; and (3) the shear stress at the top wall. Therefore, for a given partition height, the structure of the recirculating flow was dependent on the location and temperature of the partition. In the current study, the temperature of the partition, estimated by assuming it to be a fin of uniform cross section [102], approached the top wall temperature. For the non-dimensional top wall temperature of 1.4, the structure of the recirculating flow changed from a single anti-clockwise cell to approximately three cells as the partition was moved from $x/H = 0.1$ to 0.6 (the corresponding change in aspect ratio of the recirculating flow region was from approximately 0.6 to 0.1) due to an increase of the wall shear stress with an increase of distance between the heated vertical wall and the partition. The flow cell between the heated vertical wall and the partition at $x/H = 0.1$ and 0.2 is not very apparent due to the position of the partition and the inability of the laser light sheet to properly illuminate this region. When the non-dimensional top wall temperature was increased to approximately 2.3, as shown in Figure 5.13, the recirculating flow was a single-cell with the partition at $x/H = 0.4$

and 0.6, since the increased top wall temperature caused the non-dimensional temperature difference between the partition and the heated vertical wall to increase from approximately 0.4 to 1.3.

For the cases with $\theta_T \approx 1.4$ and 2.3, there is no flow separation behind the partition as in the case with the insulated top wall. At these large top wall temperatures, the upward boundary layer flow along the heated vertical wall separated and turned over before reaching the top wall, with the separated flow generally below the lip of the partition (Figures 5.12 and 5.13). In these cases, the flow attached and flowed up along the rear surface of the partition. This can be attributed to the positive buoyancy force induced by the temperature difference between the partition and the ambient air. The flow pattern on the rear surface of the partition is not very distinct in the figures when the partition was at $x/H = 0.4$ and 0.6, since the partition partially blocked the laser light sheet at these two positions. For the case with the partition at $x/H = 0.1$ and non-dimensional top wall temperatures of 1.4 and 2.3, the undulating flow at $x/H \approx 0.1$ to 0.2 moved back and flowed up along the rear surface of the partition due to the thermal effect of the partition. As a result, the shape of the undulating flow (at $x/H \approx 0.1$ to 0.2) was different from that in the cases with the partition at $x/H = 0.2, 0.4$ and 0.6 or without the partition (Figures 5.3 and 5.4).

The flow patterns with the increased height of the aluminium partition ($H_P/H = 0.125$) for non-dimensional top wall temperatures of 1.4 and 2.3 are shown in Figures 5.14 and 5.15, respectively. With an increase of the partition height, the increased surface along which the recirculating flow between the partition and the heated vertical wall was accelerated would result in the momentum of the recirculating flow to be increased compared to that in the case with the smaller partition. For the case with the non-dimensional top wall temperature of approximately 1.4 and partition

at $x/H = 0.2$, the increased partition height resulted in the undulating flow to be partially blocked. As a result, the flow separated from the lip of the partition, and then reattached and flowed up along the rear surface of the partition. For the cases with the partition at $x/H = 0.1$ and 0.2 and non-dimensional top wall temperature of approximately 2.3, the flow turned around and flowed up along the rear surface of the partition without any separation near the lip of the partition, unlike for the cases with the lower top wall temperature (Figures 5.14 (a) and (b)). This is due to the effect of the top wall temperature on the momentum of the flow approaching the partition. With an increase of the top wall temperature, the corresponding increase in the temperature of the partition will result in an increase in the momentum of the recirculating flow between the partition and the heated vertical wall, which in turn would affect the momentum of the separated flow near the corner region. In addition, the increased top wall temperature would decrease the vertical momentum of the upward boundary layer flow along the heated vertical wall as shown in Figure 4.21.

To verify that the air flow along the rear surface of the aluminium partition attached to the top wall (Figures 5.12 to 5.15) was not due to the coanda effect, an experiment was performed with a wooden partition attached to the top wall at $x/H = 0.2$. In this case, the non-dimensional height of the wooden partition was 0.125 and the non-dimensional top wall temperature of the cavity was approximately 1.4. The average non-dimensional temperature of the partition, measured by thermocouples in the wooden partition, was approximately 0.71 which is significantly lower than the top wall temperature. As shown in Figure 5.16, the flow separated from the rear surface of the wooden partition with no attached flow, which is different from the result shown in Figure 5.14 (b). Thus, it can be confirmed that the thermal effect of the aluminium partition caused the flow to move up along the rear surface of the

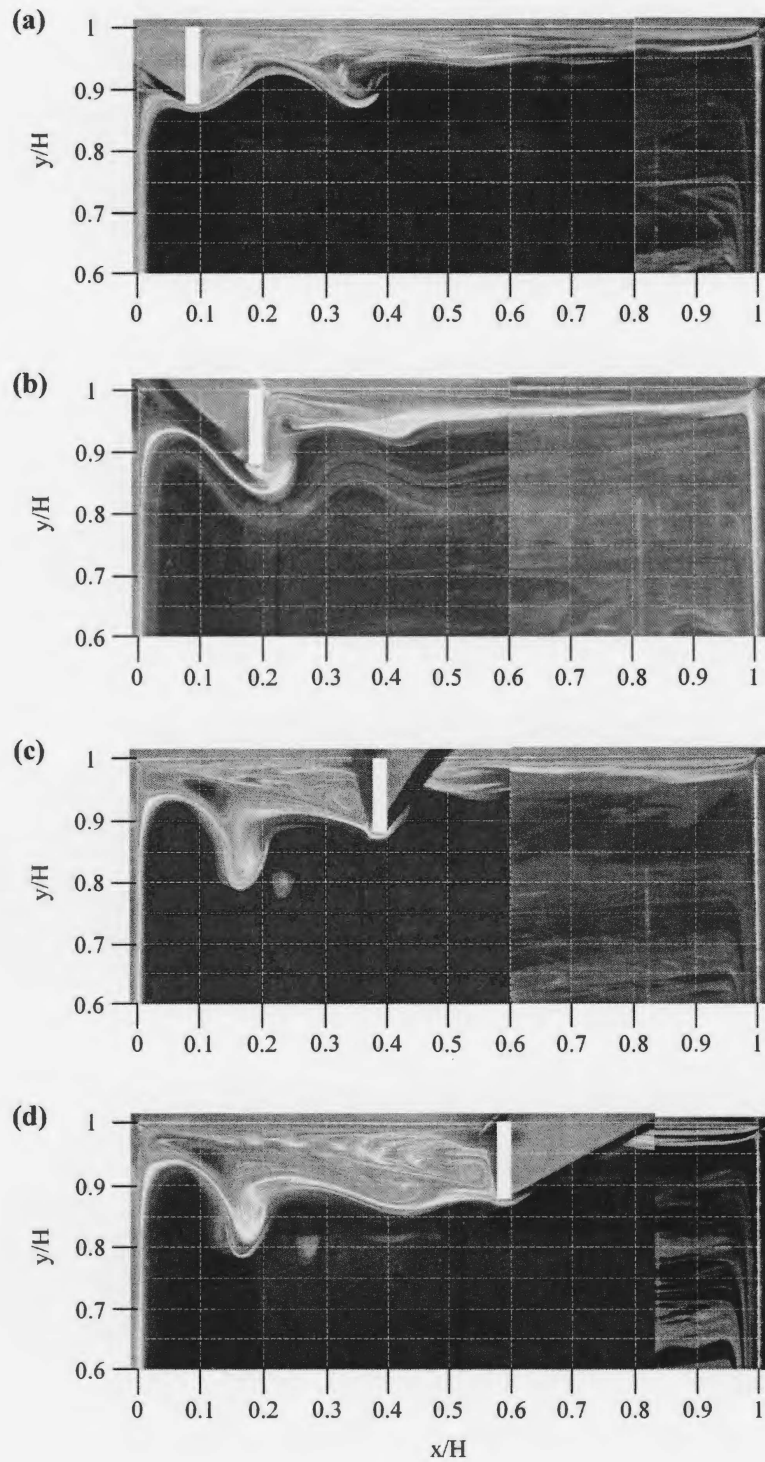


Figure 5.14: Flow patterns across the entire width of the partitioned square cavity for non-dimensional top wall temperature of approximately 1.4 with the partition ($H_P/H = 0.125$) attached at (a) $x/H = 0.1$, (b) $x/H = 0.2$, (c) $x/H = 0.4$ and (d) $x/H = 0.6$.

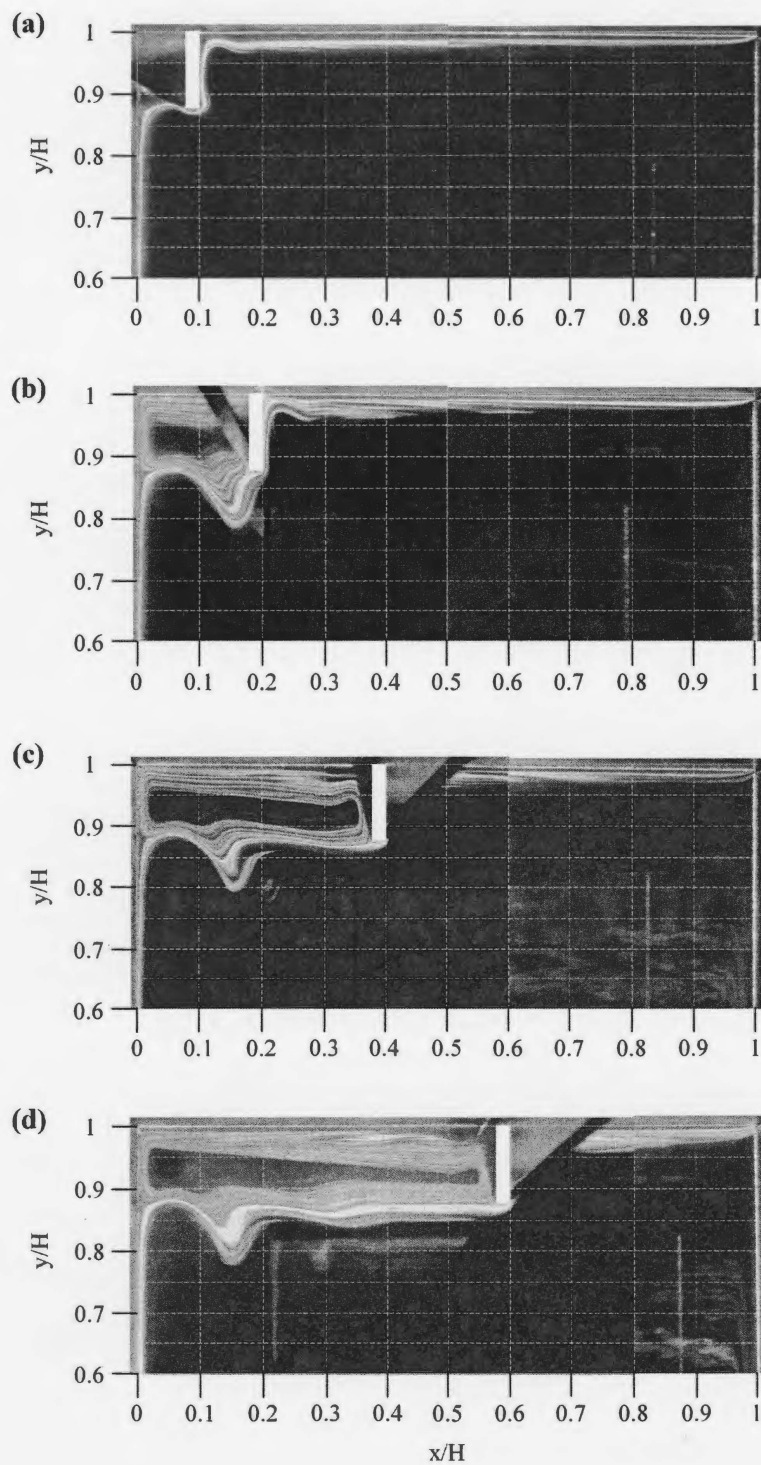


Figure 5.15: Flow patterns across the entire width of the partitioned square cavity for non-dimensional top wall temperature of approximately 2.3 with the partition ($H_P/H = 0.125$) attached at (a) $x/H = 0.1$, (b) $x/H = 0.2$, (c) $x/H = 0.4$ and (d) $x/H = 0.6$.

partition.

The temperature profiles along the heated vertical wall of the partitioned cavities and the rear surface of the partition are compared to those in the square cavity without the partition in Figures 5.17 to 5.19 for the smaller partition at $x/H = 0.2$ and 0.6 . Along most of the heated vertical wall, the partition had no significant effect on the temperature profiles, except in the region close to the partition where the flow pattern was changed due to the presence of the partition as shown in Figures 5.11 to 5.13. At $y/H \lesssim 0.7$ for the insulated top wall and $y/H \lesssim 0.9$ for the heated top wall, the discrepancies in the temperature distributions between the cavities with and without the partition on the top wall are less than 9%. For the insulated top wall case, the mixing due to the recirculating flow behind the partition resulted in the local temperature in this region ($y/H = 0.95$ and 0.965) to be approximately uniform. For the partition at $x/H = 0.2$ (Figure 5.17 (b)), the uniformity in the temperature is in the region $0.2 \lesssim x/H \lesssim 0.45$, which corresponds to the location of the recirculating flow behind the partition. With the partition at $x/H = 0.6$ (Figure 5.17 (c)), the region of the uniformity in the temperature moved to $x/H \approx 0.6$ to 0.7 . For the case with the insulated top wall, the average temperature of the top wall was lower than the temperature of the air flow along the wall, resulting in an energy transfer into the wall from the flow. As a result, the local air temperature at $y/H = 0.95$ and 0.965 in the recirculating flow region behind the partition ($0.2 \lesssim x/H \lesssim 0.45$ for the partition at $x/H = 0.2$ and $0.6 \lesssim x/H \lesssim 0.7$ for the partition at $x/H = 0.6$) was lower than that at $y/H = 0.9$. For the case without the partition (Figure 5.17 (a)), at $x/H \gtrsim 0.3$, the local temperature at $y/H = 0.95$ was larger than that at $y/H = 0.965$. The flow separation behind the partition at $x/H = 0.2$ is reflected in the non-uniformity in the temperature profiles at $y/H = 0.8$ and 0.9 in the region $0.2 \lesssim x/H \lesssim 0.3$.

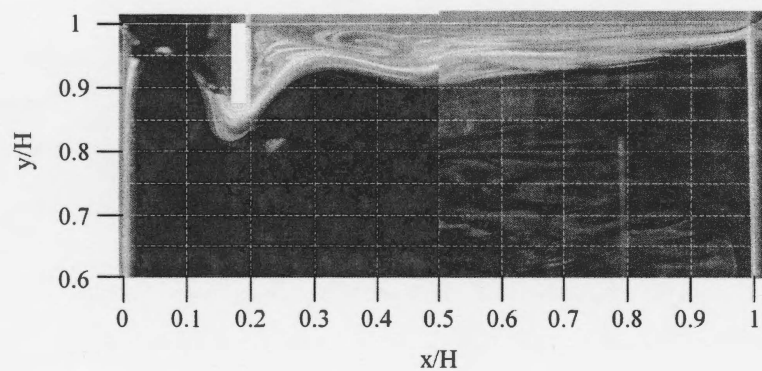


Figure 5.16: Flow pattern across the entire width of the partitioned square cavity for non-dimensional top wall temperature of approximately 1.4 with a wooden partition ($H_P/H = 0.125$) attached on the top wall at $x/H = 0.2$.

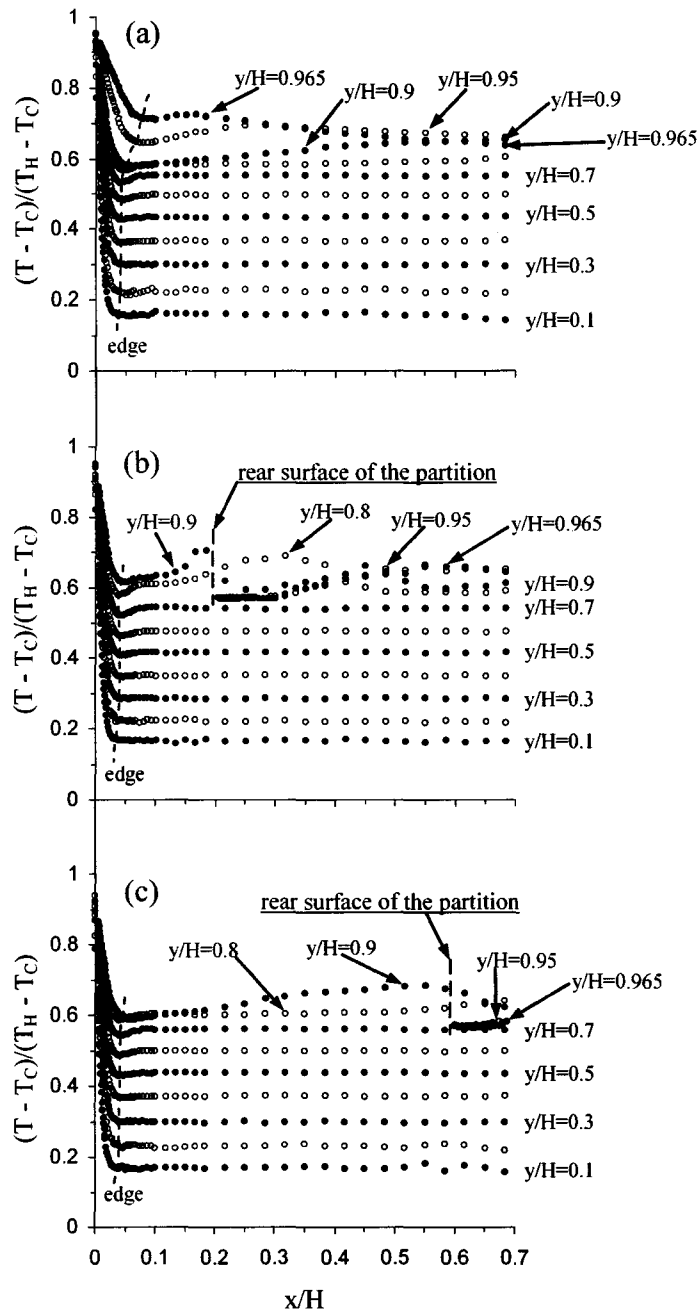


Figure 5.17: Non-dimensional temperature profiles along the heated vertical wall of the square cavity (a) without the partition and with the partition on the top wall (b) at $x/H = 0.2$ and (c) at $x/H = 0.6$ for non-dimensional top wall temperature of approximately 0.56 (insulated). Here, the non-dimensional height of the partition was 0.0625.

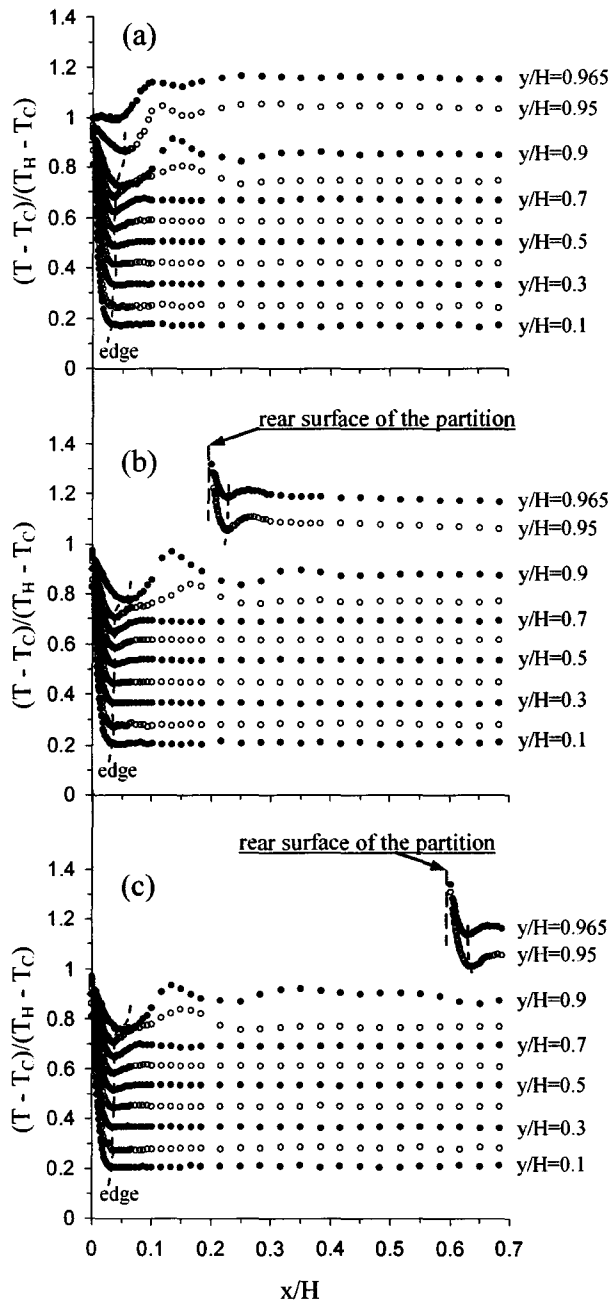


Figure 5.18: Non-dimensional temperature profiles along the heated vertical wall of the square cavity (a) without the partition and with the partition on the top wall (b) at $x/H = 0.2$ and (c) at $x/H = 0.6$ for non-dimensional top wall temperature of approximately 1.4. Here, the non-dimensional height of the partition was 0.0625.

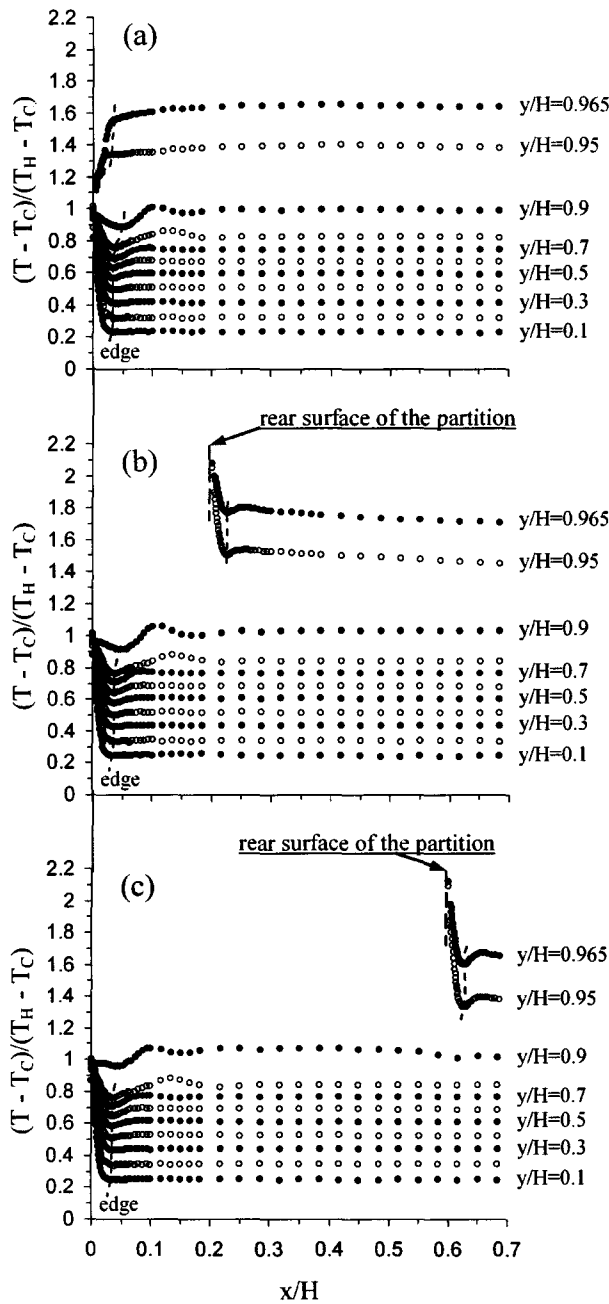


Figure 5.19: Non-dimensional temperature profiles along the heated vertical wall of the square cavity (a) without the partition and with the partition on the top wall (b) at $x/H = 0.2$ and (c) at $x/H = 0.6$ for non-dimensional top wall temperature of approximately 2.3. Here, the non-dimensional height of the partition was 0.0625.

For the partitioned cavities with non-dimensional top wall temperatures of approximately 1.4 and 2.3, a thermal boundary layer developed along the rear surface of the partition as shown by the temperature profiles in Figures 5.18 (b, c) and 5.19 (b, c). The temperature gradient near the rear surface of the partition was increased with an increase of the top wall temperature. For example, for the case with the partition at $x/H = 0.2$, the temperature gradients in the region $0.2 \lesssim x/H \lesssim 0.21$ at heights $y/H = 0.965$ and 0.95 respectively increased by approximately 190% and 220% when the non-dimensional top wall temperature increased from approximately 1.4 to 2.3. For the case with the partition at $x/H = 0.6$, the increase in the temperature gradients ($0.6 \lesssim x/H \lesssim 0.61$) at the two heights were approximately 230% and 310%, respectively. For the cavity with the partition at $x/H = 0.2$ and non-dimensional top wall temperature of 1.4 (Figure 5.18 (b)), the discrepancy in the local ambient temperatures just outside the boundary layer ($0.06 \lesssim x/H \lesssim 0.08$) at heights $y/H = 0.8$ and 0.9 was approximately 7%. With the partition at $x/H = 0.6$ (Figure 5.18 (c)), the discrepancy in the local ambient temperature in the same region ($0.06 \lesssim x/H \lesssim 0.08$ and $y/H = 0.8$ to 0.9) was less than 2% as that without the partition (Figure 5.18 (a)). These results indicate that the mixing effect of the secondary flow between the boundary layer flow along the heated vertical wall and the undulating flow is sensitive to the partition location. With an increase of the top wall temperature, the mixing region due to the secondary flow moved down, since the y-location where the upward boundary layer flow along the heated vertical wall turned over decreased. As a result, for the case with the non-dimensional top wall temperature of 2.3, the discrepancy in the ambient temperature in the region $0.06 \lesssim x/H \lesssim 0.08$ between the heights $y/H = 0.8$ and 0.9 was over 13% as shown in Figure 5.19. This discrepancy in the partitioned cavities ($\gtrsim 17\%$) was slightly larger than that in the cavity without the partition ($\approx 13\%$), since the y-location where the upward boundary layer flow along

the heated vertical wall turned over in the partitioned cavities was lower compared to that in the cavity without the partition.

When the non-dimensional height of the aluminium partition was increased to 0.125 (Figures 5.20 and 5.21), the thermal boundary layer along the rear surface of the partition resulted in the temperature distributions in the region close to the rear surface ($0.2 \lesssim x/H \lesssim 0.45$ for the partition at $x/H = 0.2$ and $0.6 \lesssim x/H \lesssim 0.7$ for the partition at $x/H = 0.6$) at $y/H = 0.9$ to be different from those in the cases with the smaller partition (Figures 5.18 and 5.19). At a given top wall temperature, the difference in the local ambient temperature just outside the boundary layer ($0.06 \lesssim x/H \lesssim 0.08$) between the heights of $y/H = 0.7$ and 0.8 became smaller with an increase of the partition height, since the mixing region due to the secondary flow between the boundary layer flow along the heated vertical wall and the undulating flow moved down. For example, for the partitioned cavities with the non-dimensional top wall temperature of approximately 1.4, this difference changed from approximately 9% to 7%, when the non-dimensional partition height was increased from 0.0625 to 0.125. With an increase of the top wall temperature, this difference was further reduced and approached zero when the non-dimensional top wall temperature was approximately 2.3 (Figure 5.21). For the case with the non-dimensional top wall temperature of 1.4 and the partition at $x/H = 0.2$ (Figure 5.20 (a)), the location where the temperature was non-uniform was further away from the heated vertical wall at $y/H = 0.8$ compared to the cases with the smaller partition (Figure 5.18 (b)) or different partition location (Figure 5.20 (b)) since the trough of the undulating flow is at $x/H \approx 0.2$ in this case compared to $x/H \approx 0.17$ with the partition at $x/H = 0.6$ or with the smaller partition. For the case with the partition at $x/H = 0.6$ and non-dimensional top wall temperature of 2.3, the temperature profile indicates a boundary layer flow moving downward along the heated vertical wall at $y/H = 0.9$ (Figure 5.21

(b)). This is due to the expansion of the recirculating flow between the heated vertical wall and the partition (Figure 5.15 (d)) with the increases of the top wall temperature and partition height. A similar thermal boundary layer was also observed in the upper left corner region of the cavity without the partition under the same non-dimensional top wall temperature as shown in Figure 5.19 (a). In this case, there is a recirculating flow between the heated vertical wall and the separated flow.

The effect of the partition with non-dimensional height of 0.0625 on the variation of the non-dimensional ambient temperature outside the boundary layer with height for the insulated top wall is shown in Figure 5.22. As expected, the ambient temperature outside the boundary layer increased approximately linearly with the height over most of the cavity. The partition at $x/H = 0.2$ resulted in the non-dimensional ambient temperature outside the boundary layer to be generally lower than that without the partition or with the partition at $x/H = 0.6$. This can be attributed to the larger recirculating flow behind the partition at $x/H = 0.2$ which could result in a higher energy transfer to the top wall compared to that in the other two cases. When the partition was at $x/H = 0.6$, the extent of the recirculating flow behind the partition was smaller, hence there is nearly no difference in the local ambient temperature outside the boundary layer compared to the cavity without the partition.

When the top wall was heated, the non-dimensional ambient temperature outside the boundary layer was nearly independent of the partition location for the investigated cases as shown in Figure 5.23. For the case with the non-dimensional top wall temperature of 1.4 (Figure 5.23 (a)), the ambient temperature outside the boundary layer in the cavity without the partition was lower than that in the partitioned cavities, indicating that the recirculating flow in the corner of the partitioned cavities transferred more heat from the top wall and the partition to the separated

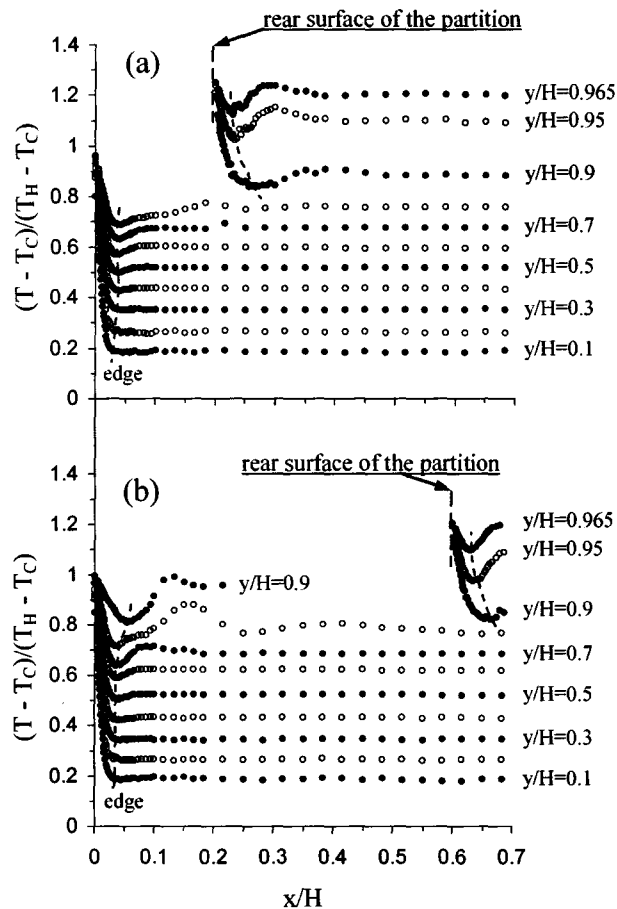


Figure 5.20: Non-dimensional temperature profiles along the heated vertical wall of the square cavity with the partition on the top wall (a) at $x/H = 0.2$ and (b) at $x/H = 0.6$ for non-dimensional top wall temperature of approximately 1.4. Here, the non-dimensional height of the partition was 0.125.

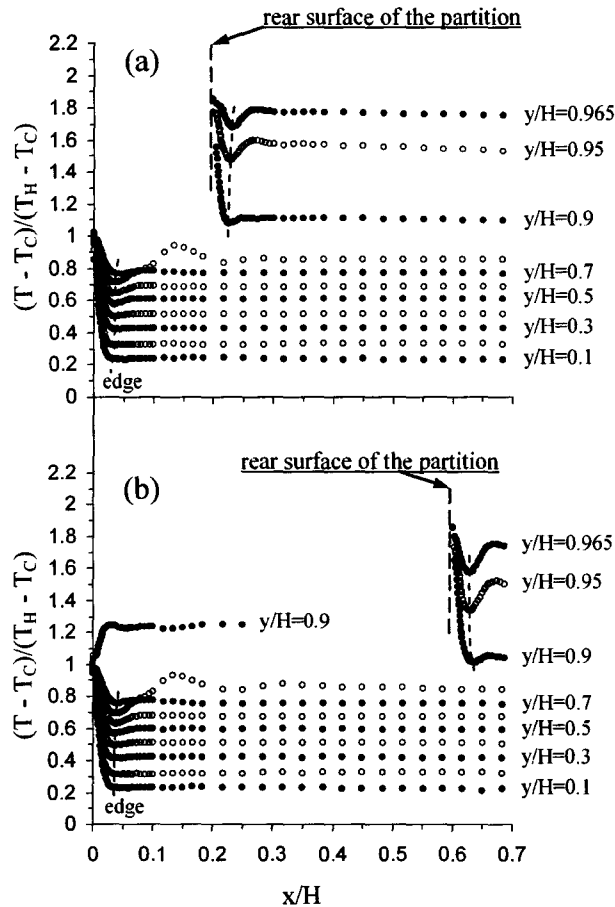


Figure 5.21: Non-dimensional temperature profiles along the heated vertical wall of the square cavity with the partition on the top wall (a) at $x/H = 0.2$ and (b) at $x/H = 0.6$ for non-dimensional top wall temperature of approximately 2.3. Here, the non-dimensional height of the partition was 0.125.

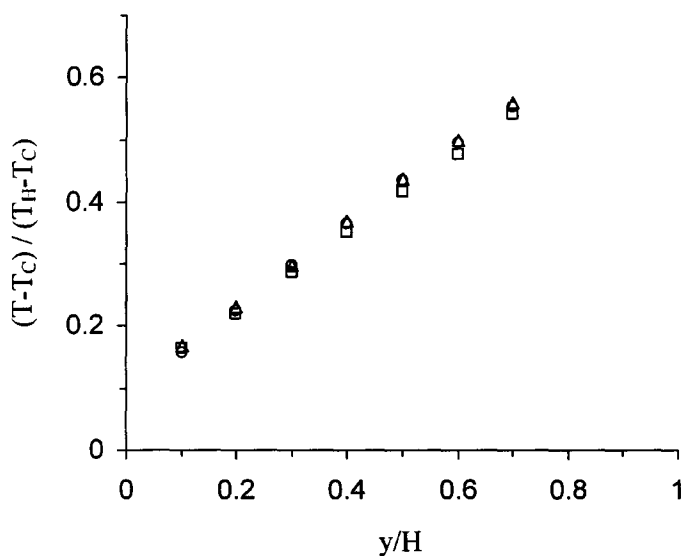


Figure 5.22: Comparison of the non-dimensional temperature outside of the boundary layer for cases with the non-dimensional top wall temperature of approximately 0.56 (insulated). \circ : without the partition, \square : the partition on the top wall at $x/H = 0.2$, and \triangle : the partition on the top wall at $x/H = 0.6$. Here, the non-dimensional height of the partition was 0.0625.

natural convection flow. For the case with the non-dimensional top wall temperature of approximately 2.3 (Figure 5.23 (b)), the difference in the local ambient temperature outside the boundary layer between the cavities with and without the partition reduced since a recirculating flow occurred in the corner region of the cavity without the partition.

The effect of the partition height on the ambient air temperature outside the boundary layer is presented in Figure 5.24. An increase in the partition height caused the ambient temperature outside the boundary layer in the region close to the bottom wall to decrease. For the case with the non-dimensional top wall temperature of 2.3, at $y/H > 0.7$, the non-dimensional ambient temperature outside the boundary layer in the cavity with the larger partition was slightly greater than that in the cavity with the smaller partition. For the partition at $x/H = 0.6$, the increase of the partition height resulted in the momentum and extent of the recirculating flow to be increased. When the partition was at $x/H = 0.2$, in addition, there would be more energy transfer into the natural convection flow from the rear surface of the partition with an increase of the partition height.

The corresponding variations of the local Nusselt number along the heated vertical wall are shown in Figures 5.25 to 5.27. At $y/H \lesssim 0.6$, there is no significant change in the local Nusselt number with changes in the top wall temperature or the partition height and location, indicating the effects of these factors on the vertical momentum of the upward boundary layer flow along the heated vertical wall and the temperature gradient at the surface of the heated vertical wall were similar. For the case with the insulated top wall (Figure 5.25), the position of the partition on the top wall affected the local Nusselt number in the region near the top of the heated vertical wall. At $y/H \gtrsim 0.7$, the local Nusselt number in the cavity with partition at $x/H = 0.2$ was lower than that in the cavities with the partition at

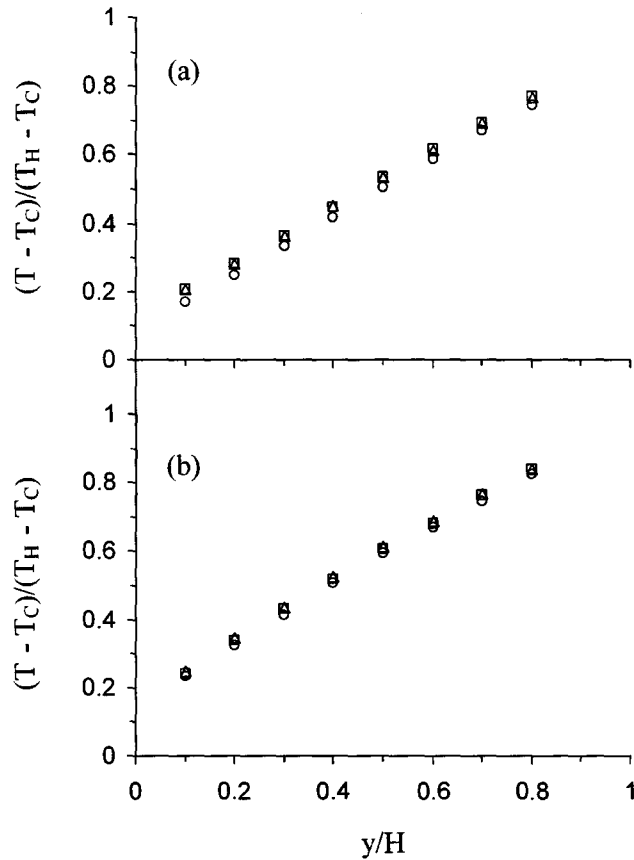


Figure 5.23: Comparison of the non-dimensional temperature outside of the boundary layer for cases with non-dimensional top wall temperatures of (a) 1.4 and (b) 2.3. ○: without the partition, □: the partition on the top wall at $x/H = 0.2$, and △: the partition on the top wall at $x/H = 0.6$. Here, the non-dimensional height of the partition was 0.0625.

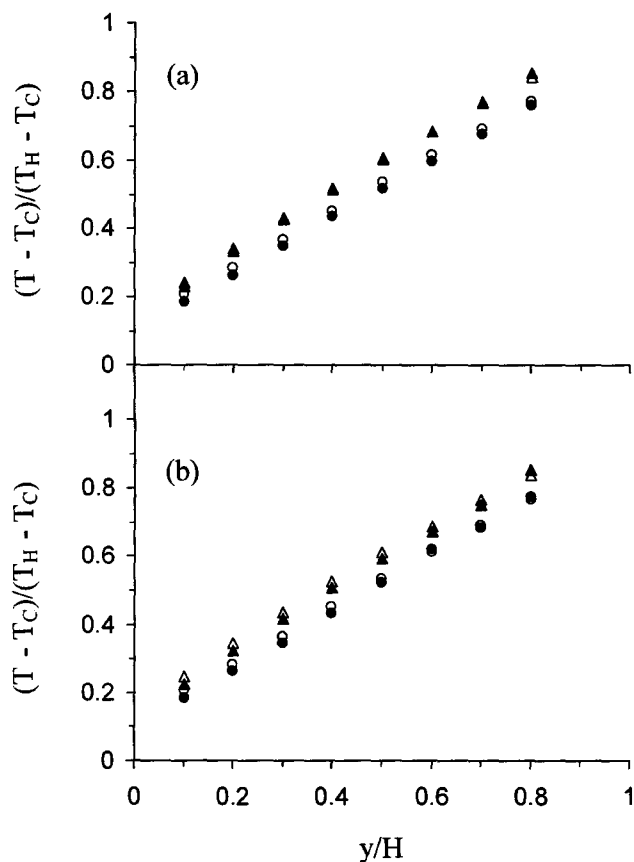


Figure 5.24: Comparison of the non-dimensional temperature outside of the boundary layer for cases with the partition on the top wall at (a) $x/H = 0.2$ and (b) $x/H = 0.6$. The non-dimensional heights of the partitions were 0.0625 (open symbols) and 0.125 (filled symbols), respectively. ○: under the non-dimensional top wall temperature of 1.4, and △: under the non-dimensional top wall temperature of 2.3.

$x/H = 0.6$ and without the partition, since the partition near the corner of the cavity reduced the momentum of the natural convection flow in this corner region. For the cavity with the partition at $x/H = 0.6$, in the region close to the top wall, the local Nusselt number was larger than that in the cavity without the partition, indicating the partition at this location can slightly increase the momentum of the natural convection flow in the corner region of the cavity. This is likely due to the lower temperature of the partition compared to that of the air flow moving along the partition as shown in Figure 5.11 (d). When the top wall was heated (Figure 5.26), at $y/H \gtrsim 0.7$, the local Nusselt number increased significantly due to the effect of the secondary flow between the undulating flow and the boundary layer flow on the heated vertical wall. In the region close to the top wall, the local Nusselt number in the cavity without the partition was slightly larger than that in the partitioned cavities due to the recirculating flow in the corner region of the partitioned cavities.

Similar to the cavity without the partition, at $y/H \gtrsim 0.7$, the local Nusselt number increased with an increase of the top wall temperature (Figure 5.27), indicating in this region the change in the top wall temperature has a larger effect on the vertical momentum of the upward boundary layer flow on the heated vertical wall than the temperature gradient at the surface of the heated vertical wall in the partitioned cavities. For the case with the partition at $x/H = 0.6$, at $y/H > 0.6$, the local Nusselt number with the smaller partition was greater than that in the cavity with the larger partition. This is likely because the momentum of the recirculating flow between the partition and the heated vertical wall increased with an increase of the partition height, which would result in a decrease of the momentum of the upward boundary layer flow along the heated vertical wall near the corner region. However, for the case with the partition close to the heated vertical wall at $x/H = 0.2$, the rear surface of the partition would increase the momentum of the natural convection flow

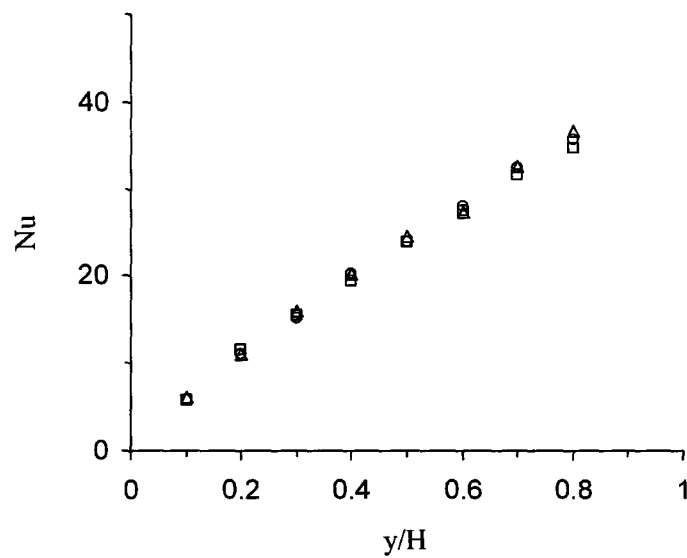


Figure 5.25: Comparison of the local Nusselt number along the heated vertical wall of the square cavity with the non-dimensional top wall temperature of approximately 0.56 (insulated). ○: without the partition, □: the partition on the top wall at $x/H = 0.2$, and △: the partition on the top wall at $x/H = 0.6$. Here, the non-dimensional height of the partition was 0.0625.

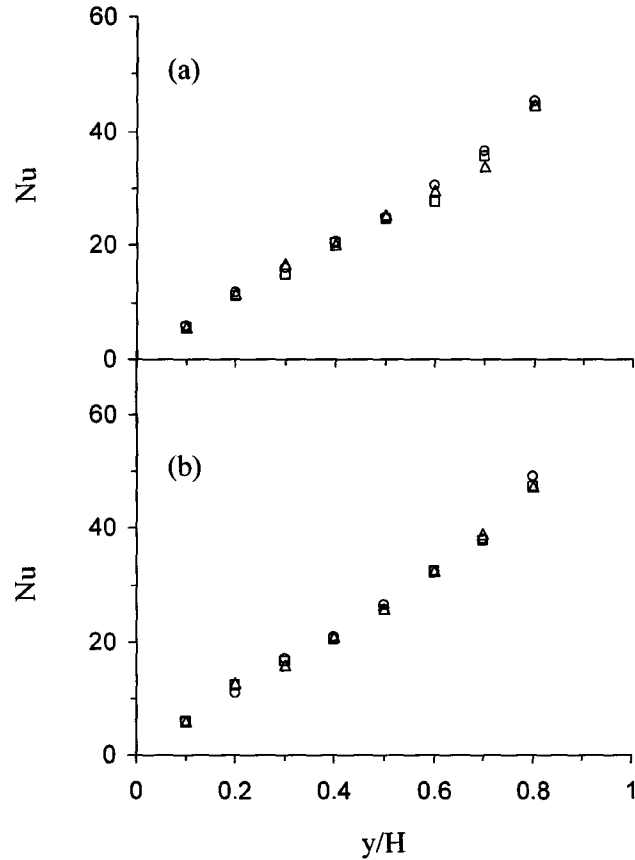


Figure 5.26: Comparison of the local Nusselt number along the heated vertical wall of the square cavity for cases with non-dimensional top wall temperatures of (a) 1.4 and (b) 2.3. ○: without the partition, □: the partition on the top wall at $x/H = 0.2$, and △: the partition on the top wall at $x/H = 0.6$. Here, the non-dimensional height of the partition was 0.0625.

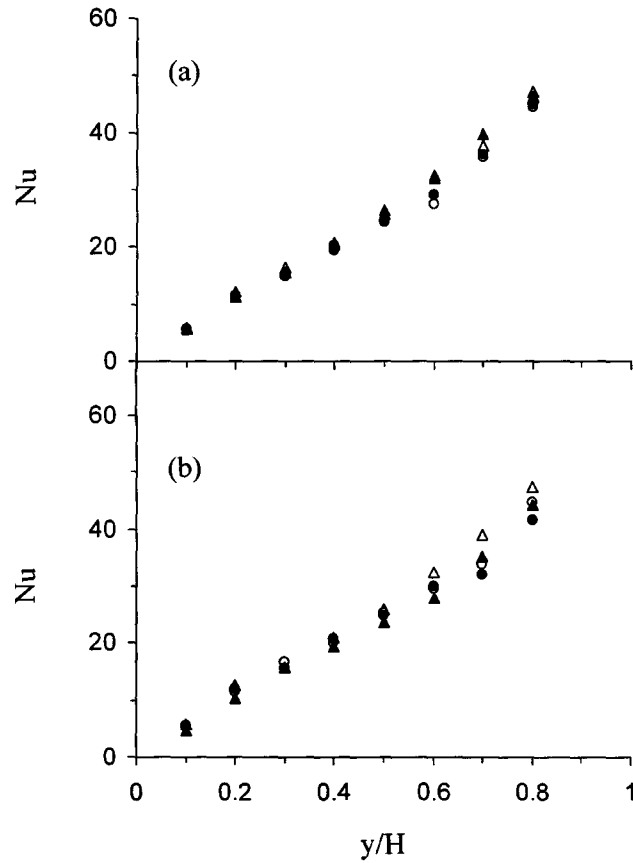


Figure 5.27: Comparison of the local Nusselt number along the heated vertical wall of the square cavity for cases with the partition on the top wall at (a) $x/H = 0.2$ and (b) $x/H = 0.6$. The non-dimensional heights of the partitions were 0.0625 (open symbols) and 0.125 (filled symbols), respectively. \circ : under the non-dimensional top wall temperature of 1.4, and \triangle : under the non-dimensional top wall temperature of 2.3.

near the location of the flow separation from the heated vertical wall. When the non-dimensional top wall temperature was 1.4, at $y/H \gtrsim 0.6$, the local Nusselt number with the larger partition was greater than that with the smaller partition, indicating the effect of the rear surface of the partition on the momentum of the convection flow was larger than the effect of the recirculating flow between the partition and the heated vertical wall. When the non-dimensional top wall temperature increased to 2.3, at $y/H \gtrsim 0.7$, the local Nusselt number decreased with an increase of the partition height, suggesting the effect of the recirculating flow was stronger than the rear surface of the partition with the increase of the partition height.

Finally, the change in the local Nusselt number with the local Rayleigh number is shown in Figure 5.28. Similar to the cavity without the partition, the data in the region $y/H \lesssim 0.7$ could be correlated by $Nu = C \cdot Ra^n$. At $y/H > 0.7$, the secondary flow between the undulating flow and the boundary layer flow on the heated vertical wall resulted in the local Nusselt number to increase significantly for the cases with the heated top wall. With the changes in the top wall temperature and partition height, the values of the constant C and the index n changed as shown in Table 5.2. For a given partition location and height, the value of the index n increased with an increase of the top wall temperature, similar to that in the cavity without the partition. For the cases with the insulated top wall, the values of the constant C and the index n in the cavity with the partition at $x/H = 0.6$ were approximately the same as those in the cavity without the partition. This partition was away from the heated vertical wall so the flow patterns in most of these two cavities were similar. In the cavity with the partition at $x/H = 0.2$, the values of C and n were approximately the same as those in the smooth walls cavity with the non-dimensional top wall temperature of 0.83. The blockage effect of the partition at $x/H = 0.2$ resulted in the flow patterns in these two cases to be similar. For the cases with the increased top wall temperature,

the partition with the non-dimensional height of 0.0625 at either $x/H = 0.2$ or 0.6 did not cause significant difference in the correlation compared to that in the cavity without the partition, since the partition mainly affected the natural convection flow in the region close to the top wall of the cavity. When the non-dimensional height of the partition was increased to 0.125, the value of the index n became slightly larger than that in the cavity with the smaller partition. For the cases with the heated top wall, the values of the constant C and the index n were nearly independent of the partition location for the currently investigated cases.

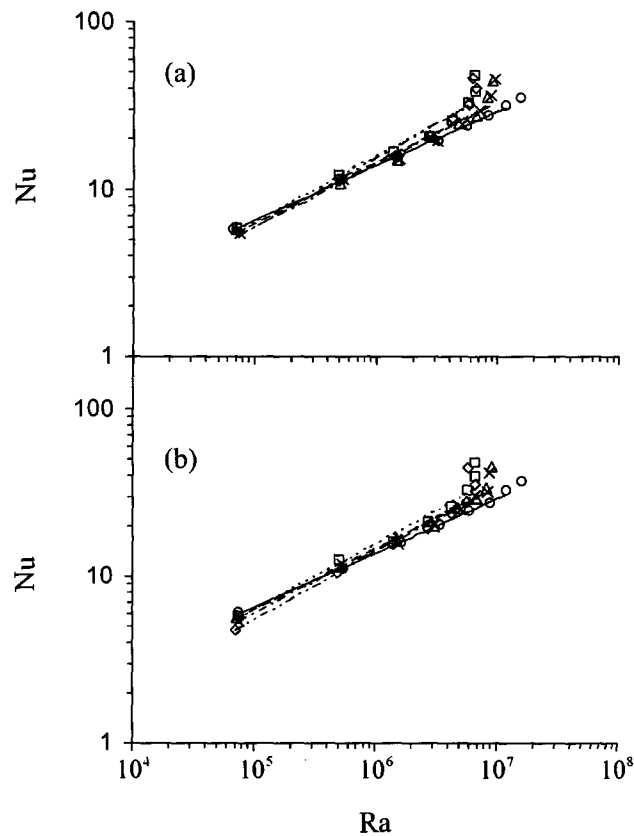


Figure 5.28: Change in the local Nusselt number with the local Rayleigh number for cases with the partition on the top wall at (a) $x/H = 0.2$ and (b) $x/H = 0.6$. Partition with the non-dimensional height of 0.0625 and θ_T of \circ : 0.56 (insulated), \triangle : 1.4 and \square : 2.3. Partition with the non-dimensional height of 0.125 and θ_T of \times : 1.4 and \diamond : 2.3.

Chapter 6

Conclusions

An experimental investigation was performed to characterize the laminar natural convection in air-filled rectangular cavities with and without a partition on the wall. The vertical walls of the cavities were maintained at uniform but different average temperatures, so a natural convection flow was driven in these cavities. The experiments were performed for a global Grashof number based on the height of the cavities, Gr_H , of approximately 1.4×10^8 to 1.8×10^8 , and non-dimensional top wall temperatures in the range 0.52 (insulated) to 2.3. In rectangular cavities with aspect ratios of 0.5, 1.0 and 2.0, the effects of the top wall temperature and the aspect ratio on the laminar natural convection were studied. In order to characterize the effect of a partition on the laminar natural convection in a square cavity, an aluminium partition with non-dimensional heights of 0.0625 and 0.125 was attached either to the heated vertical wall or top wall at $y/H = 0.65, 0.95$ and $x/H = 0.1, 0.2, 0.4$ and 0.6.

In the rectangular cavities with aspect ratios of 0.5, 1.0 and 2.0, flow visualizations and temperature measurements showed that the flow pattern and temperature profiles near the top wall were significantly changed as the top wall of the cavities was heated. When the top wall was heated with a modest top wall temperature

($\theta_T \lesssim 1.2$), the natural convection boundary layer flow remained attached along the heated vertical wall and turned around the corner before separating from the top wall. This results in an undulating flow region in the upper left corner of the cavities, causing a non-uniformity in the temperature profiles in this region. The location of the trough of the undulating flow changed with the top wall temperature, but was nearly independent of the aspect ratio of the cavities. The flow separation also caused a secondary flow in the region between the boundary layer flow along the heated vertical wall and the undulating flow. This secondary flow resulted in the temperature distributions just outside the boundary layer to be approximately uniform in this region.

For the cavities with a large top wall temperature ($\theta_T \gtrsim 1.2$), the upward natural convection boundary layer flow along the heated vertical wall separated from the heated vertical wall and turned over before reaching the top wall due to the negative buoyancy force. There is an anti-clockwise recirculating flow between the separated flow and the heated vertical wall. The extent of the recirculating flow decreased with an increase of the aspect ratio. The location of the trough of the undulating flow was insensitive to the change in the top wall temperature, which is different from that in the cases with the modest top wall temperatures, since the top wall could not directly affect the upward boundary layer flow along the heated vertical wall. For a given aspect ratio, with an increase of the top wall temperature, the y -location where the upward boundary layer along the heated vertical wall turned over decreased and the undulating flow becomes more stable.

In the rectangular cavities, the ambient temperature outside the boundary layer increased approximately linearly with the height over most of the cavity ($y/H \lesssim 0.8$). With an increase of the top wall temperature, the local ambient temperature increased. In the case with large top wall temperatures, the local ambient temperature

near the bottom wall is more sensitive to the change in the top wall temperature compared to that for the case with modest top wall temperatures. The change in the ambient temperature is more sensitive to the change in the top wall temperature with a decrease of the aspect ratio, since the contact area between the top wall and the natural convection flow along the top wall increased with a decrease of the aspect ratio. The temperature gradient $d\theta_\infty/d(y/H)$ increased with an increase of the top wall temperature. For a given aspect ratio, $d\theta_\infty/d(y/H)$ changed more rapidly with the change in the top wall temperature at modest top wall temperatures compared to the case with large top wall temperatures. The increase in the temperature gradient $d\theta_\infty/d(y/H)$ was more significant for the smaller aspect ratio cavity.

The local Nusselt number over most of the heated vertical wall was correlated to the local Rayleigh number in the form $Nu = C \cdot Ra^n$. The values of the index n for these rectangular cavities are significantly different from those in the cases with an isothermal vertical wall in either isothermal or non-isothermal surroundings due to the effect of the top and bottom walls on the stratification rate of the fluid outside the boundary layer. For a given aspect ratio, the value of the index n is nearly independent of the modest top wall temperatures, while the value of n changed with the large top wall temperatures. The average Nusselt number for the heated vertical wall \overline{Nu}_H also increased with an increase of the vertical Rayleigh number Ra_V and could be correlated by $\overline{Nu}_H = 1.0113 \cdot Ra_V^{0.2117}$ for the range of experiments performed here.

The temperature profiles predicted from the similarity solutions for the natural convection flow along an isothermal vertical wall in a stratified medium proposed by Kulkarni et al. [1] do not agree with the measurements in the current cases. The buoyancy associated with the temperature profiles predicted from the similarity solutions were negative so they could, at most, describe a decelerating boundary layer flow after it has passed through the neutral buoyancy point. The boundary

layer flow here either did not reach the solutions or overshoot them depending on the top wall temperature. The profiles predicted using the non-similarity model outlined in Chen and Eichhorn [2] were in good agreement with the measurements in the region $y/H \lesssim 0.5$. However, in the upper part of the heated vertical wall, there are some discrepancies between the experimental data and the model solution. The heat transfer from the heated vertical wall at $y/H \lesssim 0.8$ was reasonably predicted by the non-similarity model but there were some differences in the non-dimensional integral of the buoyancy force along the heated vertical wall between the experimental data and the non-similarity solutions in this region.

When an aluminium partition was attached to either the heated vertical wall or the top wall, the blockage effect and/or the thermal effect of the partition resulted in changes in the temperature and flow fields compared to those in the corresponding cavity without the partition. However, the changes are mainly limited in the vicinity of the partition. For the cases with the insulated top wall, the blockage effect of the partition dominated, resulting in flow separation and the formation of a recirculating flow behind the partition. The extent of the recirculating flow region was depended on the location of the partition. The recirculating flow caused the temperature distributions in this flow region to be relatively uniform and different from those in the corresponding cavity without the partition.

For the cavity with the partition on the heated vertical wall at $y/H = 0.65$ and with the heated top wall, the blockage effect dominated even at the large top wall temperature of $\theta_T \approx 2.3$, resulting in the y -location where the upward boundary layer flow turned over to be lower than that in the corresponding cavity without the partition. For the cavity with the partition at $y/H = 0.95$ and the $\theta_T \approx 2.3$, there is no blockage effect for the non-dimensional partition height of 0.0625, and the thermal effect increased as the non-dimensional partition height increased to 0.125.

For the cavity with the heated top wall, the change in the height of the partition at $y/H = 0.95$ resulted in changes to the ambient temperature outside the boundary layer due to the change in the recirculating flow in the corner region. The variations of the partition height and the top wall temperature affected the blockage effect of the partition, resulting in the local Nusselt number near the corner region to be affected.

When the partition was attached to the heated top wall, a recirculating flow was formed between the partition, heated vertical wall, top wall and the separated flow. This flow is likely driven by the temperature difference between the partition and the heated vertical wall. For a given partition height, the structure of the recirculating flow was dependent on the partition location and the top wall temperature. With an increase of the partition height, the region of the recirculating flow was expanded. In this case, the flow attached and flowed up along the rear surface of the partition. The temperature gradient near the rear surface of the partition was increased with an increase of the top wall temperature.

For the case with the insulated top wall, the ambient temperature outside the boundary layer and the local Nusselt number near the corner region changed with the partition location due to the blockage effect of the partition. For the case with the heated top wall, however, there are no significant changes in the ambient temperature and the local Nusselt number when the partition was moved from $x/H = 0.2$ to $x/H = 0.6$. The ambient temperature outside the boundary layer and the local Nusselt number near the corner region were affected by the partition height due to the changes in the recirculating flow between the partition and the heated vertical wall and the rear surface of the partition.

Similar to the cases without the partition, the local Nusselt number over most of the heated vertical wall of these partitioned cavities could be correlated to the local Rayleigh number in the form $Nu = C \cdot Ra^n$. For the partition with non-

dimensional heights of 0.0625 and 0.125 on the heated vertical wall at $y/H = 0.95$ as well as the partition with the non-dimensional height of 0.0625 on the top wall, the values of the constant C and the index n were approximately the same as those in the corresponding cavity without the partition, since the effect of the partition was limited to its immediate vicinity. The larger partition on the top wall resulted in the value of the index n to be larger than that in the cavity with the smaller partition. For the larger partition, the values of the constant C and the index n were nearly independent of the partition location.

The major contributions of this study to the scientific and engineering fields are:

1. Elicited the mechanisms of the laminar natural convection in rectangular cavities with various thermal boundary conditions and geometries. The new findings provide a more fundamental understanding in this field and provide insight to further develop theoretical and numerical models of natural convection in rectangular cavities.
2. Determined the extent of the effect of partitions on the laminar natural convection in a square cavity with large top wall temperatures. The experimental results extend our understanding of the effect of partitions on the natural convection in cavities. In particular, the new findings could be used in engineering applications to optimize the energy transfer in rooms, buildings and enclosed electronics cabinets.
3. Evaluated existing theoretical models for prediction of the natural convection in a square cavity with a heated top wall. The current study clearly indicated that these models can not accurately describe the characteristics of the laminar natural convection in an air-filled square cavity with large top wall temperatures.

The models considered are unable to fully capture the mechanisms for this configuration.

4. The extensive measurements provide a significant data bank for the natural convection in rectangular cavities with different geometries and thermal boundary conditions. The data could be important to benchmark future numerical simulations.

Chapter 7

Recommendations

In the current investigation, the temperature distributions in the boundary layer flow along the heated vertical wall and the flow patterns in the cavities with and without a partition on the wall were obtained. A greater fundamental understanding of the mechanism of the laminar natural convection flow in the cavities were obtained from these measurements. However, due to instrument limitations, the velocity distributions in the boundary layer flow along the heated vertical wall were not measured. It will be useful to characterize the velocity field in the boundary layer flow along the heated vertical wall using PIV, LDA or a pulsed-wire. These measurements will yield valuable information to determine the reason and location of the flow separation of the boundary layer along the heated vertical wall.

A pulsed-wire is currently being developed for velocity measurements in the cavity. The preliminary velocity measurements using the pulsed-wire for the upward boundary layer flow along the heated vertical wall of the square cavity without the partition and with the non-dimensional top wall temperature θ_T of approximately 2.3 are shown in Figure 7.1. The measurements were performed at non-dimensional heights y/H of 0.2, 0.5 and 0.8. The peak velocity of the upward boundary layer flow

at the height $y/H = 0.5$ is larger than that at heights $y/H = 0.2$ and 0.8 , similar to the result reported by Tian and Karayiannis [6]. However, the velocity distributions are skewed by the thermal diffusion, especially at low velocities, which should be compensated in order to accurately measure the velocity distributions. Developing a low cost pulsed-wire for convective flow will be very useful to determine the location of the flow separation and estimate the momentum flux of the boundary layer flow.

Velocity measurements of the recirculating flow in the upper left corner of the cavities with the heated top wall will be useful to further clarify the effect of the top wall temperature on the heat transfer characteristics in the cavity, especially in the region close to the top wall. This will provide information on the effect of the recirculating flow on the vertical momentum of the upward boundary layer flow along the heated vertical wall, which in turn could affect the heat transfer characteristics of the natural convection flow.

The measurement could be further extended to the velocity and temperature fields in the downward boundary layer flow along the cooled vertical wall of the cavity, so the heat and flow in the entire cavity could be characterized. The results shown in Figure 4.25 indicate that for the cases with large top wall temperatures, the downward flow along the cooled vertical wall could affect the local ambient temperature distributions outside the boundary layer, θ_∞ , in the region close to the bottom wall. For the cases with the heated top wall, it was observed that the natural convection flow separated from either the heated vertical wall or top wall due to the negative buoyancy force. Hence, the characteristics of the temperature field, especially in the upper part of the cavity, were affected. When the flow moves down along the cooled vertical wall, the directions of the gravity and the flow velocity are the same. This would result in an asymmetry in the temperature and flow fields between the upper left and lower right corners of the cavity. The whole field measurements will be useful

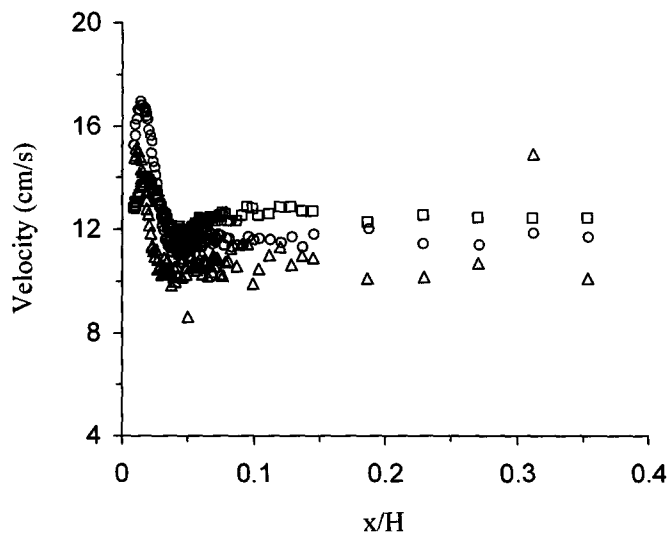


Figure 7.1: Preliminary velocity measurements by a pulsed-wire for the upward boundary layer flow along the heated vertical wall at non-dimensional heights y/H of \triangle : 0.2, \circ : 0.5 and \square : 0.8. These measurements were performed in the square cavity with smooth walls and non-dimensional top wall temperature θ_T of approximately 2.3.

to clarify the physical mechanism here.

Bibliography

- [1] A.K. Kulkarni, H.R. Jacobs, and J.J. Hwang. Similarity solution for natural convection flow over an isothermal vertical wall immersed in thermally stratified medium. *Int. J. Heat Mass Transfer*, 30:691–698, 1987.
- [2] C.C. Chen and R. Eichhorn. Natural convection from a vertical surface to a thermally stratified fluid. *Journal of Heat Transfer*, 98:446–451, 1976.
- [3] E.R.G. Eckert and W.O. Carlson. Natural convection in an air layer enclosed between two vertical plates with different temperatures. *Int. J. Heat Mass Transfer*, 2:106–120, 1961.
- [4] D.E. Cormack, L.G. Leal, and J.H. Seinfeld. Natural convection in a shallow cavity with differentially heated end walls. Part 2. Numerical solutions. *J. Fluid Mech.*, 65:231–246, 1974.
- [5] S.H. Yin, T.Y. Wung, and K. Chen. Natural convection in an air layer enclosed within rectangular cavities. *Int. J. Heat Mass Transfer*, 21:307–315, 1978.
- [6] Y.S. Tian and T.G. Karayiannis. Low turbulence natural convection in an air filled square cavity — Part I: the thermal and fluid flow fields. *Int. J. Heat Mass Transfer*, 43:849–866, 2000.

-
- [7] M.W. Nansteel and R. Greif. Natural convection in undivided and partially divided rectangular enclosures. *Journal of Heat Transfer*, 103:623–629, 1981.
- [8] K.M. Kelkar and S.V. Patankar. Numerical prediction of natural convection in square partitioned enclosures. *Numerical Heat Transfer, Part A*, 17:269–285, 1990.
- [9] R. Scozia and R.L. Frederick. Natural convection in slender cavities with multiple fins attached to an active wall. *Numerical Heat Transfer*, 20:127–158, 1991.
- [10] E. Bilgen. Natural convection in cavities with a thin fin on the hot wall. *Int. J. Heat Mass Transfer*, 48:3493–3505, 2005.
- [11] N. Seki, S. Fukusako, and H. Inaba. Visual observation of natural convective flow in a narrow vertical cavity. *J. Fluid Mech.*, 84:695–704, 1978.
- [12] M.E. Newell and F.W Schmidt. Heat transfer by laminar natural convection within rectangular enclosures. *Journal of Heat Transfer*, 92:159–168, 1970.
- [13] J.E. Drummond and S.A. Korpela. Natural convection in a shallow cavity. *J. Fluid Mech.*, 182:543–564, 1987.
- [14] S. Ostrach. Natural convection in enclosures. *Journal of Heat Transfer*, 110:1175–1190, 1988.
- [15] S. Ostrach and C. Raghavan. Effect of stabilizing thermal gradients on natural convection in rectangular enclosures. *Journal of Heat Transfer*, 101:238–243, 1979.

- [16] G.S. Shiralkar and C.L. Tien. A numerical study of the effect of a vertical temperature difference imposed on a horizontal enclosure. *Numerical Heat Transfer*, 5:185–197, 1982.
- [17] M.R. Ravi, R.A.W.M. Henkes, and C.J. Hoogendoorn. On the high-Rayleigh-number structure of steady laminar natural-convection flow in a square enclosure. *J. Fluid Mech.*, 262:325–351, 1994.
- [18] W. Wu, D. Ewing, and C.Y. Ching. The effect of the top and bottom wall temperatures on the laminar natural convection in an air-filled square cavity. *Int. J. Heat Mass Transfer*, 49:1999–2008, 2006.
- [19] A. Emery and N.C. Chu. Heat transfer across vertical layers. *Journal of Heat Transfer*, 87:110–114, 1965.
- [20] R.K. MacGregor and A.F. Emery. Free convection through vertical plane layers—moderate and high Prandtl number fluids. *Journal of Heat Transfer*, 91:391–403, 1969.
- [21] J.W. Elder. Laminar free convection in a vertical slot. *J. Fluid Mech.*, 23:77–98, 1965.
- [22] S. Wakitani. Flow patterns of natural convection in an air-filled vertical cavity. *Physics of Fluids*, 10:1924–1928, 1998.
- [23] B. Lartigue, S. Lorente, and B. Bourret. Multicellular natural convection in a high aspect ratio cavity: experimental and numerical results. *Int. J. Heat Mass Transfer*, 43:3157–3170, 2000.
- [24] S.M. Bajorek and J.R. Lloyd. Experimental investigation of natural convection in partitioned enclosures. *Journal of Heat Transfer*, 104:527–532, 1982.

- [25] N.N. Lin and A. Bejan. Natural convection in a partially divided enclosure. *Int. J. Heat Mass Transfer*, 26:1867–1878, 1983.
- [26] F. Ampofo. Turbulent natural convection in an air filled partitioned square cavity. *Int. J. Heat and Fluid Flow*, 25:103–114, 2004.
- [27] F. Ampofo. Turbulent natural convection of air in a non-partitioned or partitioned cavity with differentially heated vertical and conducting horizontal walls. *Experimental Thermal and Fluid Science*, 29:137–157, 2005.
- [28] X. Shi and J.M. Khodadadi. Laminar natural convection heat transfer in a differentially heated square cavity due to a thin fin on the hot wall. *Journal of Heat Transfer*, 125:624–634, 2003.
- [29] E. Bilgen. Natural convection in enclosures with partial partitions. *Renewable Energy*, 26:257–270, 2002.
- [30] S. Ostrach, R.R. Loka, and A. Kumar. Natural convection in low aspect-ratio rectangular enclosures. *ASME HTD*, 8:1–10, 1980.
- [31] A.T. Kirkpatrick and M. Bohn. An experimental investigation of mixed cavity natural convection in the high Rayleigh number regime. *Int. J. Heat Mass Transfer*, 29:69–82, 1986.
- [32] T. Nishimura, F. Nagasawa, and Y. Kawamura. Natural convection in horizontal enclosures with multiple partitions. *Int. J. Heat Mass Transfer*, 32:1641–1647, 1989.
- [33] O. Aydin, A. Unal, and T. Ayhan. Natural convection in rectangular enclosures heated from one side and cooled from the ceiling. *Int. J. Heat Mass Transfer*, 42:2345–2355, 1999.

- [34] M. Corcione. Effects of the thermal boundary conditions at the sidewalls upon natural convection in rectangular enclosures heated from below and cooled from above. *International Journal of Thermal Sciences*, 42:199–208, 2003.
- [35] C.J. Hoogendoorn. Natural convection in enclosures. *Proceedings of the Eighth International Heat Transfer Conference*, 1:111–120, San Francisco, 1986.
- [36] S. Ostrach. Natural convection heat transfer in cavities and cells. *Proceedings of the Seventh International Heat Transfer Conference*, 1:365–379, Washington, D.C., 1982.
- [37] J.M. Hyun. Unsteady buoyant convection in an enclosure. *Advanced Heat Transfer*, 24:277–320, 1994.
- [38] H. Ozoe, K. Yamamoto, H. Sayama, and S.W. Churchill. Natural circulation in an inclined rectangular channel heated on one side and cooled on the opposing side. *Int. J. Heat Mass Transfer*, 17:1209–1217, 1974.
- [39] J.N. Arnold, I. Catton, and D.K. Edwards. Experimental investigation of natural convection in inclined rectangular regions of differing aspect ratios. *Journal of Heat Transfer*, 98:67–71, 1976.
- [40] S.M. EISherbiny, G.D. Raithby, and K.G.T. Hollands. Heat transfer by natural convection across vertical and inclined air layers. *Journal of Heat Transfer*, 104:96–102, 1982.
- [41] V. Sernas and E.I. Lee. Heat transfer in air enclosures of aspect ratio less than one. *Journal of Heat Transfer*, 103:617–622, 1981.

- [42] D.G. Briggs and D.N. Jones. Two-dimensional periodic natural convection in a rectangular enclosure of aspect ratio one. *Journal of Heat Transfer*, 107:850–854, 1985.
- [43] R. Viskanta, D.M. Kim, and C. Gau. Three-dimensional natural convection heat transfer of a liquid metal in a cavity. *Int. J. Heat Mass Transfer*, 29:475–485, 1986.
- [44] M.S. Bohn and R. Anderson. Temperature and heat flux distribution in a natural convection enclosure flow. *Journal of Heat Transfer*, 108:471–475, 1986.
- [45] Y.S. Tian and T.G. Karayiannis. Low turbulence natural convection in an air filled square cavity — Part II: the turbulence quantities. *Int. J. Heat Mass Transfer*, 43:867–884, 2000.
- [46] N. Ramesh and S.P. Venkateshan. Experimental study of natural convection in a square enclosure using differential interferometer. *Int. J. Heat Mass Transfer*, 44:1107–1117, 2001.
- [47] F. Ampofo and T.G. Karayiannis. Experimental benchmark data for turbulent natural convection in an air filled square cavity. *Int. J. Heat Mass Transfer*, 46:3551–3572, 2003.
- [48] J. Salat, S. Xin, P. Joubert, A. Sergent, F. Penot, and P. Le Quere. Experimental and numerical investigation of turbulent natural convection in a large air-filled cavity. *Int. J. Heat and Fluid Flow*, 25:824–832, 2004.
- [49] R. Cheesewright. Natural convection from a plane, vertical surface in non-isothermal surroundings. *Int. J. Heat Mass Transfer*, 10:1847–1859, 1967.

- [50] A.E. Gill. The boundary-layer regime for convection in a rectangular cavity. *J. Fluid Mech.*, 26:515–536, 1966.
- [51] G. De Vahl Davis. Laminar natural convection in an enclosed rectangular cavity. *Int. J. Heat Mass Transfer*, 11:1675–1693, 1968.
- [52] W.M.M. Schinkel, S.J.M. Linthorst, and C.J. Hoogendoorn. The stratification in natural convection in vertical enclosures. *ASME HTD*, 8:31–38, 1980.
- [53] M. Farhangnia, S. Biringen, and L.J. Peltier. Numerical simulation of two-dimensional buoyancy-driven turbulence in a tall rectangular cavity. *International Journal for Numerical Methods in Fluids*, 23:1311–1326, 1996.
- [54] Z.J. Zhu and H.X. Yang. Numerical investigation of transient laminar natural convection of air in a tall cavity. *Heat and Mass Transfer*, 39:579–587, 2003.
- [55] D.E. Cormack, L.G. Leal, and J. Imberger. Natural convection in a shallow cavity with differentially heated end walls. Part 1. Asymptotic theory. *J. Fluid Mech.*, 65:209–229, 1974.
- [56] J. Imberger. Natural convection in a shallow cavity with differentially heated end walls. Part 3. Experimental results. *J. Fluid Mech.*, 65:247–260, 1974.
- [57] Cormack. D.E., G.P. Stone, and L.G. Leal. The effect of upper surface conditions on convection in a shallow cavity with differentially heated end-walls. *Int. J. Heat Mass Transfer*, 18:635–648, 1975.
- [58] A. Bejan, A.A. Al-Homoud, and J. Imberger. Experimental study of high-Rayleigh-number convection in a horizontal cavity with different end temperatures. *J. Fluid Mech.*, 109:283–299, 1981.

- [59] R. Yewell, D. Poulikakos, and A. Bejan. Transient natural convection experiments in shallow enclosures. *Journal of Heat Transfer*, 104:533–538, 1982.
- [60] J.E. Hart. Low prandtl number convection between differentially heated end walls. *Int. J. Heat Mass Transfer*, 26:1069–1074, 1983.
- [61] H. Ozoe, M. Ohmuro, A. Mouri, S. Mishima, H. Sayama, and S.W. Churchill. Laser-doppler measurements of the velocity along a heated vertical wall of a rectangular enclosure. *Journal of Heat Transfer*, 105:782–788, 1983.
- [62] Y. Kamotani, L.W. Wang, and S. Ostrach. Experiments on natural convection heat transfer in low aspect ratio enclosures. *AIAA Journal*, 21:290–294, 1983.
- [63] P.G. Baines. Two-dimensional plumes in stratified environments. *J. Fluid Mech.*, 471:315–337, 2002.
- [64] B.A. Meyer, J.W. Mitchell, and M.M. El-Wakil. Natural convection heat transfer in moderate aspect ratio enclosures. *Journal of Heat Transfer*, 101:655–659, 1979.
- [65] F.J. Hamady, J.R. Lloyd, H.Q. Yang, and K.T. Yang. Study of local natural convection heat transfer in an inclined enclosure. *Int. J. Heat Mass Transfer*, 32:1697–1708, 1989.
- [66] M.A.R. Sharif and W. Liu. Numerical study of turbulent natural convection in a side-heated square cavity at various angles of inclination. *Numerical Heat Transfer, Part A*, 43:693–716, 2003.
- [67] M. Rahman and M.A.R. Sharif. Numerical study of laminar natural convection in inclined rectangular enclosures of various aspect ratios. *Numerical Heat Transfer, Part A*, 44:355–373, 2003.

- [68] D. Dropkin and E. Somerscales. Heat transfer by natural convection in liquids confined by two parallel plates which are inclined at various angles with respect to the horizontal. *Journal of Heat Transfer*, 87:77–84, 1965.
- [69] K.R. Randall, J.W. Mitchell, and M.M. EI-Wakil. Natural convection heat transfer characteristics of flat plate enclosures. *Journal of Heat Transfer*, 101:120–125, 1979.
- [70] S.M. Elsherbiny. Free convection in inclined air layers heated from above. *Int. J. Heat Mass Transfer*, 39:3925–3930, 1996.
- [71] N. Yucel and H. Turkoglu. Numerical analysis of laminar natural convection in enclosures with fins attached to an active wall. *Heat and Mass Transfer*, 33:307–314, 1998.
- [72] R.L. Frederick and A. Valencia. Natural convection in central microcavities of vertical, finned enclosures of very high aspect ratios. *Int. J. Heat and Fluid Flow*, 16:114–124, 1995.
- [73] A. Nag, A. Sarkar, and V.M.K. Sastri. Effect of thick horizontal partial partition attached to one of the active walls of a differentially heated square cavity. *Numerical Heat Transfer, Part A*, 25:611–625, 1994.
- [74] R.L. Frederick. Natural convection in an inclined square enclosure with a partition attached to its cold wall. *Int. J. Heat Mass Transfer*, 32:87–94, 1989.
- [75] R.L. Frederick and A. Valencia. Heat transfer in a square cavity with a conducting partition on its hot wall. *Int. Comm. Heat Mass Transfer*, 16:347–354, 1989.

- [76] S. Shakerin, M. Bohn, and R.I. Loehrke. Natural convection in an enclosure with discrete roughness elements on a vertical heated wall. *Int. J. Heat Mass Transfer*, 31:1423–1430, 1988.
- [77] H. Ambarita, K. Kishinami, M. Daimaruya, T. Saitoh, H. Takahashi, and J. Suzuki. Laminar natural convection heat transfer in an air filled square cavity with two insulated baffles attached to its horizontal walls. *Thermal Science & Engineering*, 14:35–46, 2006.
- [78] N. Yucel and A.H. Ozdem. Natural convection in partially divided square enclosures. *Heat and Mass Transfer*, 40:167–175, 2003.
- [79] H. Turkoglu and N. Yucel. Natural convection heat transfer in enclosures with conducting multiple partitions and side walls. *Heat and Mass Transfer*, 32:1–8, 1996.
- [80] E.S. Nowak and M.H. Novak. Vertical partitions in slender rectangular cavities. *Int. J. Heat and Fluid Flow*, 15:104–110, 1994.
- [81] M. Ciofalo and T.G. Karayiannis. Natural convection heat transfer in a partially-or completely-partitioned vertical rectangular enclosure. *Int. J. Heat Mass Transfer*, 34:167–179, 1991.
- [82] S. Acharya and R. Jetli. Heat transfer due to buoyancy in a partially divided square box. *Int. J. Heat Mass Transfer*, 33:931–942, 1990.
- [83] D.A. Olson, L.R. Glicksman, and H.M. Ferm. Steady-state natural convection in empty and partitioned enclosures at high Rayleigh numbers. *Journal of Heat Transfer*, 112:640–647, 1990.

- [84] K.S. Chen, A.C. Ku, and C.H. Chou. Investigation of natural convection in partially divided rectangular enclosures both with and without an opening in the partition plate: measurement results. *Journal of Heat Transfer*, 112:648–652, 1990.
- [85] T. Nishimura, M. Shiraishi, F. Nagasawa, and Y. Kawamura. Natural convection heat transfer in enclosures with multiple vertical partitions. *Int. J. Heat Mass Transfer*, 31:1679–1686, 1988.
- [86] R. Jetli and S. Acharya. End wall effects on thermal stratification and heat transfer in a vertical enclosure with offset partitions. *The Canadian Journal of Chemical Engineering*, 66:563–571, 1988.
- [87] E. Zimmerman and S. Acharya. Free convection heat transfer in a partially divided vertical enclosure with conducting end walls. *Int. J. Heat Mass Transfer*, 30:319–331, 1987.
- [88] T. Nishimura, M. Shiraishi, and Y. Kawamura. Natural convection heat transfer in enclosures with an off-center partition. *Int. J. Heat Mass Transfer*, 30:1756–1758, 1987.
- [89] H.J. Shaw, C.K. Chen, and J.W. Cleaver. Cubic spline numerical solution for two-dimensional natural convection in a partially divided enclosure. *Numerical Heat Transfer*, 12:439–455, 1987.
- [90] R. Jetli, S. Acharya, and E. Zimmerman. Influence of baffle location on natural convection in a partially divided enclosure. *Numerical Heat Transfer*, 10:521–536, 1986.

- [91] T.W. Tong and F.M. Gerner. Natural convection in partitioned air-filled rectangular enclosures. *Int. Comm. Heat Mass Transfer*, 13:99–108, 1986.
- [92] M.W. Nansteel and R. Greif. An investigation of natural convection in enclosures with two- and three-dimensional partitions. *Int. J. Heat Mass Transfer*, 27:561–571, 1984.
- [93] D. Duxbury. An interferometric study of natural convection in enclosed plane air layers with complete and partial central vertical divisions. *Ph.D. thesis*, University of Salford, 1979.
- [94] E.M. Sparrow, H. Quack, and C.J. Boerner. Local nonsimilarity boundary-layer solutions. *AIAA Journal*, 8:1936–1942, 1970.
- [95] E.M. Sparrow and H.S. Yu. Local non-similarity thermal boundary-layer solutions. *Journal of Heat Transfer*, 93:328–334, 1971.
- [96] W.J. Minkowycz and E.M. Sparrow. Local nonsimilar solutions for natural convection on a vertical cylinder. *Journal of Heat Transfer*, 96:178–183, 1974.
- [97] M.W. Nansteel, S.S. Sathel, and P.S. Ayyaswamy. Discontinuous boundary temperatures in heat transfer theory. *ASME Proc. Heat Transfer*, pages 123–126, 1986.
- [98] R.B. Chinnakotla, D. Angirasa, and R.L. Mahajan. Parametric study of buoyancy-induced flow and heat transfer from L-shaped corners with asymmetrically heated surfaces. *Int. J. Heat Mass Transfer*, 39:851–865, 1996.
- [99] J.P. Holman. Heat transfer. *Sixth Edition*, McGraw-Hill Book Company, 1986.

- [100] W. Wu. The effect of stable stratification on the natural convection in a square cavity caused by a horizontal temperature difference. *Master's Thesis*, McMaster University, Hamilton, Ontario, Canada, 2004.
- [101] H.W. Coleman and W.G. Steele. Experimentation and uncertainty analysis for engineers. *Second Edition*, John Wiley and Sons, Inc., New York, 1999.
- [102] F.P. Incropera and D.P. DeWitt. Introduction to heat transfer. *Fourth Edition*, John Wiley and Sons, Inc., 2002.